

---

# **MODELLING RIVER ICE FREEZE-UP ON THE RED RIVER NEAR NETLEY CUT**

---

by

**Melissa Aynslie Marie Haresign**

A Thesis submitted to the Faculty of Graduate Studies of  
University of Manitoba  
In partial fulfillment of the requirements for the degree of

**Master of Science**

Department of Civil Engineering  
University of Manitoba  
Winnipeg, Manitoba, Canada

Copyright © 2012 by Melissa Aynslie Marie Haresign

---

## **ABSTRACT**

CRISSP2D, a two-dimensional finite element model, was used to undertake a comprehensive hydrodynamic, thermodynamic, and dynamic ice study on the Red River near Netley Cut in order to determine the cut's effect on the local hydrodynamics and freeze-up processes.

Open water hydrodynamic and thermodynamic models were developed, calibrated, and verified such that the measured data and simulation results were in acceptable agreement. These models were used as input to the dynamic ice model which was able to adequately predict ice thickness within the study area once the air-ice heat transfer coefficient was calibrated.

The geometry of the dynamic ice model was subsequently altered to simulate the effects of sealing Netley Cut. The geometry change resulted in no noticeable difference in simulated ice thickness, but did affect the hydrodynamics within the study area. In particular, the water velocity in the Red River downstream of Netley Cut and water surface elevation upstream of Netley Cut both increased noticeably.

## **ACKNOWLEDGEMENTS**

First and foremost I offer my sincerest gratitude to my advisor, Dr. Shawn Clark. He has supported me throughout my thesis with his patience and knowledge while having the confidence in me to allow me to work independently. Shawn's knowledge and enthusiasm for water resources engineering has undoubtedly led me to towards a successful M.Sc. thesis and a fulfilling career.

I would also like to acknowledge the assistance from several individuals within the Water Resources Group at the University of Manitoba. In particular, Jarrod Malenchak, whose expertise of CRISSP2D was invaluable throughout this project. I would also like to thank the students who assisted with data collection, including Parsa Aminian, Tyson Dyck, Garrett Ward, Brittany Dupont, Milan Bileljanin, Andrew Weiss, and Kevin Sagan.

I would like to acknowledge the funding contributions from the University of Manitoba, the National Science and Engineering Research Council, and Manitoba Water Stewardship, without which this research would not have been possible.

Last, but certainly not least, I would like to thank my family and friends who have always shown support. In particular, my parents whose unconditional love and encouragement have allowed me to pursue challenges and achieve goals that at one time seemed unreachable.

## TABLE OF CONTENTS

ABSTRACT.....	ii
ACKNOWLEDGEMENTS.....	iii
TABLE OF CONTENTS.....	iv
LIST OF FIGURES.....	viii
LIST OF TABLES.....	xiii
LIST OF COPYRIGHTED MATERIAL FOR WHICH PERMISSION WAS OBTAINED .....	xiv
NOMENCLATURE.....	xv
CHAPTER 1 <i>INTRODUCTION</i> .....	1
1.1     PROJECT OVERVIEW.....	1
1.2     DESCRIPTION OF THE STUDY AREA .....	4
1.2.1     LAKE WINNIPEG .....	5
1.2.2     THE RED RIVER .....	6
1.2.3     THE NETLEY-LIBAU MARSH.....	8
1.3     PROJECT OBJECTIVES.....	18
CHAPTER 2 <i>LITERATURE REVIEW</i> .....	19
2.1     INTRODUCTION .....	19
2.2     SURFACE HEAT EXCHANGE .....	20

---

## TABLE OF CONTENTS

---

2.2.1	SHORTWAVE RADIATION .....	21
2.2.2	LONGWAVE RADIATION.....	22
2.2.3	EVAPORATIVE HEAT TRANSFER .....	23
2.2.4	CONDUCTIVE HEAT TRANSFER .....	24
2.2.5	PRECIPITATION.....	25
2.3	LINEAR APPROXIMATION OF THE ENERGY BUDGET .....	26
2.4	FREEZE-UP PROCESSES.....	28
2.4.1	LAKE ICE FORMATION .....	29
2.4.2	RIVER ICE FORMATION .....	33
CHAPTER 3	<i>NUMERICAL MODEL</i> .....	40
3.1	INTRODUCTION TO CRISSP2D .....	40
3.2	MODEL COMPONENTS.....	41
3.2.1	HYDRODYNAMIC MODULE .....	42
3.2.2	WATER TEMPERATURE MODULE.....	43
3.2.3	THERMAL ICE MODULE.....	44
3.2.4	DYNAMIC ICE MODULE .....	45
3.3	MODEL REQUIREMENTS.....	46
3.3.1	DATA REQUIREMENTS .....	47
3.3.2	BOUNDARY AND INITIAL CONDITIONS .....	48

---

**TABLE OF CONTENTS**

---

3.3.3	MODEL CALIBRATION .....	49
CHAPTER 4	<i>DATA ACQUISITION</i> .....	51
4.1	INTRODUCTION .....	51
4.2	BATHYMETRY.....	52
4.3	OPEN WATER DATA COLLECTION .....	55
4.4	PRE-FREEZE-UP DATA COLLECTION.....	60
4.5	WINTER DATA COLLECTION .....	61
CHAPTER 5	<i>MODEL DEVELOPMENT</i> .....	67
5.1	FINITE ELEMENT MESH DEVELOPMENT.....	67
5.2	BOUNDARY CONDITIONS .....	70
5.3	INITIAL CONDITIONS.....	73
CHAPTER 6	<i>HYDRODYNAMIC MODEL</i> .....	74
6.1	HYDRODYNAMIC CALIBRATION .....	74
6.2	HYDRODYNAMIC VERIFICATION .....	83
CHAPTER 7	<i>DYNAMIC ICE MODEL</i> .....	87
7.1	INTRODUCTION .....	87
7.2	CALIBRATION OF WATER-AIR HEAT TRANSFER COEFFICIENT.....	88
7.3	DYNAMIC ICE MODEL CALIBRATION .....	92
7.3.1	BOUNDARY CONDITIONS.....	94

---

## TABLE OF CONTENTS

---

7.3.2	INITIAL CONDITIONS .....	95
7.3.3	INITIAL FREEZE-UP PERIOD .....	96
7.3.4	CALIBRATION OF ICE GROWTH.....	99
7.3.5	DISCHARGE AND WATER SURFACE ELEVATION MEASUREMENTS.....	102
7.4	DYNAMIC ICE VERIFICATION .....	104
7.4.1	2010-2011 WINTER SEASON .....	104
7.4.2	2011-2012 WINTER SEASON.....	112
7.5	DISCUSSION OF DYNAMIC ICE MODEL.....	120
7.5.1	THE INFLUENCE OF WATER VELOCITY ON ICE THICKNESS .....	120
7.5.2	THE INFLUENCE OF FRAZIL ICE PRODUCTION ON ICE GROWTH .....	123
7.5.3	THE INFLUENCE OF SNOW AND WIND ON ICE THICKENING .....	126
7.6	THE EFFECT OF SEALING NETLEY CUT .....	127
CHAPTER 8	<i>CONCLUSION</i> .....	130
8.1	PRJOECT SUMMARY .....	130
8.2	CONCLUSIONS .....	134
8.3	RECOMMENDATIONS & FUTURE WORK.....	135
REFERENCES	.....	139
APPENDIX A	.....	146

## LIST OF FIGURES

Figure 1.1: Study Area. ....	4
Figure 1.2: Netley-Libau Marsh Vegetated Area Change between 1979 and 2001 .....	10
Figure 1.3: Conceptual diagram of some factors thought to be contributing to the decline of emergent vegetation. ....	11
Figure 1.4: Change in river bed bathymetry between 1998 and 2001 at Red River flow split.....	14
Figure 1.5: Change in river bed bathymetry between 1998 and 2001 at mouth of main channel.....	14
Figure 1.6: Erosion of Netley Cut between 1923 and 2003. ....	16
Figure 4.1: Bathymetry obtained in 2009 hydrometric survey.....	52
Figure 4.2: Bathymetry obtained from 1957 hydrometric survey. ....	53
Figure 4.3: Bathymetry obtained from University of Manitoba ADCP survey.....	54
Figure 4.4: Location of pressure transducers in the summer of 2010.....	57
Figure 4.5: Argonaut locations, summer 2009.....	59
Figure 4.6: Ice thickness measurement locations in winter 2009-2010. ....	61
Figure 4.7: Ice thickness measurement locations in winter 2011.....	62
Figure 4.8: Ice thickness measurement locations in winter 2010-2011. ....	63



---

## LIST OF FIGURES

---

Figure 4.9: Ice thickness measurement locations in winter 2011-2012. ....	65
Figure 5.1: Finite element mesh.....	69
Figure 6.1: Reach boundaries and locations of calibration gauges.....	77
Figure 6.2: Hydrodynamic calibration at Red River flow split.....	79
Figure 6.3: Hydrodynamic calibration at Devils Creek. ....	80
Figure 6.4: Hydrodynamic calibration at Netley Creek. ....	80
Figure 6.5: Hydrodynamic Calibration at Breezy Point .....	81
Figure 6.6: Hydrodynamic calibration at Selkirk. ....	81
Figure 6.7: Hydrodynamic verification at Red River flow split.....	83
Figure 6.8: Hydrodynamic verification at Devils Creek. ....	84
Figure 6.9: Hydrodynamic verification at Netley Creek. ....	84
Figure 6.10: Hydrodynamic verification at Breezy Point.....	85
Figure 6.11: Hydrodynamic verification at Selkirk. ....	85
Figure 7.1: Thermodynamic calibration of the water-air heat transfer coefficient at Devils Creek. ....	89
Figure 7.2: Thermodynamic calibration of water-air heat transfer coefficient at Red River flow split.....	90
Figure 7.3: The Wolverine used to pre-cut ice covers prior to natural break-up. ....	93
Figure 7.4: Amphibex ice breaker unit. ....	93

---

## LIST OF FIGURES

---

Figure 7.5: Simulated ice type during the initial freeze-up period of 2009 at a) hour 10, b) hour 20, c) hour 30, d) hour 40.....	98
Figure 7.6: Calibration simulation at Peguis Church in winter 2009-2010. ....	101
Figure 7.7: Calibration Simulation downstream of Netley Cut in winter 2009-2010. ....	101
Figure 7.8: Comparison of modelled and measured WSE at Selkirk in winter 2009-2010.....	103
Figure 7.9: Ice concentration during freeze-up period, a) November 17, 2010 b) November 18, 2010 c) November 19, 2010 d) November 20, 2010. ....	105
Figure 7.10: Comparison between a) modelled results and b) a RADARSAT image from November 29, 2010. ....	106
Figure 7.11: Dynamic ice model verification at Sugar Island during 2010-2011 winter season. ....	108
Figure 7.12: Dynamic ice model verification at Netley Cut during 2010-2011 winter season.	108
Figure 7.13: Verification simulation of WSE at Red River flow split in 2010-2011 winter season. ....	110
Figure 7.14: Verification simulation of WSE at Devils Creek in 2010-2011 winter season.....	111
Figure 7.15: Verification simulation of WSE at Breezy Point in 2010-2011 winter season. ....	111
Figure 7.16: Verification simulation of WSE at Selkirk in 2010-2011 winter season.....	112
Figure 7.17: Comparison between the modelled results at the onset of freeze-up and the observations made in the field on November 16, 2011. ....	114

---

## LIST OF FIGURES

---

Figure 7.18: Comparison between model results and aerial photo on December 1, 2011.....	115
Figure 7.19: Dynamic ice model verification at Selkirk during 2011-2012 winter season.....	116
Figure 7.20: Dynamic ice model verification at Hwy. 4 during 2011-2012 winter season. ....	117
Figure 7.21: Dynamic ice model verification upstream of Netley Cut during 2011-2012 winter season.....	117
Figure 7.22: Comparison of measured and simulated water surface elevation at Devils Creek during the 2011-2012 winter season. ....	119
Figure 7.23: Comparison of measured and simulated water surface elevation at Selkirk during the 2011-2012 winter season.....	119
Figure 7.24: Comparison of simulated and measured ice thickness in the east and main channel.....	123
Figure 7.25: The influence of a) frazil ice on b) ice thickness in simulated results. ....	124
Figure 7.26: Comparison of modelled water surface elevation with Netley Cut open and sealed.....	128
Figure A. 1: Dynamic ice calibration upstream of Peguis Church in winter 2009-2010.....	147
Figure A. 2: Dynamic ice calibration at Breezy Point in winter 2009-2010.....	147
Figure A. 3: Dynamic ice calibration at Netley Cut in winter 2009-2010.....	147
Figure A. 4: Dynamic ice verification upstream of Sugar Island in 2010-2011 .....	147
Figure A. 5: Dynamic ice verification at Hwy. 4 in 2010-2011 .....	149

---

## LIST OF FIGURES

---

Figure A. 6: Dynamic ice verification at Breezy Point in 2010-2011 .....	149
Figure A. 7: Dynamic ice verification at Goldeye Lake in 2010-2011.....	150
Figure A. 8: Dynamic ice verification at Goldeye Creek in 2010-2011.....	150
Figure A. 9: Dynamic ice verification at Netley Creek in 2010-2011.....	151
Figure A. 10: Dynamic ice verification downstream of Netley Creek in 2010-2011. ....	151
Figure A. 11: Dynamic ice verification upstream of Netley Cut in 2010-2011.....	152
Figure A. 12: Dynamic ice verification downstream of Netley Cut in 2010-2011.....	152
Figure A. 13: Dynamic ice verification at Netley Lake in 2010-2011.....	153
Figure A. 14: Dynamic ice verification at Breezy Point in 2011-2012. ....	153
Figure A. 15: Dynamic ice verification upstream of Netley Cut in 2011-2012.....	154
Figure A. 16: Dynamic ice verification downstream of Netley Cut in 2011-2012 .....	154
Figure A. 17: Dynamic ice verification in main channel in 2011-2012.....	155
Figure A. 18: Dynamic ice verification in east channel in 2011-2012 .....	155

## LIST OF TABLES

Table 1.1: Changes in aquatic vegetation in the Netley-Libau Marsh between 1979 and 2001.....	10
Table 2.1: Albedo of Great Lakes Ice. ....	22
Table 2.2: Typical values of $\gamma$ .....	31
Table 4.1: Average proportion of Red River flow passing through different channels....	56
Table 6.1: Mesh sensitivity analysis.....	75
Table 6.2: Manning’s n values for different reaches. ....	76
Table 6.3: Comparison of simulated and measured flow split for hydrodynamic calibration.....	82
Table 6.4: Comparison of simulated and measured flow split for hydrodynamic verification.....	86
Table 7.1: RMSE analysis for dynamic ice calibration simulations. ....	100
Table 7.2: Comparison of modelled and measured discharge proportions for 2009-2010 winter season. ....	103
Table 7.3: Comparison of modelled and simulated discharge proportions for the 2010-2011 winter season.....	109
Table 7.4: Comparison of modelled and measured discharge proportions for 2011-2012 winter season. ....	118

## LIST OF COPYRIGHTED MATERIAL FOR WHICH PERMISSION WAS OBTAINED

ITEM	SOURCE	PAGE
Figure 1.1: Study Area	Grosshans et al., 2004	4
Figure 1.2: Netley-Libau Marsh Vegetated Area Change between 1979 and 2001	Grosshans et al., 2004	10
Figure 1.3: Conceptual diagram of some factors thought to be contributing to the decline of emergent vegetation	Grosshans et al., 2004	11

## NOMENCLATURE

Symbol	Dimensions	Description
$\varphi_{wa}$	$[\text{Wm}^{-2}]$	Rate of heat loss from the water to the atmosphere
$\varphi_R$	$[\text{Wm}^{-2}]$	Net short-wave radiation
$\varphi_B$	$[\text{Wm}^{-2}]$	Net long-wave radiation
$\varphi_H$	$[\text{Wm}^{-2}]$	Sensible heat flux from the air
$\varphi_E$	$[\text{Wm}^{-2}]$	Latent heat flux from water vapour
$\varphi_P$	$[\text{Wm}^{-2}]$	Heat flux from precipitation
$\varphi_G$	$[\text{Wm}^{-2}]$	Heat flux at the flow boundaries
$\varphi_{ri}$	$[\text{Wm}^{-2}]$	Solar radiation under cloudy skies
$R_t$		Albedo
$\varphi_{cl}$	$[\text{Wm}^{-2}]$	Short wave radiation reaching the earth under clear skies
$C$		Cloud cover
$\varphi_{bs}$	$[\text{Wm}^{-2}]$	Long wave radiation emitted by the water surface
$\varphi_{ba}$	$[\text{Wm}^{-2}]$	Long wave radiation reaching the river surface
$\varphi_{br}$	$[\text{Wm}^{-2}]$	Radiation reflected back by the river surface
$\sigma$	$[\text{Wm}^{-2}\text{K}^{-4}]$	Stefan-Boltzmann constant
$T_s$	$[\text{°K}]$ or $[\text{°C}]$	Surface water temperature
$T_a$	$[\text{°K}]$ or $[\text{°C}]$	Air temperature
$\varepsilon_a$		Emissivity of the atmosphere
$e_s$	$[\text{Pa}]$	Saturated vapour pressure corresponding to the water surface temperature
$e_a$	$[\text{Pa}]$	Vapour pressure corresponding to the air temperature 2 m above the ground

---

## Nomenclature

---

$v_a$	[m/s]	Wind velocity 2 m above the water surface
$v_{az}$	[m/s]	Wind velocity at a height of $z$ m
$R$		Bowen's ratio
$T_w$	[°K] or [°C]	Water temperature
$A_s$	[m <sup>2</sup> s <sup>-1</sup> ]	Mass of snow accumulation over unit area of water surface per unit time
$L_i$	[Jkg <sup>-1</sup> ]	Latent heat of fusion of ice
$C_p$	[J°C <sup>-1</sup> kg <sup>-1</sup> ]	Specific heat of ice
$V$	[km]	Visibility
$h_{wa}$	[W°Cm <sup>-2</sup> ]	Open water heat transfer coefficient
$\varphi_{wi}$	[Wm <sup>-2</sup> ]	Heat transfer from river water to ice
$h_{wi}$	[W°Cm <sup>-2</sup> ]	Water-ice heat transfer coefficient
$T_m$	[°C]	Melting temperature of ice (0°C)
$V_w$	[m/s]	Water velocity
$D_h$	[m]	Hydraulic diameter
$c_{wi}$	[m <sup>0.4</sup> s <sup>0.8</sup> ]	Air-ice heat transfer constant
$N_u$		Nusselt Number
$K_w$	[W°C <sup>-1</sup> m <sup>-1</sup> ]	Thermal conductivity of water
$N$		Surface ice concentration
$\varphi_i$	[Wm <sup>-2</sup> ]	Heat flux from ice to air
$t$	[s]	Time
$h_i$	[m]	Ice thickness
$\varphi_T$	[Wm <sup>-2</sup> ]	Total surface heat exchange
$k_i$	[Wm <sup>-1</sup> °C <sup>-1</sup> ]	Thermal conductivity of ice



---

## Nomenclature

---

$S$		Number of degree days of freezing
$h_s$	[m]	Thickness of the snow cover
$k_s$	[Wm <sup>-1</sup> °C <sup>-1</sup> ]	Thermal conductivity of the snow
$H_a$	[Wm <sup>-1</sup> °C <sup>-1</sup> ]	Heat transfer coefficient that accounts for the thermal resistance between the uppermost surface and the air
$\rho_i$	[kgm <sup>-3</sup> ]	Density of ice
$\rho_s$	[kgm <sup>-3</sup> ]	Density of snow
$\rho_w$	[kgm <sup>-3</sup> ]	Density of water
$e_T$	[kgm <sup>-1</sup> s <sup>-2</sup> ]	Thermal energy in the ice-water mixture in the suspended layer
$\varphi_{ss}$	[Wm <sup>-2</sup> ]	Rate of heat gain on unit area through top and bottom boundaries
$\varphi_{sk}$	[Wm <sup>-2</sup> ]	Rate of heat loss on unit area through top and bottom boundaries
$C_v$		Volumetric ice concentration
$E$	s <sup>-1</sup>	Net volumetric rate of loss of frazil due to mass exchanges with the surface layer and at the bed
$C_{pw}$	[J° C <sup>-1</sup> kg <sup>-1</sup> ]	Specific heat of water
$T_s$	[°C]	Surface water temperature
$\alpha$	[Wm <sup>-2</sup> ]	Linear heat transfer constant
$\beta$	[Wm <sup>-2</sup> °C <sup>-1</sup> ]	Linear heat transfer coefficient
$u$	[m/s]	Local depth averaged velocity
$W$	[m/s]	Wind velocity 2 m above the water surface
$b$		Wind utilization coefficient
$B$	[m]	Width of channel
$v_b'$	[m/s]	Buoyant velocity of frazil particles on the water surface

---

## Nomenclature

---

$v_z'$	[m/s]	Vertical fluctuating component of the water velocity
$V_c$	[m/s]	Maximum velocity for dynamic border ice growth
$W$	[m]	Width of border ice

---

**1.1 PROJECT OVERVIEW**

The province of Manitoba is known for, and relies heavily on, its abundance of natural water resources for both recreation and economic benefit. It is home to Lake Winnipeg, the tenth largest freshwater lake in the world, as well as a plethora of other lakes, rivers and wetlands. However, over the past several decades the health of Lake Winnipeg and its surrounding coastal wetland, the Netley-Libau Marsh, has been deteriorating (Grosshans et al., 2004). This prompted the Government of Manitoba to initiate hydrodynamic studies of the Netley-Libau Marsh and surrounding area.

A particular region of interest is Netley Cut, an opening in the western bank of the Red River that allows a significant portion of the flow to enter Netley Lake. This opening plays an important role in the local hydrodynamics of the Red River and its mouth in

---

## INTRODUCTION

---

Lake Winnipeg. Netley Cut was initially excavated in the early 1900's to allow for boat passage to the lakes along the south border of Lake Winnipeg. However, since then the cut has increased in size due to erosion. The creation and growth of Netley Cut has altered the flow pattern through the Red River, as a portion of the flow is now routed through Netley Lake rather than flowing directly into Lake Winnipeg.

Suggestions have been put forth to seal Netley Cut, preventing flow into Netley Lake and hopefully revitalizing the marsh and helping to restore the health of Lake Winnipeg. However, it is hypothesized that sealing Netley Cut will exacerbate the challenges that Manitobans face with ice jamming every winter. During ice break-up, ice jams typically form in the vicinity of Netley Cut, often resulting in severe flooding and substantial property damage to homes and cottages upstream. The cut is perceived to help alleviate these jams, as ice sheets are able to flow into Netley Lake, relieving some of the congestion in the river. However, if sealed, some fear that the consequences of ice jamming in the Red River may become even more severe.

The issues surrounding ice jamming on the Red River have become so severe that the province of Manitoba has recently invested in specialized equipment to cut and break up the ice prior to the natural break-up period. Each winter, Manitoba Water Stewardship executes a cutting program in the reaches most prone to ice jamming, hoping that these efforts will ease the natural break-up process and minimize the severity and frequency of ice jams. Typically the cutting is refined to areas where the ice

thickness exceeds approximately 50 cm. As a result, ice thickness has to be manually measured and equipment is dispatched if deemed necessary. Due to the sheer size of the river, this program can take weeks to complete each year. Reliable predictions of ice thickness could help to optimize this mitigation strategy.

Winter safety has also been a longstanding problem on the Red River. Each year, there are numerous accounts of people and vehicles falling through thin ice, often resulting in serious injury or death. Typically, these individuals are under the impression that the ice is thick enough to safely walk or drive on, which is not always the case. Understanding and being able to predict the ice formation processes on the Red River may aid in preventing some of these tragedies.

The purpose of this research is to provide a better understanding of the hydrodynamics and ice processes on the Red River in the vicinity of Netley Cut. This includes an assessment of the area in its current state, as well as a preliminary, yet quantitative assessment of the potential impacts that closing the cut might have on ice cover formation in the study area. This objective will be reached by completing various field programs to collect a variety of different data sets during both the open water and ice covered seasons. These data sets will serve as the input to a CRISSP2D model that is capable of simulating the hydrodynamics and river ice freeze-up processes in the study area. The results obtained in this study will aid in improving winter safety on the Red River by working to prevent thin ice accidents. In addition, model results will assist in

planning efficient ice jam mitigation strategies and help alleviate some of consequences of ice jamming in the study area each year.

## **1.2 DESCRIPTION OF THE STUDY AREA**

This study concentrates on the area immediately south of Lake Winnipeg (shown in Figure 1.1). This includes the Netley-Libau Marsh, Netley Cut, and the portion of the Red River that extends from Selkirk to Lake Winnipeg. The total reach length included in this

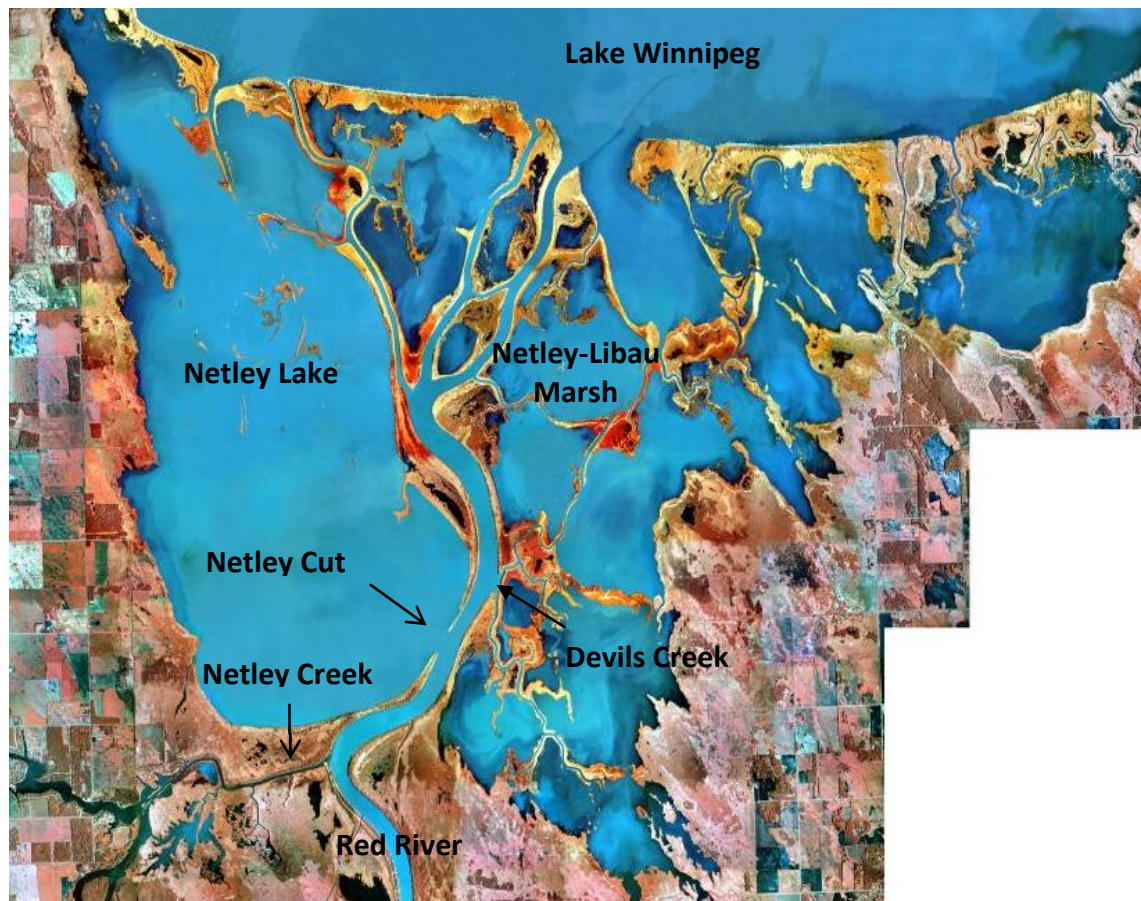


**Figure 1.1: Study Area.**

study was approximately 33 km and includes two tributary inflows at Netley Creek and Devils Creek. Historically, this portion of the river has been most problematic to Manitobans with ice jam and flooding concerns nearly every break up season.

### **1.2.1 LAKE WINNIPEG**

Lake Winnipeg plays a large role in the economic and recreational livelihood of Manitobans. It is the tenth largest freshwater lake in the world and is considered to be Canada's sixth Great Lake, having a surface area of approximately 24,500 km<sup>2</sup>. For a lake of its size, Lake Winnipeg is unusually shallow, having a mean water depth of only about 12 m (Herdendorf, 1982). In addition, it has a large fetch length, making it susceptible to wind effects and resulting in water that is typically well mixed. Particularly in the smaller south basin there is virtually no stratification of temperature, oxygen or dissolved elements occurring in the lake. Lake Winnipeg is also known to have large water level fluctuations due to wind set-up and set-down. The physical characteristics of the lake (length, breadth) are such that persistent prairie winds drive surface water currents and cause water levels to increase by up to a metre at downwind locations.

The Lake Winnipeg watershed is quite vast, covering approximately 984,000 km<sup>2</sup> and draining portions of four Canadian provinces and four American states. There are three major inflows to the lake: the Saskatchewan River, the Red River, and the Winnipeg River. These inflows are greatest in the spring and summer due to run-off from snow

melt and heavier precipitation. Water passing through the lake has served 5.5 to 6 million people, their urban and rural centres, 55 million hectares of Canadian agricultural land, and between 17 and 20 million livestock (Salki, 2002). The water exits the lake via the Nelson River and discharges into Hudson Bay.

Unfortunately, the health of Lake Winnipeg has deteriorated significantly over the past few decades due to the cumulative effects of eutrophication (Salki, 2002). This steady ecologic decline can be attributed to a variety of factors including an increase in human population, lack of tertiary sewage treatment, intensive cropping and use of fertilizers, increased cattle and hog production, changes in flow patterns, flooding, and erosion (Salki, 2002). Each of these factors contribute to increasing the nutrient load entering Lake Winnipeg and are discussed at length in the subsequent sections of this chapter.

### **1.2.2 THE RED RIVER**

The Red River watershed is one of the largest in North America, covering approximately 127,000 km<sup>2</sup>. The river is a mild, meandering Prairie river, having a total reach length of approximately 885 km and originating in South Dakota. The Red River is one of few rivers that flow north in North America, spreading through the Netley-Libau Marsh, and eventually discharging into Lake Winnipeg. The flow can vary significantly from year to year. Several extreme floods have occurred in the past several decades, most notably in 1950, 1979, 1997, and 2009.



In the winter, sub-zero air temperatures cause the Red River and surrounding wetlands to freeze over. Typically, the freeze-up process begins with a skim ice cover forming on the lakes and wetlands. This is often followed by skim ice or strips of border ice forming along the banks of the Red River. As winter proceeds, the skim ice thickens thermally downward and the border ice strips increase in size until a competent ice cover has formed. Depending of meteorological and hydraulic conditions during the freeze-up period frazil particles and frazil pans may also form. Once the ice cover has formed it generally remains in place for the entire winter.

When spring approaches, ice break-up is typically triggered by snowmelt and warmer temperatures. Thermal processes cause the ice cover to deteriorate, while increasing flow rates cause the ice to detach from the river banks. The ice breaks into large pieces and, as discharge continues to increase, the pieces are transported downstream. Occasionally, these moving ice sheets become arrested in a particular location. This often coincides with the blocks hitting an intact and relatively strong ice cover. However, there are other factors that can influence the formation of ice jams, including channel constrictions, tight bends, and rapid decreases in channel slope.

The Red River is particularly susceptible to ice jamming. This can be partially attributed to the fact that the river flows north into colder regions where the ice is often still intact. Additionally, the meandering nature of the river provides many opportunities for ice to

become lodged. Once an ice jam forms, the water level upstream continues to rise until the jam is released or an equilibrium water level is reached. This often results in severe flooding of the communities upstream of the jam. In Manitoba, the most severe ice jams occur north of Winnipeg, generally between Selkirk and Lake Winnipeg.

Along its path, the Red River flows through several urban and industrial centres, waste water treatment plants, vast areas of chemical-intensive agriculture and farmland, all of which contribute to its poor water quality. As a result, the Red River is the largest contributor of nitrogen and phosphorus to Lake Winnipeg (Grosshans et al., 2004) and this nutrient loading has continued to grow over time. Analyses of water samples collected from the river near Selkirk between 1978 and 1999 have indicated a 28% increase in total nitrogen and a 58% increase in total phosphorus (Jones and Armstrong, 2001). These excessive nutrient loadings have significantly contributed to the ecologic decline of both Lake Winnipeg and the Netley-Libau Marsh (discussed further in Section 1.2.3.4).

### **1.2.3 THE NETLEY-LIBAU MARSH**

The Netley-Libau Marsh is a large, freshwater wetland that is situated on the south shore of Lake Winnipeg. It covers approximately 26,000 ha of land and is comprised of a variety of lakes and channels that connect the Red River to Lake Winnipeg. The marsh plays several important ecological roles in the Lake Winnipeg watershed. It is an

important bird breeding and nesting area, and a spawning area for Lake Winnipeg fish (Venema et al., 2005). However, arguably the most important function of the marsh is that its vegetation acts as a filter, removing nutrients and pollutants from the water before they reach Lake Winnipeg (Kadlec and Knight, 1996).

Over the last few decades, the marsh has experienced a significant decline in its overall vegetated area (Grosshans et al., 2004). Aerial views of the marsh in 1979 and 2001 (Figure 1.2) indicate that the extents of nearly all species of vegetation are shrinking. This has resulted in a substantial growth of the open water area, increasing nearly 25% in this time period. There has been a notable loss of uplands and islands, particularly within Netley Lake, where only a few scattered remnants now remain. Lakes have expanded and merged, and several channel banks have been breached. Furthermore, there have been shifts in dominant vegetation types, documented in Table 1.1, which have further altered the ecological processes occurring in the marsh.

The overall changes in the marsh area are thought to be attributable to a number of factors which are described in subsequent sections of this text and include the cessation of dredging in the Red River, the increasing size of Netley Cut, large incoming nutrient loads, flooding in the Lake Winnipeg watershed, and Lake Winnipeg Regulation (Grosshans et al., 2004). The consequences and interactions between these factors are shown conceptually in Figure 1.3. As depicted, factors are interconnected in feedback cycles, making a simple solution difficult to establish. As a result of these changes, the

---

## INTRODUCTION

---

marsh's ability to remove nutrients from the water has been significantly impaired, allowing more nutrients and pollutants to enter Lake Winnipeg, exacerbating the eutrophication process.

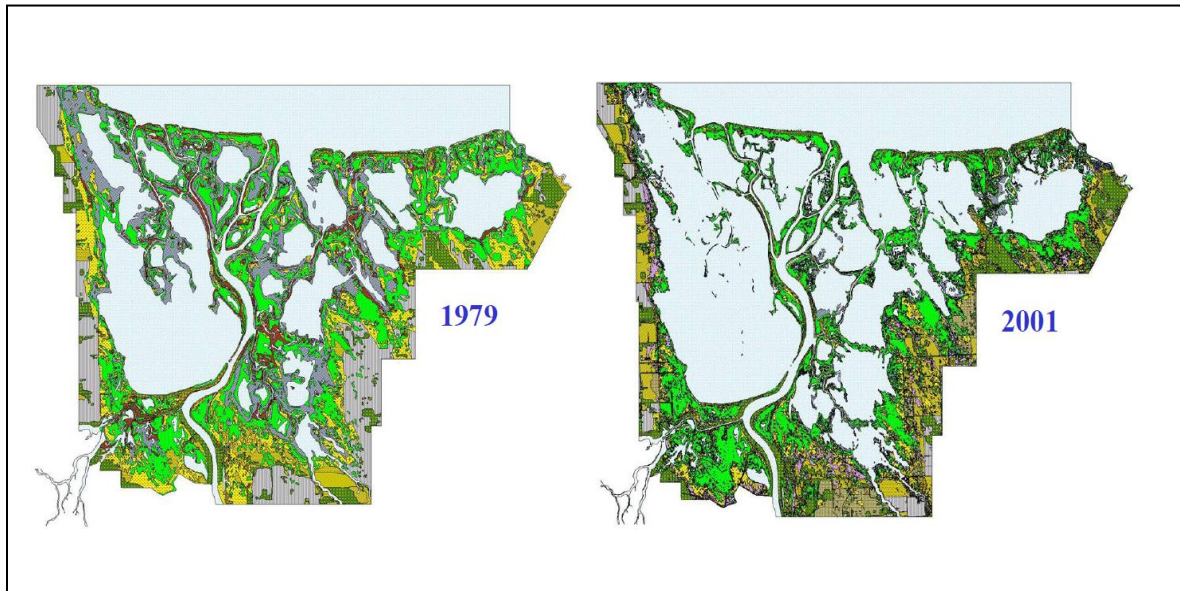


**Figure 1.2: Netley-Libau Marsh Vegetated Area Change between 1979 and 2001 (Grosshans et al., 2004)**

**Table 1.1: Changes in aquatic vegetation in the Netley-Libau Marsh between 1979 and 2001 (Grosshans et al., 2004).**

Vegetation	1979		2001	
	Area (ha)	%	Area (ha)	%
Open Water	8884	34.5	13125	50.9
Bulrush	3247	12.6	317	1.2
River bulrush and sedge	922	3.6	166	0.6
Cattail	4987	19.3	4620	17.9
Giant Reed	650	2.5	732	2.8
Total	25774		25773	



### **1.2.3.1 Changes in Flow Patterns**

Major contributors to the ecological decline of the marsh are the significant changes in flow patterns it has experienced over the years, causing the marsh to become less hydraulically isolated from Lake Winnipeg (Verbiwski, 1986). As a result of this interconnectivity, it is quite common for large volumes of water to be exchanged between Lake Winnipeg and the Netley-Libau Marsh. During wind set-up and set-down, extreme fluctuations in water levels allow water to flow through breaches in the beach ridge that separates Lake Winnipeg from the marsh (Verbiwski, 1986). These events result in the frequent exchange of nutrients and pollutants between the marsh and lake and often cause local flooding and erosion of the upland areas during wind set-up and expose extensive mudflats during wind set-down.

As a result of the hydraulic interconnectivity between the lake and the marsh, generally Lake Winnipeg dictates water levels within the Netley-Libau Marsh. As a result, it has a significant impact on the structure of the marsh and its aquatic vegetation (Grosshans et al., 2004). Periods of high water have the tendency to cause emergent marsh habitat to decline and open water area to increase, while periods of low water tend to allow the marsh bottom to be exposed, allowing for germination of emergent vegetation. Since marsh levels cannot be controlled independently of lake levels, it is likely that only an extreme drought will allow for the rejuvenation of vegetation within the marsh. This is evidenced by the temporary re-growth of some of the emergent plant species during extremely dry conditions in 2003 (Grosshans et al., 2004).

The water level in Lake Winnipeg has been regulated to remain between 216.6 m and 217.9 m, since 1975, when Manitoba Hydro undertook the Lake Winnipeg Regulation Project. Although this has played a role in maintaining a more constant lake level, it prevents the extended dry periods required for germination of new vegetation, resulting in negative ecological consequences on the Netley-Libau Marsh (Grosshans et al., 2004).

Other changes in flow patterns may have resulted from the cessation of dredging the mouth of the Red River. Historically, this region has been dredged to allow for easier boat navigation. The practice began in 1884, becoming more frequent until it was being dredged annually between 1960 and 1998 (KGS Group, 2002). On an annual basis, an average of 55,000 m<sup>3</sup> of material was removed from the river, with approximately 75% of that being removed from the mouth of the main channel (KGS Group, 2002). In 1998 the dredging was slowed until it eventually ceased in 1999. Between 1998 and 2001 changes in the bottom profile of the dredging locations varied between a few centimetres and up to one metre in some locations (KGS Group, 2002). Figures 1.4 and 1.5 show river bed bathymetry at the Red River flow split and the mouth of the main channel surveyed between 1998 and 2001.

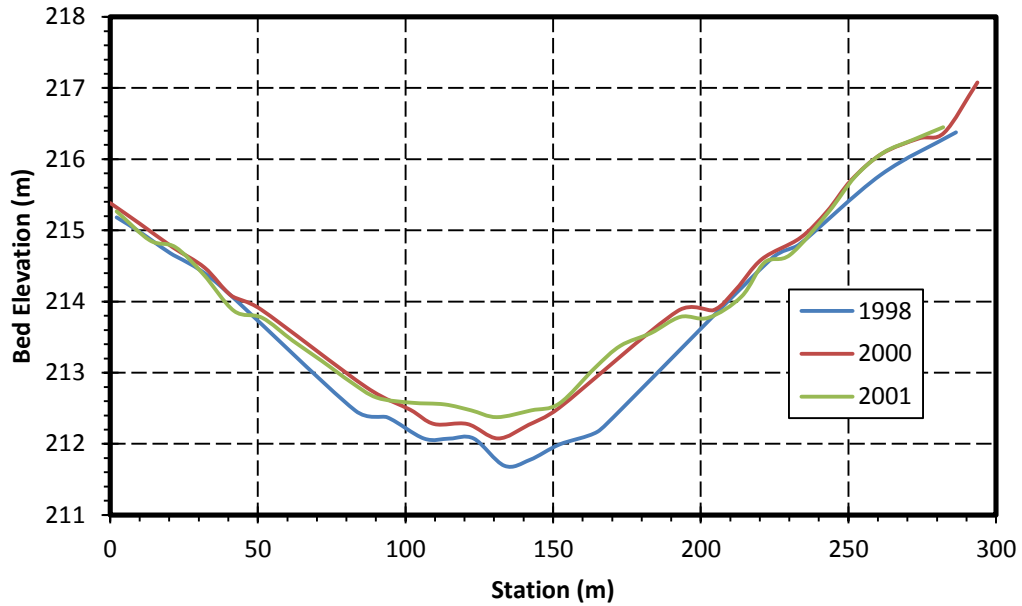


Figure 1.4: Change in river bed bathymetry between 1998 and 2001 at Red River flow split (KGS Group, 2002).

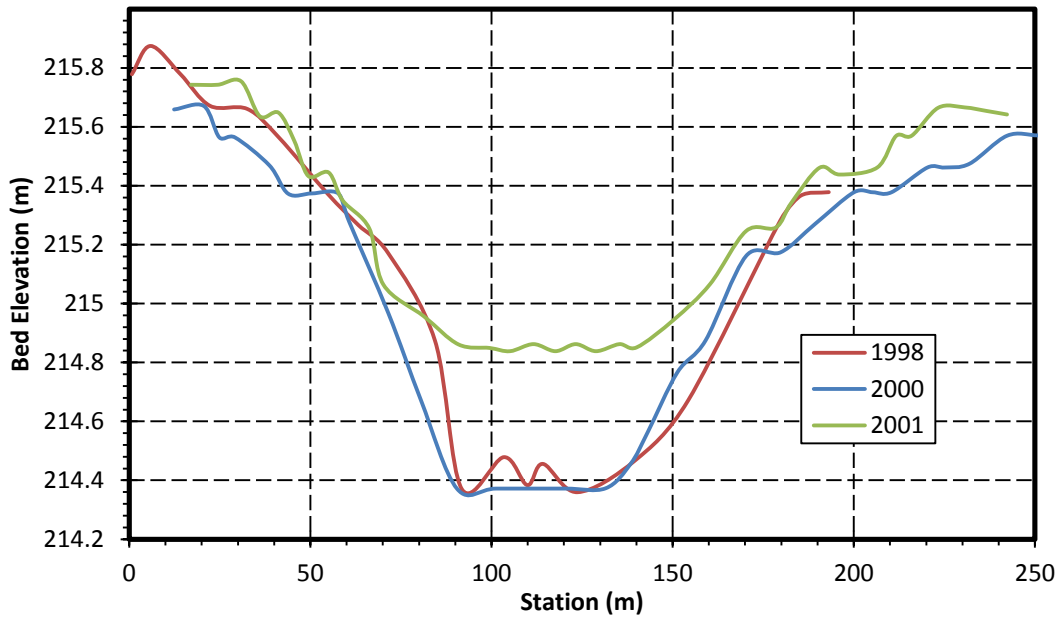


Figure 1.5: Change in river bed bathymetry between 1998 and 2001 at mouth of main channel (KGS Group, 2002).



It is clear from Figures 1.4 and 1.5 that the cessation of dredging, particularly within the study area, has caused significant infilling of the channel and it is believed that this trend will continue as long as the dredging program is discontinued. In fact, it is conceivable that the main channel may eventually become completely impassible if dredging in this area continues to be suspended (KGS Group, 2002). To compensate for this, it is highly likely that the infilling process will hasten the natural process of channel migration within the Netley-Libau Marsh area and will almost certainly lead to an enlargement of other existing channels and/or the establishment of new waterways (KGS Group, 2002). Most notably, this phenomenon is evidenced by a growing proportion of flow being routed through Netley Lake via Netley Cut.

#### **1.2.3.2 Netley Cut**

Netley Cut was initially excavated in 1913 by the federal government as a means of allowing boat access to Netley Lake. In addition, excavating Netley Cut provided a means for water entering Netley Lake during wind set-up on Lake Winnipeg to exit more quickly and drain valuable hayfields (Grosshans et. al, 2004). At the time of excavation, the cut was approximately 5 m wide. However, erosion quickly became a problem, causing the cut to begin increasing in size almost immediately (shown in Figure 1.6). Since its original excavation, several attempts have been made to seal the cut and prevent further erosion, none of which have had long term success. As a result, the cut remains open today and is now approximately 400 m wide, passing approximately 37% of the Red River flow into Netley Lake.

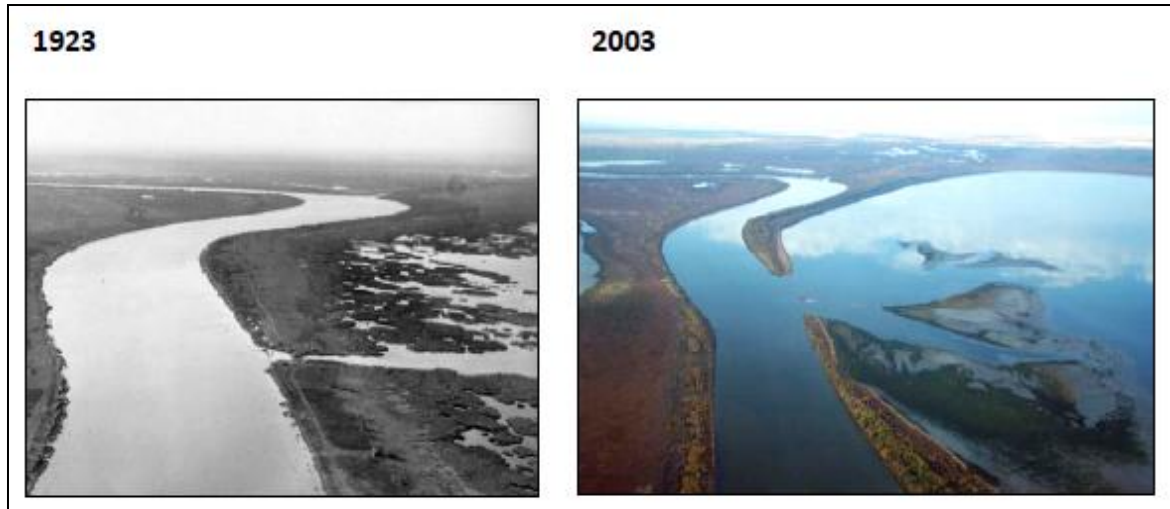


**Figure 1.6: Erosion of Netley Cut between 1923 and 2003 (IISD, 2011).**

The consequence of this flow change over the years is that larger quantities of river-bourne silt, debris, nutrients, and pollutants are able to enter the marsh via Netley Cut (Grosshans et al., 2004). As a direct result, Netley Lake has been experiencing declines in aquatic vegetation, erosion of smaller channels, upland, and emergent islands, and increases in turbidity and algal blooms (Grosshans et al., 2004).

### **1.2.3.3 Flooding**

The Red River itself is undoubtedly contributing to the ecologic decline of the marsh as well. Large flow events and associated flooding are very common, particularly during the spring freshet. During these periods of high flow, erosion of the riverbanks occurs, which may possibly lead to the collapse of weak points in the banks. In addition, the flooding that results from significant flow events often causes large parts of the marsh to be submerged for extended periods of time. This effectively drowns the existing vegetation

and prevents the dry conditions required for germination and the re-growth of new aquatic vegetation.

However, the most substantial impact of flooding within the Red River basin is the significant spike in nutrient concentration associated with the overland flow. The river flows through vast agricultural land where abundant nutrient-rich fertilizers are used on crops. When flooding occurs, these nutrients are transported by the Red River into the Netley-Libau Marsh and/or Lake Winnipeg.

#### **1.2.3.4 Nutrient Load**

As discussed previously, the Red River contributes a significant portion of the nutrient load to Lake Winnipeg. Nutrient enrichment, particularly nitrogen and phosphorus, poses a threat to the health of both the Netley-Libau Marsh and Lake Winnipeg. When these nutrients accumulate in the water, algal blooms typically result from the excessive nutrient enrichment and often lead to the loss of aquatic vegetation. The algae may form a thick layer, essentially shading the existing vegetation from the sun and competing with said vegetation for nutrients in the water (Phillips et al., 1978). As the aquatic vegetation dies off, the area becomes more susceptible to erosion, since the roots of aquatic plants often act as stabilizing mechanisms (Carper and Bachmann, 1984). In turn, additional nutrients may be released from disturbed sediments, further stimulating algal growth.

Due to some of the flow pattern changes discussed previously, more of this nutrient load is being routed directly into the Netley-Libau Marsh. Early marsh surveys indicate that historically, the marsh was in a healthy 'clear water' state where aquatic vegetation was abundant (McCleod and Moir, 1944). The marsh remained this way into the early 1980s. However, since then, the Netley-Libau Marsh has transformed into a 'turbid state' where aquatic vegetation has become much sparser and the algal concentration has become comparable to that of eutrophic lakes (Wetzel, 2001). Scheffer (1998) has suggested that there exists a critical threshold of algae production that initiates the decline of aquatic vegetation, and once reached, it is very difficult to recover from, even upon reducing the nutrient load.

### **1.3 PROJECT OBJECTIVES**

This research contains a thorough investigation of the river ice dynamics on the Red River near Netley Cut. The main objectives of this research were to:

- 1) Provide a better understanding of the hydrodynamics of the Netley-Libau Marsh area under open water and ice covered conditions.
- 2) Develop a means of modelling the freeze-up and mid-winter ice processes on the Red River near the Netley-Libau Marsh.
- 3) Simulate the effects that altering or sealing Netley Cut would have on local ice processes

The following sections of this thesis provide details on how the above goals were met.

---

**2.1 INTRODUCTION**

Many ice formation processes are quite complex in nature and thus can be difficult to reproduce accurately with a numerical model. Understanding the governing equations and assumptions associated with the chosen numerical model are essential for creating an accurate representation of the physical world. The following sections of this chapter are intended to familiarize the reader with the major processes that are being reproduced by CRISSP2D, including surface heat exchange, the energy budget, and the mechanisms that govern freeze-up processes on lakes and rivers.

## **2.2 SURFACE HEAT EXCHANGE**

Water changes temperature as a direct result of surface heat exchange. This heat transfer between the water and air is controlled by a number of meteorological mechanisms, including air temperature, humidity, wind velocity, barometric pressure, sun and cloud conditions, and precipitation. An energy balance approach is often used in order to use these mechanisms to quantify surface heat exchange.

Due to the turbulent nature of the flow in most rivers, it is often assumed that the water is well mixed in the vertical direction and therefore, the entire water column warms and cools at approximately the same rate as the water on the surface. It follows that changes in water temperature can be quantified by considering an energy balance at the water surface. This energy balance, including only the most significant heat fluxes as determined by the quantity of heat per unit time, is shown in Equation 2.1 below

$$\varphi_{wa} = \varphi_R + \varphi_B + \varphi_H + \varphi_E + \varphi_P + \varphi_G \quad (2.1)$$

where  $\varphi_{wa}$  is the net heat flux to the water column [ $Wm^{-2}$ ],  $\varphi_R$  is the net short-wave radiation [ $Wm^{-2}$ ],  $\varphi_B$  is the net long-wave radiation [ $Wm^{-2}$ ],  $\varphi_H$  is the sensible heat flux from the air [ $Wm^{-2}$ ],  $\varphi_E$  is the latent heat flux from water vapour [ $Wm^{-2}$ ],  $\varphi_P$  is the heat flux from precipitation [ $Wm^{-2}$ ],  $\varphi_G$  is the heat flux at the flow boundaries [ $Wm^{-2}$ ].

### 2.2.1 SHORTWAVE RADIATION

The net short-wave radiation is often the most dominant term in the energy balance. Its value is always positive, constituting an energy gain. Its magnitude is based on numerous intricate astronomical and geographical relationships, including latitude and longitude, local apparent time, local standard time, and the solar constant. These formulations are complex in nature and are detailed in Ashton (1986). However, only a portion of the radiant energy passing into the atmosphere actually reaches the surface of the earth. Thus, the net shortwave radiation ( $\varphi_R$ ) can be calculated as

$$\varphi_R = (1 - R_t)\varphi_{ri} \quad (2.2)$$

where  $\varphi_{ri}$  is the solar radiation under cloudy skies [ $Wm^{-2}$ ] and  $R_t$  is the albedo or reflectivity which is a function of latitude and surface properties. The reflectivity of water typically ranges from 6% to 10% and can be calculated using formulae developed by Anderson (1954). Suggested albedos of various ice types are given in Table 2.1. The short wave radiation reaching the earth under cloudy skies ( $\varphi_{ri}$ ) can be calculated as

$$\varphi_{ri} = \varphi_{cl}(1 - 0.0065C^2) \quad (2.3)$$

where  $\varphi_{cl}$  is the short wave radiation reaching the earth under clear skies [ $Wm^{-2}$ ] and  $C$  is the cloud cover in tenths.

**Table 2.1: Albedo of Great Lakes Ice (Bolsenga, 1969).**

Ice Type	Albedo (%)
Clear lake ice (snow free)	10
Bubbly lake ice (snow free)	22
Ball ice (snow free)	24
Refrozen Pancake (snow free)	31
Slush Curd (snow free)	32
Slush ice (snow free)	41
Brash ice (snow between blocks)	41
Snow ice (snow free)	46

### 2.2.2 LONGWAVE RADIATION

The long-wave radiation accounts for the heat radiated from a physical body and thus, will always be an energy loss. The long wave radiation often contributes significantly to the overall energy flux, particularly on clear winter nights (Andersson and Andersson, 1992). This type of radiation accounts for the net balance of the atmospheric long wave radiation reaching the river surface, the fraction of the atmospheric radiation reflected back by the river surface, and the long wave radiation emitted by the river surface. As a result, the net long wave radiation can be written as

$$\varphi_B = \varphi_{bs} - (\varphi_{ba} - \varphi_{br}) \quad (2.3)$$



where  $\varphi_{bs}$  is the long wave radiation emitted by the water surface [ $Wm^{-2}$ ],  $\varphi_{ba}$  is the long wave radiation reaching the river surface [ $Wm^{-2}$ ],  $\varphi_{br}$  is the radiation reflected back by the river surface [ $Wm^{-2}$ ].

The components of Equation 2.3 are primarily calculated using the Stefan-Boltzmann law. If expressions for the Stefan-Boltzmann law are substituted into Equation 2.3 and appropriate emissivity coefficients are utilized, the net heat flux from long wave radiation can be written as

$$\varphi_B = 0.97\sigma[T_s^4 - \varepsilon_a(1 + kC^2)T_a^4] \quad (2.4)$$

where  $\sigma$  is the Stefan-Boltzmann constant ( $5.67 \times 10^{-8} Wm^{-2}K^{-4}$ ),  $T_s$  is the surface water temperature [ $^{\circ}K$ ],  $T_a$  is the air temperature [ $^{\circ}K$ ],  $\varepsilon_a$  is the emissivity of the atmosphere (calculated by relationships developed by Satterlund, 1979),  $k$  is an empirical constant, and  $C$  is the cloud cover (in tenths).

### **2.2.3 EVAPORATIVE HEAT TRANSFER**

When air and water are in contact, water will evaporate as long as the relative humidity is less than 100%. There have been numerous formulae developed to estimate evaporation, but for winter conditions the Rimsha-Donchenko (1957) formula is recommended. This formula is expressed as

$$\varphi_E = \frac{4.1855}{8.64} (1.56K_N + 6.08v_a)(e_s - e_a) \quad (2.5)$$

where  $K_N = 8 + 0.35(T_s - T_a)$ ,  $T_s$  is the temperature on the river surface [°C],  $T_a$  is the air temperature [°C],  $e_s$  is the saturated vapour pressure corresponding to the water surface temperature [Pa],  $e_a$  is the vapour pressure corresponding to the air temperature at 2 m above the ground [Pa], and  $v_a$  is the wind velocity at 2 m above the water surface. If there is no data available for 2 m above the ground,  $v_a$  can be calculated as

$$v_a = v_{az} \left(\frac{2}{z}\right)^{0.15} \quad (2.6)$$

where  $v_{az}$  is the wind velocity at a height of  $z$  m above the ground.

#### **2.2.4 CONDUCTIVE HEAT TRANSFER**

Bowen (1926) concluded that the heat exchange due to convection by air is a fixed ratio of that by evaporation such that

$$\varphi_H = R\varphi_E \quad (2.7)$$

where  $R$  is Bowen's ratio. If Equation 2.7 is combined with the Rimsha-Donchenko (1957) formula, the following expression for conductive heat transfer is obtained

$$\varphi_H = \frac{4.1855}{8.64} (K_N + 3.9\nu_a)(T_s - T_a) \quad (2.8)$$

where  $T_s$  and  $T_a$  are measured in [°K].

### **2.2.5 PRECIPITATION**

Precipitation that falls into open water may cause a considerable heat flux. When snow falls, it melts in the water and effectively lowers the temperature of the water. Additionally, the lower the air temperature, the more heat is required to raise the temperature of the snow to that of the water. However, in near 0°C water, fallen snow may not melt completely. Instead, it may transform into snow slush and the heat loss due to the snow is only that required to cool the water to 0°C. The heat loss from precipitation can be calculated from Equation 2.9

$$\varphi_P = A_s [L_i + C_p(T_w - T_a)] \quad (2.9)$$

where  $T_a$  is the air temperature [°C],  $T_w$  is the water temperature [°C],  $A_s$  is the mass of snow accumulation over unit area of water surface per unit time [ $m^2s^{-1}$ ],  $L_i$  is the latent heat of fusion of ice ( $3.3484 \times 10^5 Jkg^{-1}$ ), and  $C_p$  is the specific heat of ice ( $4.1855 \times 10^3 J^\circ Ckg^{-1}$ ). If  $A_s$  is not available via direct measurement, it can be estimated using Mellor's (1966) formula

$$A_s = \frac{78.5}{86400} V^{-2.375} \quad (2.10)$$

where  $V$  is the visibility in [km]. Generally Equation 2.10 is valid for  $1 < V < 10$  under calm conditions. Alterations to Equation 2.10 are required if these conditions are not met.

### **2.3 LINEAR APPROXIMATION OF THE ENGERY BUDGET**

One of the most important aspects of any river ice model is its ability to simulate the surface heat exchange processes accurately. The formulations for calculating surface heat exchange detailed in Section 2.2 often require meteorological data that is often not readily available. As a result, it may be beneficial to use simplified linearized formulae and calibrate the heat exchange coefficients during the modeling process. In CRISSP2D, both the detailed thermal budget method and linearized formulation are available. The method used is chosen based on input data availability and the modeller's preference.

The heat transfer between open water and the atmosphere ( $\phi_{wa}$ ) can be expressed as

$$\phi_{wa} = h_{wa}(T_w - T_a) \quad (2.11)$$

where  $h_{wa}$  is the open water heat transfer coefficient [ $Wm^{-2}C^{-1}$ ] and  $T_w$  and  $T_a$  are measured in [°C]. Typically  $h_{wa}$  has a value of approximately  $20 W^{\circ}C^{-1}m^{-2}$  (Lal and

Shen, 1991) but should be calibrated based on location and model application. A similar relationship exists for the heat transfer from river water to ice ( $\varphi_{wi}$ ). At the ice-water interface the heat transfer depends on the water temperature and flow condition and may be expressed as

$$\varphi_{wi} = h_{wi}(T_w - T_m) \quad (2.12)$$

where  $h_{wi}$  is the water-ice heat transfer coefficient [ $Wm^{-2}C^{-1}$ ],  $T_w$  is measured in  $^{\circ}C$ , and  $T_m$  is melting temperature of ice ( $0^{\circ}C$ ). Where fully developed flow exists ( $Re > 2200$ ),  $h_{wi}$  can be calculated as

$$h_{wi} = c_{wi} \frac{V_w^{0.8}}{D_h^{0.2}} \quad (2.13)$$

where  $V_w$  is the water velocity [m/s],  $D_h$  is the hydraulic diameter [m], and  $c_{wi}$  is an input constant that varies with flow conditions, ice conditions, and water temperature [ $m^{0.4}s^{0.8}$ ] (Jayasundra, 2007). In applications where  $Re < 2200$  and laminar flow is present,  $h_{wi}$  may be calculated as

$$h_{wi} = \frac{N_u K_w}{D_h} \quad (2.14)$$

where  $N_u$  is the Nusselt Number,  $K_w$  is the thermal conductivity of water [ $W^{\circ}C^{-1}m^{-1}$ ].

The total heat exchange in the model domain is the sum of the heat exchange at the

water-air interface and the water-ice interface. Thus, the total surface heat exchange can be expressed as

$$\varphi_T = (1 - N)\varphi_{wa} + N\varphi_{wi} \quad (2.15)$$

where  $N$  is the surface ice concentration and  $\varphi_{wa}$  and  $\varphi_{wi}$  are defined in Equations 2.11 and 2.12, respectively. The preceding equations do not account for the heat transfer between the river bed and the water. Typically this source of heat transfer is considered to be negligible in comparison to the much more significant surface energy exchange (Shen and Yapa, 1984).

## **2.4 FREEZE-UP PROCESSES**

The mechanisms described in the preceding section are all responsible for cooling water to the freezing point during the winter season. Once the majority of the water in rivers or surface water of lakes has cooled to the freezing point, ice will begin to form. Differences in ice formation between rivers and lakes arise because of the turbulent condition of most rivers. In the absence of strong winds, the formation of ice crystals on a lake will cause an ice cover to form. However, rivers typically have sufficient turbulence to submerge surface ice crystals, assuming water velocity is greater than approximately 0.6 m/s. As a result, the ice cover formation is heavily dependent on water velocity and other hydraulic conditions. River and lake ice formation processes are discussed in detail in the following sections.

### 2.4.1 LAKE ICE FORMATION

In the absence of strong winds, lake water tends to be calm. The absence of turbulence allows the lake to stratify, allowing the warmer, more dense water to fall to the bottom. As a result of this stratification, a thin layer of very cold water can develop at the surface and once the surface becomes sufficiently cold, crystallization can begin. External seeding is often required to initiate this process (Ashton, 1986). Crystallization typically begins in calm bays and along shore lines. The ice tends to form in the shape of needles, randomly oriented particles, and ice with a dendritic pattern. Given the appropriate conditions, this primary ice cover can spread quickly, as its growth in the lateral direction tends to be considerably faster than its growth in the vertical direction.

The rate of ice thickening on lake may be approximated using the degree-day method. Assuming steady-state conditions and that the heat transfer between the water and ice is negligible, the ice growth rate can be written as

$$\varphi_i dt = \rho_i L_i dh_i \quad (2.16)$$

where  $\varphi_i$  is the heat flux from ice to air [ $Wm^{-2}C^{-1}$ ],  $\rho_i$  is the density of the ice [ $kgm^{-3}$ ],  $t$  is time [s], and  $h_i$  is the ice thickness [m]. If it is assumed that the temperature of the ice at the ice-air interface is equal to that of the air, Equation 2.16 can be written as

$$\varphi_i = \frac{k_i(T_m - T_a)}{h_i} \quad (2.17)$$

where  $k_i$  is the thermal conductivity of ice [ $Wm^{-1}C^{-1}$ ] and  $T_a$  is measured in [ $^{\circ}C$ ]. If Equation 2.16 and Equation 2.17 are combined and integrated, letting  $t = 0$  correspond to  $h = 0$ , the Stefan equation is obtained (Equation 2.18).

$$h_i = \left(\frac{2k_i}{\rho_i L_i}\right)^{\frac{1}{2}} [(T_m - T_a)t]^{\frac{1}{2}} \quad (2.18)$$

To evaluate this Equation 2.18, a summation is made, since air temperature varies with time. This expression can be written as

$$S = \sum (T_m - T_a)t \quad (2.19)$$

where  $S$  is the number of degree-days of freezing. This expression can be further simplified by combining the appropriate values of density, thermal conductivity, the latent heat of fusion, and a coefficient that adjusts for observed ice thickness into a single coefficient,  $\gamma$ . Thus, Equation 2.18 can be simplified to

$$h_i = \gamma\sqrt{S} \quad (2.20)$$



where  $\gamma < \sqrt{\frac{2k_i}{\rho_i L}}$  and varies based on wind and snow conditions on the lake. Typical values of  $\gamma$  are given in Table 2.2.

**Table 2.2: Typical values of  $\gamma$  (Michel, 1971).**

Condition	$\gamma$ ( $mm \cdot ^\circ C^{-0.5} \cdot day^{-0.5}$ )
Theoretical maximum	0.034
Windy lakes with no snow	0.027
Average lake with snow	0.017-0.024
Average river with snow	0.014-0.017
Sheltered small river with rapid flow	0.07-0.014

Snow tends to have an insulating effect on the ice and thus, alternate computations to calculate ice thickness under a snow cover are required. Equation 2.21 shows a heat flux balance taking the snow cover into consideration

$$\frac{dh_i}{dt} = \frac{1}{\rho_i L_i} \frac{T_m - T_a}{\frac{h_i}{k_i} + \frac{h_s}{k_s} + \frac{1}{H_a}} \quad (2.21)$$

where  $h_s$  is the thickness of the snow cover [m],  $k_s$  is the thermal conductivity of the snow [ $Wm^{-1}^\circ C^{-1}$ ], and  $H_a$  is a heat transfer coefficient that accounts for the thermal resistance between the uppermost surface and the air [ $Wm^{-1}^\circ C^{-1}$ ]. The value of  $k_s$  depends mainly on the density of the snow. Measured data has shown a significant amount of scatter and thus, no simple relation to calculate thermal conductivity of snow exists. To approximate the value of  $k_s$ , Mellor (1977) has suggested Equation 2.22

$$k_s = 0.021 + 4.2 \times 10^{-4} \rho_s + 2.2 \times 10^{-9} \rho_s^3 \quad (2.22)$$

where  $\rho_s$  is the density of the snow [ $kgm^{-3}$ ].

Gray and Prowse (1993) suggest that typical snow densities range from  $50 kgm^{-3}$  for newly fallen snow to  $280 kgm^{-3}$  for wind toughened snow. These correspond to thermal conductivities of  $0.042 Wm^{-1}K^{-1}$  and  $0.17 Wm^{-1}K^{-1}$ , respectively. These thermal conductivity values are 1-2 orders of magnitude lower than that of ice which is approximately  $2.43 Wm^{-1}K^{-1}$  at  $-20^\circ C$ , as given by Dorsey (1940). As a result, the snow cover has a correspondingly higher insulating effect.

Ice has a relatively low specific gravity (SG = 0.92) which allows the ice cover to become submerged once an adequate snow cover has formed. Typically, this requires only a relatively light snow cover, depending on the density of the snow. Additionally, the ice cover usually contains cracks that allow water to seep through and flow laterally from hole to hole, complicating the process of snow ice formation. The combination of these phenomena cause the snow to become wet and form what is known as snow ice. The density of snow ice is typically between  $880 kgm^{-3}$  and  $900 kgm^{-3}$  (Ager, 1962). It is possible for snow ice to form several times throughout the winter.

## **2.4.2 RIVER ICE FORMATION**

The primary factor that differentiates the formation of lake ice from river ice is turbulence. Since turbulence intensity can vary significantly between rivers, and even between reaches on the same river, the freeze-up processes on rivers tend to be more complex in nature. On most rivers there is typically an intricate series of processes that occur before a competent ice cover is formed. These steps are described in the following sections of this chapter.

### **2.4.2.1 Supercooling and Frazil Ice Production**

Frazil ice crystals will form throughout the entire depth of the flow if the temperature of an open reach of turbulent water drops below 0°C, becoming supercooled. Typically, the production of frazil particles is greatest when there is a strong net heat flux. As a result, frazil ice formation tends to follow a diurnal cycle with most production occurring at night (Beltaos, 1995). These frazil particles are typically disk-shaped and their size can vary based on the turbulence intensity of the flow (Clark, 2006). During frazil ice production, the water is supercooled and the ice particles are referred to as active. Active frazil ice particles are very sticky and will adhere to other frazil particles, resulting in the formation of frazil flocs. Due to their size, frazil flocs have increased buoyancy which causes them to rise to the water surface. These flocs will eventually group together and form frazil pans. Frazil pans may freeze together or accumulate near the banks and form border ice dynamically. Since supercooling can only occur where heat

exchange with the atmosphere is possible, frazil production decreases as large ice pans are formed and eventually ceases once a competent ice cover has formed.

In CRISP2D the supercooling of water is formulated using the conservation of thermal energy of the ice water mixture in the suspended layer and solved using the finite element method. The Lagrangian form of the conservation of energy equation is expressed as

$$\frac{de_T}{dt} = \varphi_{ss} - \varphi_{sk} + \rho_i L_i E \quad (2.23)$$

and

$$e_T = \rho_w C_{pw} (1 - C_v) T_w - \rho_i C_v L_i \quad (2.24)$$

where  $e_T$  is the thermal energy in the ice-water mixture in the suspended layer [ $kgm^{-1}s^{-2}$ ],  $C_v$  is the volumetric ice concentration,  $T_w$  is the water temperature [ $^{\circ}C$ ],  $\rho_w$  is the density of water [ $kgm^{-3}$ ],  $C_{pw}$  is the specific heat of water [ $J^{\circ}Ckg^{-1}$ ],  $\varphi_{ss}$  is the rate of heat gain per unit area through top and bottom boundaries [ $Wm^{-2}$ ] and  $\varphi_{sk}$  is the rate of heat loss through top and bottom boundaries [ $Wm^{-2}$ ],  $E$  is the net volumetric rate of loss of frazil due to mass exchanges with the surface layer and at the bed [ $s^{-1}$ ].

Water temperature and frazil ice transport simulations take into account the transport of thermal energy of the mixture due to advection and diffusion, heat exchanges at the water surface, bed, and between suspended ice and water. These simulations also account for mass exchange at the bed and between the suspended layer and the surface ice, as well as heat and mass exchanges related to the frazil ice suspension. When a mass exchange between layers occurs, the ice parcel thickness is recalculated, and the concentration of ice is reset accordingly.

Ice parcels are allowed to move freely through the model domain, forming flocs and pans and changing size and shape via interactions with other particles and reach boundaries. Often the pans will accumulate along the leading edge of existing border ice, contributing to the production of dynamic border ice. Alternatively, the ice may become lodged in a channel, forming a bridging point and initiating the development of a competent ice cover. The latter process is controlled by a stopping criterion, which is a specified velocity that allows the ice particles to come to rest.

Once a continuous ice cover has been established, heat exchange between the water and air is no longer possible and the model stops simulating the production of frazil particles. From this point forward, the growth and decay of the ice cover is modeled with the following linearized heat exchange formulation

$$\rho_i L_i \frac{dh_i}{dt} = -\phi_R + \alpha + \beta(T_s - T_a) - h_{wi}(T_w - T_m) \quad (2.25)$$

where  $\alpha$  is a linear heat transfer constant [ $Wm^{-2}$ ],  $\beta$  is a linear ice-air heat transfer coefficient [ $Wm^{-2}C^{-1}$ ], and  $T_s$  is measured in [ $^{\circ}C$ ].

#### **2.4.2.2 Border Ice Formation**

In rivers, ice covers may first appear as static border ice developed in the form of skim ice along the banks. The thermal and mechanical conditions of the river govern the border ice formation process. First, the thermal condition requires the water surface temperature to drop to the freezing temperature, allowing ice crystals to form and remain intact. Second, the mechanical conditions must be such that the turbulence is not strong enough to carry the surface ice crystals deeper into the water column. CRISP2D evaluates the follow four conditions at each node in the model domain:

- 1) The surface water temperature,  $T_s$ , is less than a critical value,  $T_{cr}$ , where

$$T_s < T_{cr} < 0^{\circ}C$$

- 2) The buoyant velocity of frazil particles is greater than the vertical fluctuating component of the water velocity ( $v_b > v_z'$ )

- 3) The local depth averaged velocity is less than a critical velocity

- 4) The node must either be a land boundary node or two previously established border ice nodes must be adjacent to the node in question.

The water surface temperature,  $T_s$ , is calculated at each node using an empirical formulation developed by Matousek and Vaclav (1984a, 1984b) and is given as

$$T_s = T_w - \frac{\varphi_{wa}}{1130u + bV_a} \quad (2.26)$$

where  $u$  is the local depth averaged velocity [m/s],  $T_w$  is the depth averaged water temperature[°C],  $b$  is the wind utilization coefficient which is related to the width of the channel surface, and  $B$  [m], and is given as

$$b = \begin{cases} 15 & \text{when } B \leq 15m \\ -0.9 + 5.87 \ln B & \text{when } B > 15m \end{cases} \quad (2.27)$$

Matousek (1984) also developed an equation to calculate the buoyant velocity of frazil particles on the water surface,  $v_b'$  [m/s], which is given in Equation 2.28.

$$v_b' = -0.025T_s + 0.005 \quad (2.28)$$

To calculate the vertical fluctuating component of the water velocity ( $v_z'$ ), Lal and Shen (1989) modified Matousek's equation (1984) (which only took into consideration bed

shear effects) in order to account for both bed and wind shear effects using the approach for vertical mixing in lakes (Fischer et al., 1979).

If any particular node satisfies the above conditions for the formation of static border ice, the node will be assigned a surface ice concentration of  $N = 1.0$  and an initial solid ice thickness of 0.001 m. From that point forward, the formed static border ice will be subject to thermal growth and decay (as per Equation 2.25).

In addition to static border ice, CRISSP2D also models the formation of dynamic border ice. This type of border ice grows due to the accretion of surface ice to the existing static ice. This type of border ice formation is what allows for the progressive closure of the river and ultimately bridging between the ice on either side of the banks. Relationships to model dynamic border ice growth have been developed by Michel et al. (1982), Newbury (1968), and Miles (1993). CRISSP2D uses the following relationship developed by Michel et al. (1982) to calculate the lateral growth of border ice

$$\frac{dW}{dt} = \frac{\phi_{wa}}{\rho_i L_i} 14.1 V_*^{-0.93} N^{1.08} \quad (2.29)$$

where  $W$  is the width of the border ice [m],  $V_* = \frac{u}{V_c}$ ,  $V_c$  is the maximum velocity for dynamic border ice growth [m/s], and  $N$  is the surface ice concentration. Previous



researchers have observed the range in  $V_c$  to be between 0.4 m/s and 1.2 m/s (Matousek, 1984; Shen and Van DeValk, 1984; Michel 1982).

### **2.4.2.3 Skim Ice Formation**

In portions of the river with particularly low water velocity and low turbulence intensity, skim ice may form on the water surface. Similarly to border ice formation, skim ice formation is modelled based on criteria defined by Matousek (1984b). In order for skim ice to form, the following three criteria must be satisfied:

- 1) The surface water temperature must be below freezing ( $T_s < 0^\circ\text{C}$ )
- 2) The buoyant velocity of surface frazil particles must be greater than the vertical fluctuating component of the water velocity ( $v_b' > v_z'$ )
- 3) The element must not previously be covered by any type of ice

In each element where the above conditions are satisfied, an initial skim ice parcel is generated using a user defined thickness and an ice concentration of 1.0.

---

**3.1 INTRODUCTION TO CRISSP2D**

As previously mentioned, the numerical model used in this study is the Comprehensive River Ice Simulation Processes (CRISSP2D). The model, developed at Clarkson University under the supervision of Dr. Hung Tao Shen, is unique in the fact that it is the only comprehensive two-dimensional river ice model currently available. Large hydropower companies, including Manitoba Hydro, provided the motivation for the model development. As such, the model was developed as a tool to help mitigate a large variety of ice-related issues relating to hydropower production.

CRISSP2D is a coupled, two-dimensional finite element model that contains hydrodynamic, thermodynamic, and dynamic ice components. These components work together to allow the model to simulate ice formation, movement, stoppage, and

jamming in rivers and lakes. It is capable of simulating a large variety of hydrodynamic and thermal ice processes including:

- 1) An unsteady flow model capable of modelling transitional flow conditions
- 2) Water temperature calculations that include supercooling events
- 3) Simulation of freeze up processes, including frazil ice, anchor ice, border ice, skim ice, and surface ice runs
- 4) Simulation of dynamic transport of surface ice and ice jam evolution
- 5) Simulation of thermal growth/decay of ice covers as well as mechanical break up conditions.

The large range of processes described above has allowed this model to be successfully applied in several different applications (discussed further in Section 3.4).

## **3.2 MODEL COMPONENTS**

The CRISSP2D model is divided into a number of sub-modules that have different roles and perform different calculations within the model structure. These sub-modules can be turned on or off at the user's discretion and used in different combinations depending on the application at hand. The portions of the model that are most relevant to this study are discussed in the subsequent sections of this chapter.

### 3.2.1 HYDRODYNAMIC MODULE

The hydrodynamic sub-component of CRISSP2D can be used to simulate a variety of flow regimes by solving the two-dimensional, depth averaged, unsteady St. Venant equations for the conservation of mass and the conservation of momentum. These equations, shown below, are slightly modified to incorporate the surface ice and surface flow effects within the model, allowing the model to simulate flow through an ice jam (Lui et al., 1998). As a result, the CRISSP2D is capable of simulating grounded ice jams, which is a feature exclusive to CRISSP2D.

$$\frac{\partial H}{\partial t} + \frac{\partial(q_{ix})}{\partial x} + \frac{\partial(q_{iy})}{\partial y} = \frac{\partial}{\partial t}(Nt'_i) \quad (3.1)$$

$$\frac{\partial q_{ix}}{\partial t} + \frac{\partial}{\partial x} \left( \frac{q_{ix}^2}{H_i} \right) + \frac{\partial}{\partial y} \left( \frac{q_{ix} q_{iy}}{H_i} \right) = \frac{1}{\rho} (\tau_{sx} - \tau_{bx}) + \frac{1}{\rho} \left( \frac{\partial T_{xx}}{\partial x} + \frac{\partial T_{yx}}{\partial y} \right) - gH_i \frac{\partial z}{\partial x} \quad (3.2)$$

$$\frac{\partial q_{iy}}{\partial t} + \frac{\partial}{\partial x} \left( \frac{q_{ix} q_{iy}}{H_i} \right) + \frac{\partial}{\partial y} \left( \frac{q_{iy}^2}{H_i} \right) = \frac{1}{\rho} (\tau_{sy} - \tau_{by}) + \frac{1}{\rho} \left( \frac{\partial T_{xy}}{\partial x} + \frac{\partial T_{yy}}{\partial y} \right) - gH_i \frac{\partial z}{\partial y} \quad (3.3)$$

where

$$T_{xy} = \varepsilon_{xy} \left( \frac{\partial q_{tx}}{\partial y} + \frac{\partial q_{ty}}{\partial x} \right) \quad (3.4)$$

In the above equations,  $H$  is the total water depth [m],  $q_t$  is the total unit width water discharge [ $\text{m}^2/\text{s}$ ],  $N$  is the ice concentration between 0 and 1,  $t'_i$  is the submerged ice thickness [m],  $H_t$  is the equivalent water depth for the total water discharge [m],  $\rho$  is the density of water [ $\text{kg}/\text{m}^3$ ],  $\tau_s$  is the surface shear stress [ $\text{N}/\text{m}^2$ ],  $\tau_b$  is the bed shear stress in [ $\text{N}/\text{m}^2$ ], and  $\varepsilon_{xy}$  is the generalized eddy viscosity coefficients.

The above equations are solved using an explicit finite element implementation of the streamline upwind Petrov-Galerkin concept (Shen and Chen, 1993; Lui and Shen, 2003).

### **3.2.2 WATER TEMPERATURE MODULE**

CRISSP2D has the capability to simulate water temperature, supercooling, and frazil ice production by solving the energy equation using the finite element method. Equations 2.23 and 2.24 account for the advection and diffusion related to the transport of thermal energy, the source and sink terms due to heat transfer at the river bottom and the surface, the heat exchange between the suspended frazil and the river water, as well as the mass exchanges between suspended and surface ice.

The solution to Equations 2.23 and 2.24 is found by employing a lumped formulation of the Galerkin finite element method to solve the conservation equations of water temperature and suspended frazil concentration, including advection, diffusion, and heat source/sink terms at the top and bottom boundaries (Liu and Shen, 2005).

Furthermore, the program calculates changes in water temperature and frazil concentration on a nodal basis using a Lagrangian form of the equations. These changes are subsequently coupled with the finite element calculations and a complete solution for water temperature and suspended frazil concentration is obtained.

### **3.2.3 THERMAL ICE MODULE**

The thermodynamic module in CRISP2D is governed by energy exchanges that are present between the atmosphere, ice cover, water, and riverbed. If detailed meteorological data is available, comprehensive energy budget calculations, including contributions from solar radiation, back radiation, evaporative heat transfer, conductive heat transfer, and heat transfer due to precipitation (as discussed in Section 2.2) can be carried out. Otherwise, CRISP2D will approximate the energy budget equations linearly, as discussed in Section 2.3.

The thermal ice module also contains calculations for the thermal growth and decay of an ice floe or ice cover. This is an important part of the simulation process because the existence and characteristics of an ice cover can have significant effects on the flow regime and break-up processes. This module carries out calculations (Equation 2.25) that allow an ice cover to grow thermally downward, or melt from either the top or bottom. The model also accounts for the insulating effects of the presence of frazil ice

deposited on the underside of an ice cover, which can accelerate the growth of the ice cover at the bottom boundary.

An additional important part of the ice simulation process is mass exchanges that occur between the suspended and surface ice layers as well as the suspended layer and the river bed. Where open water exists, frazil ice particles may be deposited to the surface layer of water. If an ice cover is already in place, the frazil particles may be deposited to the underside of the ice cover, increasing its thickness. It is also possible for these deposited frazil particles to be re-entrained into the suspended layer if the water is sufficiently turbulent. Mass exchange between the suspended layer and the river bed is accounted for within the anchor ice module. This module is not particularly relevant to this study and will not be discussed further within this thesis.

Several other thermal ice formation processes are simulated within the thermal module of CRISSP2D, including the formation of skim ice, border ice, frazil ice, and anchor ice. The equations and criteria that govern these processes are discussed at length in Section 2.4.2 (excluding anchor ice, as it is not relevant to this study).

### **3.2.4 DYNAMIC ICE MODULE**

When coupled with the hydrodynamic and thermodynamic modules, the ice dynamic sub-component of CRISSP2D can simulate a wide variety of ice processes. Surface ice

dynamics are simulated using a Lagrangian discrete parcel method (Chen, 1993; Shen et al., 2000). This method considers the ice as a continuum and represents the ice using a sufficiently large number of individual particles. This technique is considered valid as long as ice particles are much smaller than the river width and sufficiently large in comparison to the ice floes in the river. Each particle has its own mass, momentum and energy and is tracked throughout the model domain. Each parcel also has its own properties, including position, velocity, thickness, density, mass, concentration, and internal stress and strain. Non-advective terms in the ice dynamics equations are determined from neighbouring parcels within a given distance. In order to calculate the internal stresses of the parcels, a viscoelastic-plastic model is used (Ji et al., 2004). Using this formulation, the forces at the boundaries of the model can be calculated.

The dynamic ice module also gives the user the option to forgo dynamic ice calculations and, instead, employ free drift calculations. This option may be advantageous in some applications since the dynamic ice calculations are quite computationally demanding. The free drift calculations simply track the ice parcel evolution as it travels down the river, not considering any interactions with other parcels.

### **3.3 MODEL REQUIREMENTS**

The process of working with the CRISSP2D model is similar to that of most numerical models. The steps that are typically followed are outlined below:



- 1) Generate the finite element mesh
- 2) Prepare the input data
- 3) Complete a hydrodynamic calibration and verification
- 4) Complete a dynamic ice calibration and verification
- 5) Complete scenario simulations
- 6) Present and analyze model results

The detail and accuracy to which these steps can be carried out largely depends on the quantity and quality of available data. Often the user is required to make numerous simplifying assumptions regarding bathymetry, boundary conditions, and calibration parameters. The model contains several switches that turn on or off different subcomponents or processes within the model. As such, data requirements vary based on which sub-components are switched on. Specific data requirements and input information for the different subcomponents are described further in the following sections.

### **3.3.1 DATA REQUIREMENTS**

Similar to most numerical models, obtaining input data for CRISSP2D can be difficult or even impossible in some applications. Although CRISSP2D is not extremely data intensive, it does require the input of a number of different data sets. First, reach boundary geometry and river bed bathymetry are required in order to construct a finite

element mesh that is a reasonable representation of the actual study area. This may be in the form of two-dimensional cross-sections or a collection of x, y, z scatter point data.

CRISSP2D requires other typical hydrodynamic information, including river discharge and water surface elevation at flow boundaries and calibration gauges. In order to carry out thermodynamic and dynamic ice simulations, the input of meteorological data is also required. The minimum model requirement is air temperature, but if available, a more complete weather data set may be used (air temperature, pressure, dew point, cloud cover, wind speed, precipitation).

There are several other optional data sets that may be input in the model if available. These include boundary ice fluxes, frazil ice concentration, water temperature measurements, surface ice conditions, ice jam locations, anchor ice locations, and many others. If such field data is available and is of reasonable quality, it will likely improve the quality of the numerical model.

### **3.3.2 BOUNDARY AND INITIAL CONDITIONS**

Since CRISSP2D is an unsteady model, boundary conditions are typically specified as time series. Each open boundary in a CRISSP2D model requires a discharge or water surface elevation boundary condition (or a combination of the two). For sub-critical flow, one boundary condition must be specified at each boundary, while supercritical flow requires both discharge and water surface elevation boundaries to be specified.

When simulating with the dynamic ice module, an additional water temperature boundary condition and an ice concentration boundary condition are required. Typically these are located at the upstream boundary of the model.

Typically the initial conditions for a hydrodynamic simulation are generated by a cold start run. To increase model stability during the cold start, the water surface elevation boundary is typically slowly ramped down from an artificially high level to match the elevation corresponding to time  $t = 0$  in the desired simulation. Likewise, the flow at the discharge boundaries is typically slowly ramped up from zero until flow conditions at time  $t = 0$  is reached. Once these conditions are achieved, the model is run at steady-state for several hours until the water level and discharge are stable at all nodes. This simulation is subsequently used to hot-start subsequent simulations. When simulating ice processes with the dynamic ice module, it is typical to initiate the simulation before the freeze-up period begins, having the initial conditions be free of ice. Existing steady-state hydrodynamic and thermodynamic simulations typically provide initial water depths, velocities, water temperatures, etc. at each node.

### **3.3.3 MODEL CALIBRATION**

Calibration is an extremely important part of the modelling process. Typically, when working with CRISSP2D, an open water hydrodynamic model is first developed and calibrated. This model is often used as the base for the following thermodynamic and

ice dynamic models. Typically, the hydrodynamic model is calibrated by comparing simulated water surface profiles to measured ones. Thus, it is optimal to have data for several water surface elevation gauges within the model domain. Other hydrodynamic data sets may also aid in the calibration of the open water model, including discharge and water velocity measurements.

Winter data is often more difficult to obtain, causing calibration of the dynamic ice model to be much more challenging. As such, a variety of different data sources have been employed to ensure that the model is performing reasonably well. These include photos of ice formation through the winter, under ice discharge or velocity measurements, ice thickness measurements, or frazil ice concentration measurements.

---

**4.1 INTRODUCTION**

Although interest in the Netley-Libau Marsh area is high, there has not been any recent numerical modelling of the area. As a result, bathymetric data had to be compiled from a variety of sources, including a comprehensive bathymetric survey carried out on the Netley-Libau Marsh. Additionally, extensive field work was conducted in order to collect the data sets required to complete this research project. Both winter and summer field programs were initiated to obtain water surface elevation (WSE) data, open water and ice covered discharge data, water velocity measurements, and ice thickness measurements. The details of how these measurements were made are described in the following sections of this chapter.

## 4.2 BATHYMETRY

Bathymetric data for the entire study area was not readily available and as such, it had to be compiled from a variety of different sources. Lake bed elevations for Netley Lake as well as river bed elevations for the portion of the Red River that extends from downstream of Netley Cut to Lake Winnipeg were obtained from a hydrometric survey that was performed in October 2009 by Aquatics ESI using sonar technology. The survey provided coverage of the aforementioned regions (shown in Figure 4.1) on a 1 m by 1 m grid. However, the west branch of the Red River was not covered in this survey because it was too shallow to accommodate the equipment used.

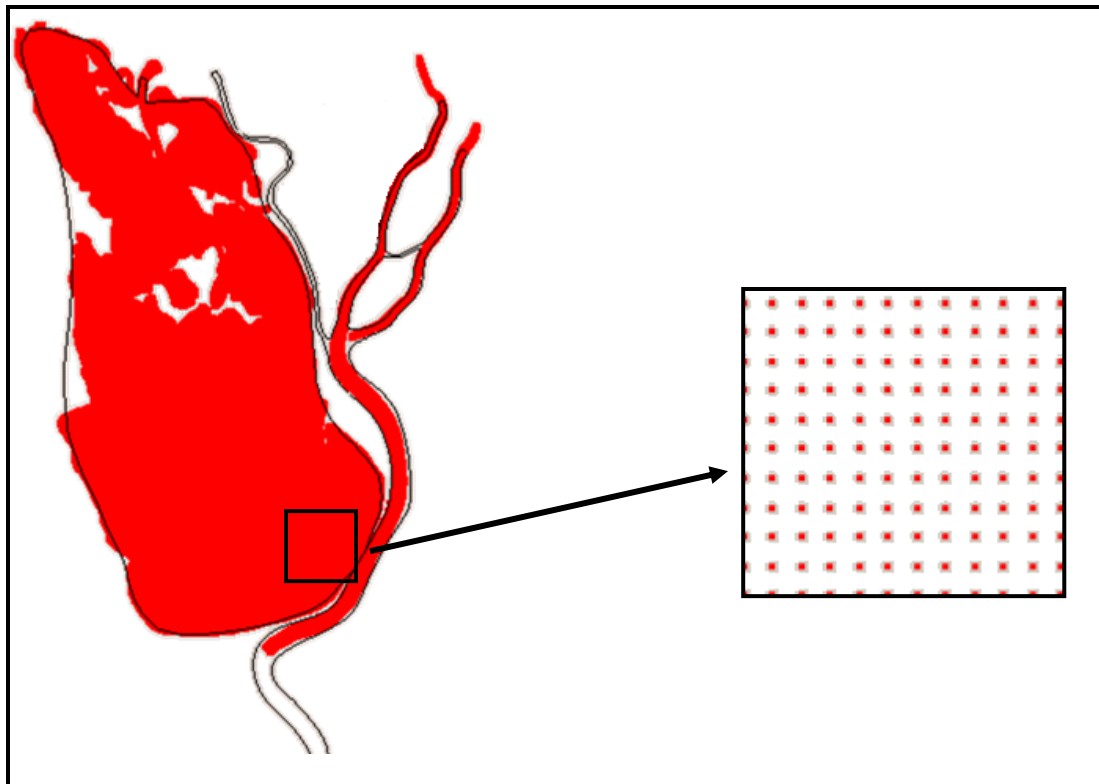


**Figure 4.1: Bathymetry obtained in 2009 hydrometric survey.**

Upstream of Netley Cut, river bed elevations were modeled using cross sections obtained from a hydrometric survey completed in 1957. The cross sections were approximately 200 m apart and extend to the upstream model boundary, as shown in Figure 4.2. Ideally, more recent cross sections would have been used, but no such data existed nor did the resources to conduct a hydrometric survey of this portion of the river. It is likely that the channel has eroded and widened over the past five decades, causing the geometry of the portion of the river to be slightly inaccurate. However, this transformation in river bed geometry was somewhat accounted for during the hydrometric calibration of the model (detailed in Chapter 6).

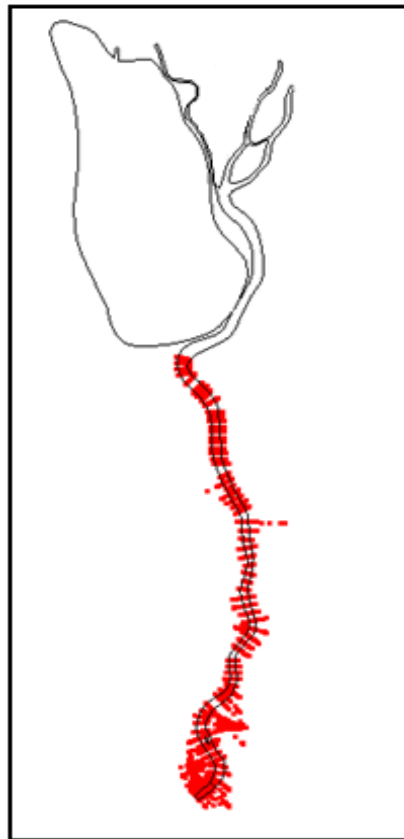


**Figure 4.2: Bathymetry obtained from 1957 hydrometric survey.**

---

## DATA ACQUISITION

---

To supplement these two sources, and provide coverage of the smaller west branch of the Red River, cross sectional bathymetry measured with an Acoustic Doppler Current Profiler (ADCP) by the University of Manitoba in July 2009 was incorporated into the model (shown in Figure 4.3). Only one cross section across the west channel was measured and thus, the channel was assumed to have constant cross sectional geometry along its length. This channel carries a very small proportion of the total flow and any discrepancies between actual and simulated river bed geometry were considered insignificant.

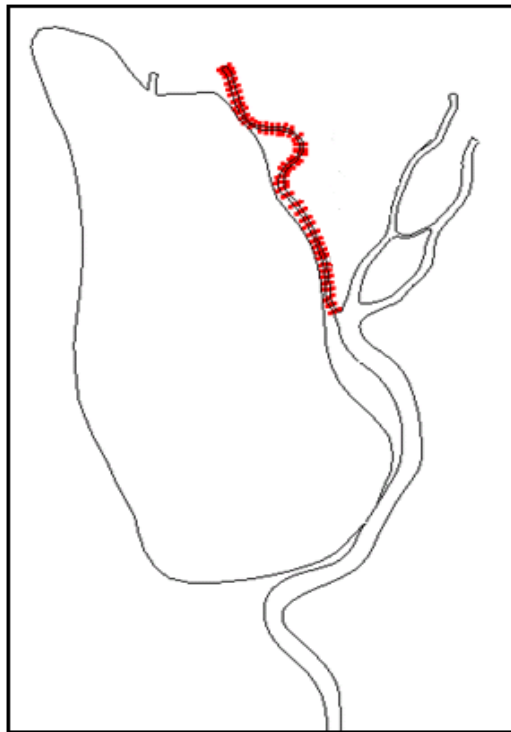


**Figure 4.3: Bathymetry obtained from University of Manitoba ADCP survey.**



### **4.3 OPEN WATER DATA COLLECTION**

Field work and data collection in the study area began in the open water season of 2009. During this season, the main focus was taking discharge measurements at various locations to determine the approximate portion of the total flow that discharges through Netley Cut and various channels downstream. These measurements were made with the River Surveyor system, which is comprised of an ADCP mounted to a floating hydroboard. The River Surveyor system was attached to a motor boat which was slowly driven from bank to bank perpendicular to flow at each point of interest. As the boat traveled, the River Surveyor continuously measured water velocity profiles and river bed bathymetry so that the discharge through each cross section could be calculated.

Discharge measurements were taken over six days between June and July. The main points of interest were upstream of Netley Cut, across Netley Cut and downstream of Netley Cut. In addition, measurements were made where the Red River splits into three channels, taking measurements in each of the east, main, and west channels. Discharge had the tendency to vary somewhat depending on the flow and wind conditions. The average proportions of the total discharge flowing through each channel are shown in Table 4.1. This analysis assisted in understanding the hydrodynamics of the study area and provided valuable information to be used during the hydrodynamic calibration and verification of the numerical model.

**Table 4.1: Average proportion of Red River flow passing through different channels.**

<b>Location</b>	<b>Percent of Total Flow</b>
Red River upstream of Netley Cut	100
Netley Cut	37.1
West Channel	0.7
Main Channel	27.4
East Channel	28.3
Error	6.5

A more extensive field program was carried out in the open water season of 2010. The main purpose of this field program was to collect data essential for the hydrodynamic calibration of the numerical model. This primarily consisted of measuring water surface elevation at various locations within the study area to be used for boundary condition inputs and calibration gauges. The data was collected by installing a series of Solinst Levelloggers throughout the Netley-Libau Marsh at representative locations. These loggers contained pressure transducers to measure water depth and also measured water temperature at a specified time interval. The locations of the pressure transducers are shown in Figure 4.4.

In addition to the levelloggers, a barologger was installed within the study area (shown in Figure 4.4) to measure barometric pressure. Data from the barologger was subsequently used to convert the raw water level data read by each levellogger into an accurate water depth measurement. This was accomplished by subtracting the air pressure from the total pressure read by each levellogger.

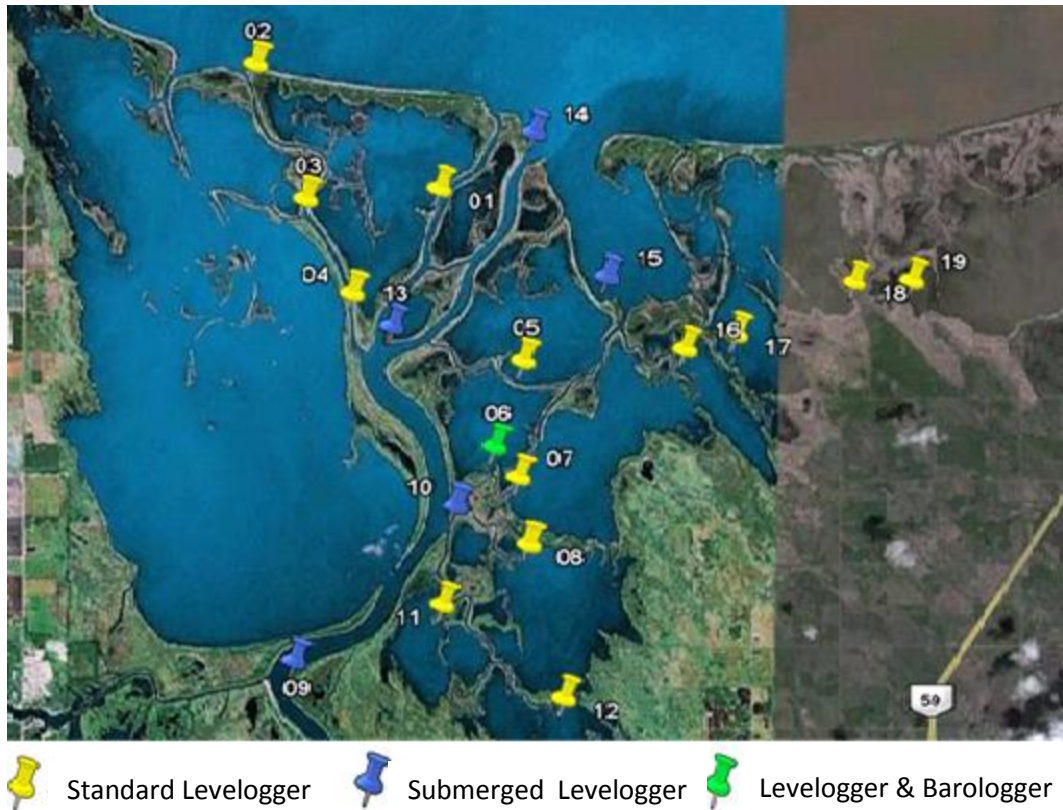


**Figure 4.4: Location of pressure transducers in the summer of 2010.**

The pressure transducers measured water depth at five minute intervals, which were subsequently averaged into hourly measurements. However, the model requires water surface elevation data, rather than water depth data. Since, both the elevation of the bed and water surface were unknown at each gauge location and there were no known benchmarks within the vicinity of these gauges, the water surface elevation at each gauge could not be measured directly. Instead, the water level data was transformed into water surface elevation data by assuming that in a period of minimal wind influence, the water surface elevation at Gauge 2 would equal that of Gimli, a slightly more northerly station on Lake Winnipeg monitored by Water Survey of Canada. Thus,

by finding the offset between the two gauges during a period of minimal wind influence, the remainder of the data could be adjusted by this constant offset to produce a reasonable estimate of the water surface elevation at Gauge 2 over the entire open water season.

A similar process was used to adjust the gauges further upstream. However, to estimate the water surface elevation at these gauges the slope of the Red River had to be taken into account. A longitudinal profile of the Red River indicated that the average slope between Selkirk and Lake Winnipeg was approximately 0.0000123. As a result, each gauge was adjusted based on this assumed slope and its distance upstream from Gauge 2. This method is not entirely accurate as it assumes that water in the channel is flowing at normal depth. In reality, the Red River does not flow at normal depth, but rather it typically forms a M1 water surface profile. Nevertheless, the aforementioned estimations of water surface elevation were the most reasonable estimates that could be made with the available data.

In addition to the pressure transducers, Sontek Argonauts were installed in several smaller tributaries that discharge to or from the Red River (locations shown in Figure 4.5). When secured to the channel bottom, these devices are able to profile the water velocity within the channel by sending out sound waves and calculating the water velocity based on the return echo. Data from the Argonauts indicated that Devils Creek (Argonauts 1 and 2) is the only tributary downstream of Netley Cut that has the capacity

to carry a significant amount of flow into or out of the Red River. The cross sectional geometries of these channels were surveyed using the River Surveyor system and the continuity equation was used to estimate flow through Devils Creek. This data was subsequently used as a boundary condition for the open water hydrodynamic calibration of the numerical model (discussed further in Chapter 6).

In the subsequent open water season of 2011, additional discharge measurements around the Netley Cut area were taken in order to verify the measurements taken in the previous summers. It was found that these measurements agreed well with the measurements previously taken.



**Figure 4.5: Argonaut locations, summer 2009.**

#### **4.4 PRE-FREEZE-UP DATA COLLECTION**

One of the main objectives of the pre-freeze-up field program was to monitor the water temperature throughout the study reach as the water cooled down prior to freeze-up. In late fall, three approximately equally spaced temperature gauges were installed along the main channel of the Red River between Selkirk and Netley Creek. It was not possible to install gauges further downstream due to access restrictions during the winter months. The gauges were removed just prior to freeze-up and the data obtained was used in calibrating the open water heat loss coefficient between the water and the air in the numerical model. The purpose of this calibration process was to attempt to reproduce water temperature trends within the river. This was accomplished by adjusting the water-air heat transfer coefficient until there was good agreement between measured and simulated water temperatures. Proper calibration of the water-air heat transfer coefficient will help ensure that the model cools the water at an appropriate rate, allowing the model to begin simulating ice formation at the appropriate time.

In addition, several photos were taken at the time of freeze up to document the processes that were occurring in different portions of the study area. This included both photos taken from the ground, as well as aerial photos taken from an airplane above the study area.

## 4.5 WINTER DATA COLLECTION

Field work was conducted and data was collected in the winter seasons of 2009-2010, 2010-2011, and 2011-2012. Throughout all of these winter seasons, the primary focus of the field program was to collect ice thickness measurements that could be used for calibrating and verifying the CRISSP2D freeze-up model. Measurements were collected throughout the study area, particularly along the Red River and in the Netley Cut area.

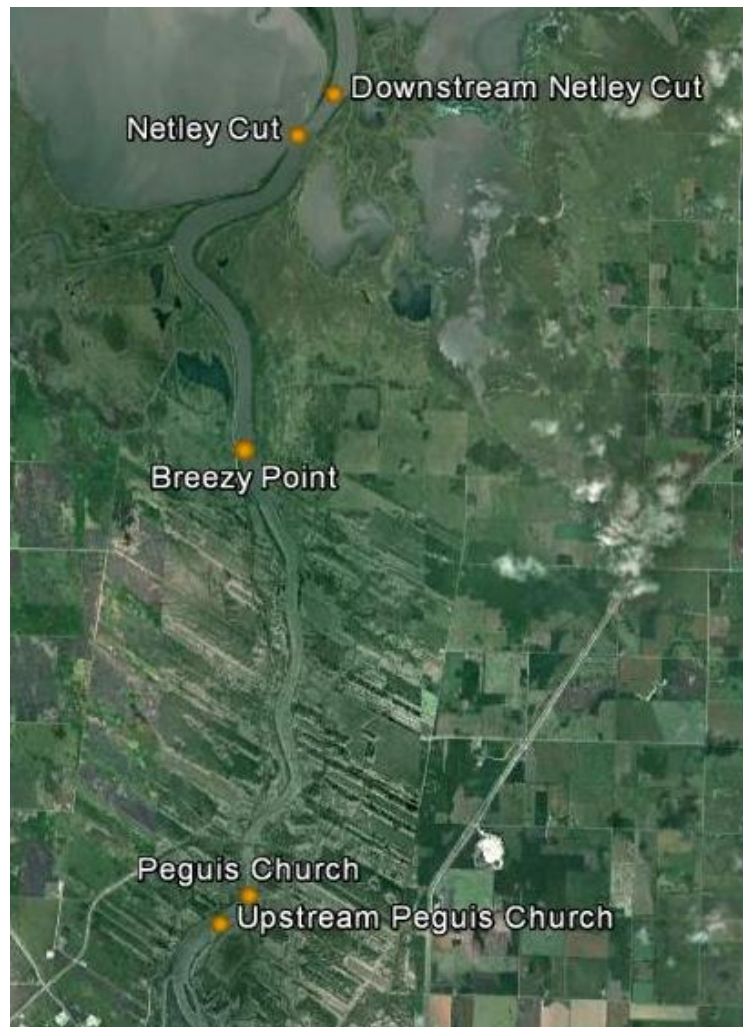


**Figure 4.6: Ice thickness measurement locations in winter 2009-2010.**

In the 2009-2010 winter season, the focus of the field program was to determine the proportion of the Red River flow that discharges through Netley Cut during the winter season. Under ice discharge measurements were taken across Netley Cut and downstream of Netley Cut using a Sontek Flow Tracker. These measurements were supplemented with ice thickness data taken by Manitoba Water Stewardship at various cross sections on the Red River between Selkirk and Netley Creek which were used in the calibration of the dynamic ice model. The locations of these cross sections are shown in Figure 4.6.

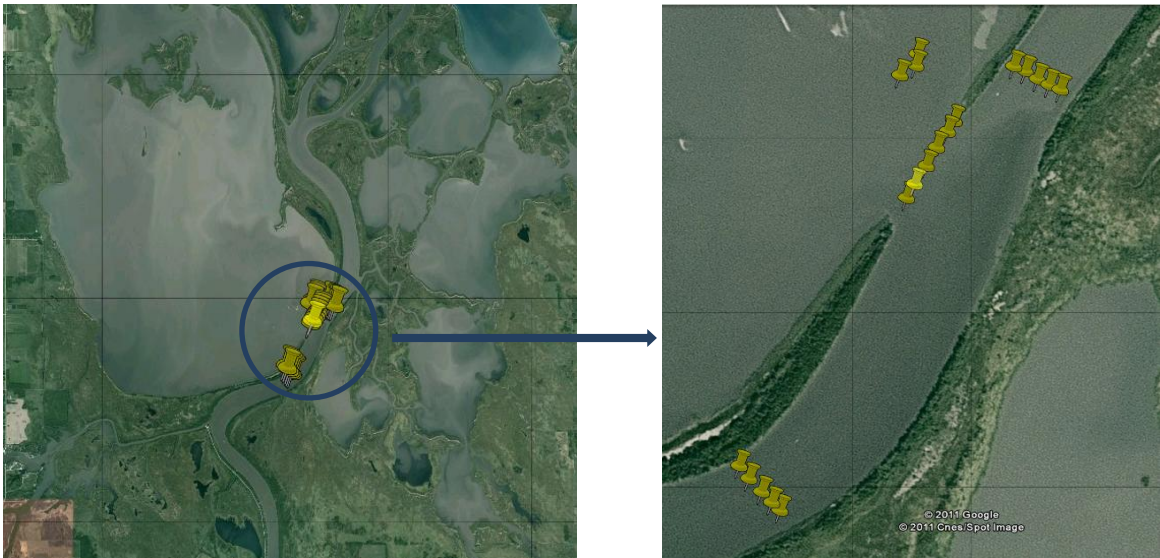


**Figure 4.7: Ice thickness measurement locations in winter 2011.**

In the 2010-2011 winter season, under ice discharge measurements were once again taken in the Netley Cut area. In addition, ice thickness measurements were taken upstream, downstream and across Netley Cut as well as in Netley Lake, as shown in



Figure 4.7. The purpose of these measurements was to test the model's ability to simulate ice growth in the vicinity of Netley Cut, the main area of interest of this research project. To supplement this data, additional ice thickness measurements were taken at numerous locations along the Red River over the freeze-up period. The locations of these measurements are shown in Figure 4.8.

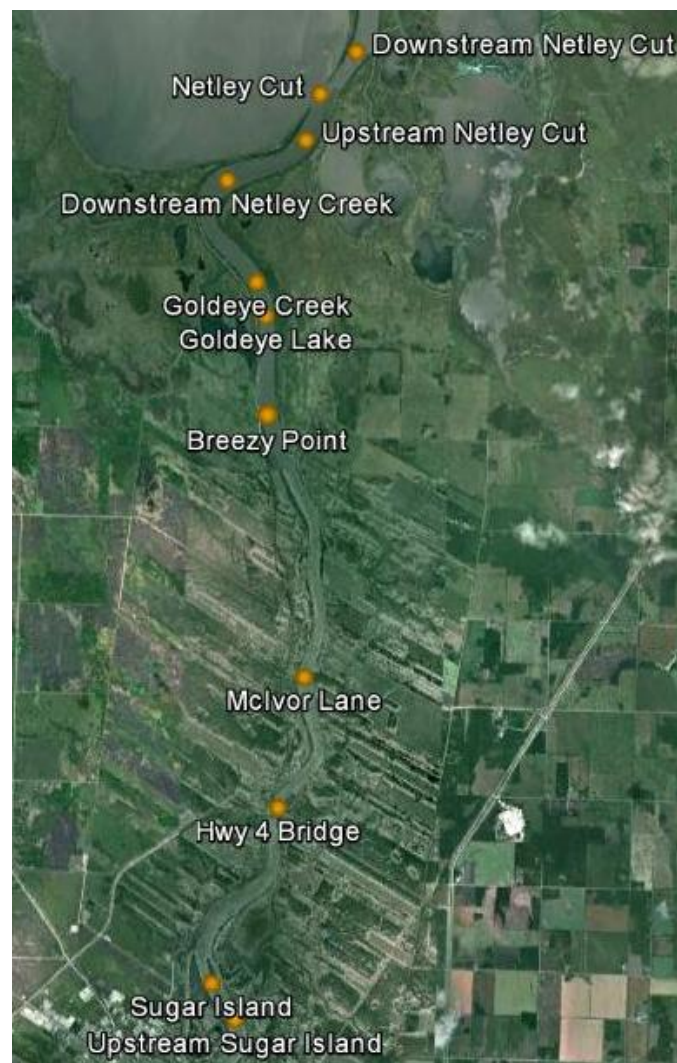


**Figure 4.8: Ice thickness measurement locations in winter 2010-2011.**

The most extensive field program was conducted in the 2011-2012 winter season. The main focus of this field program was to take ice thickness measurements at various cross sections along the Red River to help with the validation of the dynamic ice model. Certain limitations existed due to safety precautions and winter time access to the river. For this reason, three cross sections were selected to monitor: Selkirk, Hwy 4 Bridge, and Breezy Point (shown in Figure 4.9). Each of these cross sections was easily accessible by car. At each of these cross sections, ice thickness and water depth were measured at 10-30 m intervals across the width of the river. Measurements were taken at each cross section four times throughout the winter season. Additionally, water temperature measurements were taken periodically at these locations throughout the winter season. However, ice thickness measurements were limited by the Province's efforts to break the ice up artificially prior to natural break up. Specialized equipment is used to cut and break-up the ice with the intentions of easing the ice-jamming problems that often occur during natural break up. This process typically begins in late February and often exposes large areas of open water, making it unsafe to access large portions of the river. As a result, some of the measurements were limited to a particular portion of the cross section, where a thick ice cover was still intact.

To supplement the ice thickness measurements taken during this winter season, additional ice thickness measurements were taken across Netley Cut and in the east branch of the Red River. The River Surveyor system was also used to measure under ice

discharge in the east channel to provide an approximation of the flow split at the Red River Delta.



**Figure 4.9: Ice thickness measurement locations in winter 2011-2012.**

Finally, two airplane trips were taken over the study area during this winter season. The first was just after freeze-up had occurred in most areas of the reach. Photos were taken to document the timing of the freeze-up and the types of freeze-up processes that were occurring. The second flight was taken near the end of the winter, prior to break-up. The objective of this flight was to document the break-up mechanisms as well as the timing of the break-up and. However, no substantial break-up had yet occurred at the time of this flight.

---

**5.1 FINITE ELEMENT MESH DEVELOPMENT**

The finite element mesh used for this study was developed in SMS 10.0. This program provides a user friendly graphical interface for mesh development and its output files can be easily converted into CRISP2D input files.

In order to begin creating the mesh, a georeferenced satellite image of the study area was imported into SMS 10.0. Using this image, the extents of model domain were defined by tracing an outline, known as the map, around the area to be modelled. The model included all branches of the Red River as well as Netley Lake and its outlet to Lake Winnipeg. The model extends approximately 21 km upstream of Netley Cut to Selkirk, Manitoba. This location was chosen as the upstream extent of the model because of its

close proximity to a Water Survey of Canada discharge gauge that could provide data for an inflow boundary condition at that location. The model terminates approximately 12 km downstream of Netley Cut where it discharges into Lake Winnipeg, having a total reach length of approximately 33 km. It was deemed that the remainder of the Netley-Libau Marsh would not contribute significantly to the ice processes on the Red River in the vicinity of Netley Cut and, thus, was excluded from the model for simplicity and computational time considerations.

Once the model domain was defined, vertices were added to the map as a means of defining element boundaries. The vertices were distributed such that the number of elements across each channel would remain relatively consistent throughout the model domain. The narrower channels required smaller elements in order to maintain the computational integrity of the mesh, while larger elements were used in the wider channels in order to optimize computational efficiency. Where intersections of large and small elements existed in the mesh, the regions were integrated with gradual element size transitions. To further decrease computational time, even larger elements were used in Netley Lake since it is a low flow region and is of less hydraulic importance than other portions of the mesh. The completed finite element mesh is illustrated in Figure 5.1.

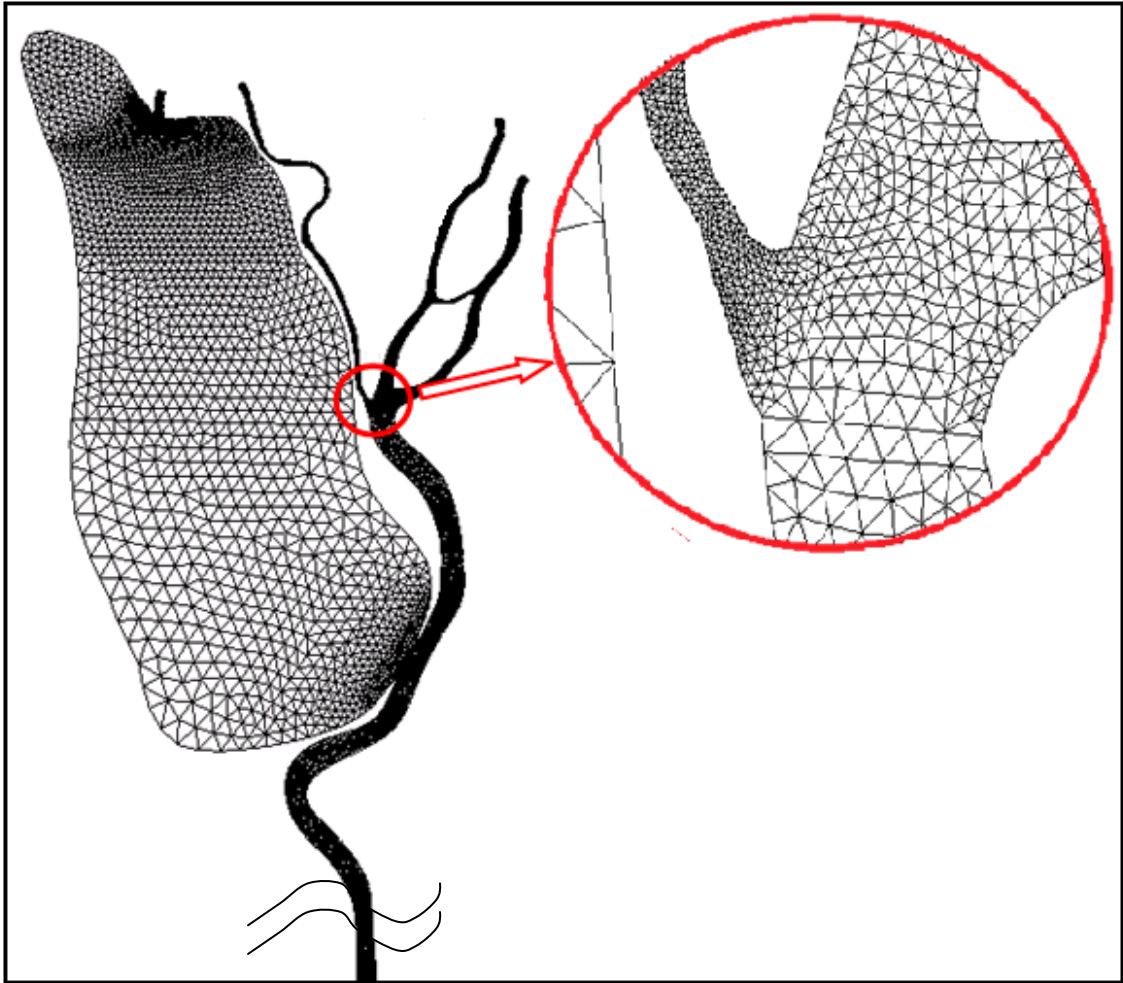


**Figure 5.1: Finite element mesh.**

Several iterations were required to determine the optimal element sizes. Meshes that were too coarse resulted in large continuity errors during the hydrodynamic calibration of the model. Thus, element sizes were adjusted until a continuity error of approximately 1% was obtained. This corresponded to having approximately six elements spanning the width of each channel. Using less than six elements across any channel led to poor continuity within the model (discussed further in Section 6.1). The resulting mesh contained approximately 14,500 nodes and 25,700 linear, triangular

elements, covering a surface area of approximately 63 km<sup>2</sup>. The nodes were numbered from upstream to downstream for computational efficiency since an upwind scheme is used to solve the unsteady flow equations.

Node elevations were established based on bathymetric data from the study area. This data was imported into SMS 10.0 and a linear interpolation scheme was used to interpolate it to the mesh nodes. Generally, the linear interpolation of the bathymetry created a reasonable approximation of the channel geometries. In some instances, however, node elevations were altered manually to create better model stability, particularly at the inlet and outlets of the model.

## **5.2 BOUNDARY CONDITIONS**

The hydrodynamic model required several boundary conditions to be established. At the upstream extent of the model, a discharge (flux) boundary condition was specified using hourly discharge data from Water Survey of Canada Gauge 05OJ005 (Red River at Selkirk). Further downstream, two additional flux boundaries were specified at Netley Creek (hourly discharge data from Water Survey of Canada Gauge 05OJ008) and Devils Creek (hourly data obtained from an Argonaut installed during a field program as discussed in Section 4.3). All other incoming tributaries were considered to be negligible.



The downstream extent of the model consists of four outlets to Lake Winnipeg and each of these outlets was assumed to have an identical water surface elevation. Thus, hourly water surface elevation data collected from a gauge installed immediately downstream of Netley Lake (Gauge 2 in Figure 4.4) was used to force the model at each of the outlets at the downstream end. It was important to use a gauge immediately downstream of the model outlets due to the nature of the water level fluctuations of Lake Winnipeg. Since Lake Winnipeg is a large, shallow lake situated in the Prairies, its water surface elevation is highly affected by wind speed, direction and duration. Constant winds in a particular direction often result in wind set-up over the lake. Due to this phenomenon, it is not uncommon for there to be an elevation difference of over a metre between the north and south shore of the lake. CRISP2D does not have the capacity to deal with this phenomenon directly. Thus, it is important that the gauge be located close enough to the model boundary to incorporate these effects. Furthermore, wind set-up and set down often result in backflow through the river channels. Thus, it was critical that the outlet boundaries also allow flow to return to the model.

Boundary data at Gauge 2 was only available between June 16, 2010 and October 16, 2010. Thus, outflow boundary data was not directly available for any winter freeze-up season. To remedy this, an empirical relationship between the water surface elevation at Gauge 2 and Water Survey of Canada Gauge 05SB006 (Lake Winnipeg at Gimli) was developed:

$$E_2 = 1.0997E_G - 21.7677 \quad (5.1)$$

where  $E_2$  is the water surface elevation at Gauge 2 [m] and  $E_G$  is the water surface elevation at Water Survey of Canada Gauge 05SB006 [m], located at Gimli, Manitoba. Using this relationship, the boundary data for the model outflow could be extrapolated into the winter season since Gauge 05SB006 is operated year round.

Similarly, the discharge data at Devils Creek was only measured for a two week period in the summer of 2010. In order to obtain data for the entire calibration, verification, and winter freeze-up time frames, the existing data needed to be extrapolated. The magnitude of the discharge that enters or exits the Red River via Devils Creek is largely governed by water levels in the Netley-Libau Marsh, which are in turn governed by the water level of Lake Winnipeg. As a result, it was found that an empirical relationship to calculate flow at Devils Creek could be developed using data from Gauge 05SB006:

$$Q_D = -71.5642X_1 - 83.0538X_2 - 251.396X_3 - 177.180X_4 - 28.2553 \quad (5.2)$$

where, at each time step,  $Q_D$  is the flow from Devils Creek [cms],  $X_1$  is the change in water surface elevation at Gauge 05SB006 over the following 5 hours [m],  $X_2$  is the change in water surface elevation at Gauge 05SB006 over the previous 5 hours [m],  $X_3$  is the change in water surface elevation at Gauge 05SB006 over the following 3 hours, lagged 5 hours [m], and  $X_4$  is the change in water surface elevation at Gauge 05SB006

over the previous 5 hours, lagged 3 hours [m]. The previously described variables were chosen based on a detailed stepwise regression analysis.  $Q_D$  can be either negative or positive to represent inflows and outflows, respectively.

The dynamic ice module of CRISP2D requires an additional water temperature boundary condition to be specified. Since no continuous water temperature data was available within the study area, this boundary was established at the upstream extent of the model and was assumed to be constant at 0.01°C during the freeze-up period. This value is consistent with several point measurements taken in the field during the 2011-2012 winter season.

### **5.3 INITIAL CONDITIONS**

At the beginning of a new hydrodynamic simulation, CRISP2D sets a constant water surface elevation throughout the entire model domain. As such, hot-start files for each simulation were generated, where the model was allowed to reach steady-state using inlet discharge and outlet water surface elevations corresponding to the first hour of each simulation. This allowed an appropriate water surface profile to be generated, as well as appropriate velocity and depth values at each node to be calculated and input as the initial conditions of the model. Utilizing a hot-start file greatly improved the model's accuracy and stability, particularly in the beginning of the simulation.

---

**6.1 HYDRODYNAMIC CALIBRATION**

The time period chosen for hydrodynamic calibration was June 24, 2010 to August 3, 2010. This period was chosen due to data availability and because it was deemed representative of the large fluctuations that can occur in the water surface elevation of Lake Winnipeg. The range in measured water surface elevation at Gauge 2 during this period was 217.6 m to 218.5 m, including many peaks and troughs to test the model's ability to simulate relatively rapid changes in water surface elevation. There were three primary objectives during the hydrodynamic calibration of this model: preserving continuity throughout the model, obtaining simulated water surface profiles matching those measured during the field program, and correctly approximating the proportion of flow that discharges through Netley Cut and each of the branches of the Red River.

The choice of element size was found to significantly affect the model's ability to preserve continuity within its domain. Large continuity errors were found to be associated with having an insufficient number of elements across any channel, and led to falsely high steady-state water surface profiles during the hot-start simulations. A mesh sensitivity analysis with various numbers of elements was completed to determine the optimum number of elements across any given channel. A summary of this analysis is given in Table 6.1. As shown in Table 6.1, there is a clear threshold where accuracy is severely compromised by lowering the computational time, namely, five elements. Little accuracy advantage was gained by using more than six elements across the channels, however, the computational time increases significantly. As a result of this analysis, the mesh was finalized with 6 elements across each channel. This proved to be an optimal balance of computational time and continuity error.

**Table 6.1: Mesh sensitivity analysis.**

<b>Number of Elements Across Channel</b>	<b>Real Time Required to Simulate 1 Hour (min)</b>	<b>Approximate Steady-State Continuity Error (%)</b>
5	2.0	21%
6	3.0	1.5%
7	5.3	1.1%
8	7.5	0.9%

The second objective of the hydrodynamic calibration was to attempt to duplicate the measurements taken in the field program, namely the water surface elevations at various gauges throughout the model domain and the flow split proportions. In the model, discharge, and ultimately water surface elevation, can be controlled by adjusting the Manning's roughness coefficients in different portions of the mesh. The mesh was divided into nine distinct reaches (shown in Figure 6.1) so that the properties of each section of the model could be adjusted independently of the others. Typically, the reaches were chosen such that the beginning and end coincided with a calibration gauge (shown in Figure 6.1). To obtain the correct water surface profile, the roughness coefficient of each reach was adjusted iteratively from downstream to upstream until the simulated and measured water surface profiles at the various calibration gauges were in good agreement. The final values for Manning's  $n$  are shown in Table 6.2, ranging between 0.018 and 0.025 in the channels and 0.055 in Netley Lake.

**Table 6.2: Manning's  $n$  values for different reaches.**

<b>Reach</b>	<b>Manning's <math>n</math></b>
1: Netley Lake Outlet	0.055
2: West Channel	0.025
3: Main Channel	0.025
4: East Channel	0.025
5: Main-East Interconnecting Channel	0.025
6: Netley Lake	0.055
7: Red River between Devils Creek and Flow Split	0.025
8: Red River between Netley Creek and Flow Split	0.025
9: Red River between Breezy Point and Netley Creek	0.025
10: Red River between Selkirk and Breezy Point	0.018

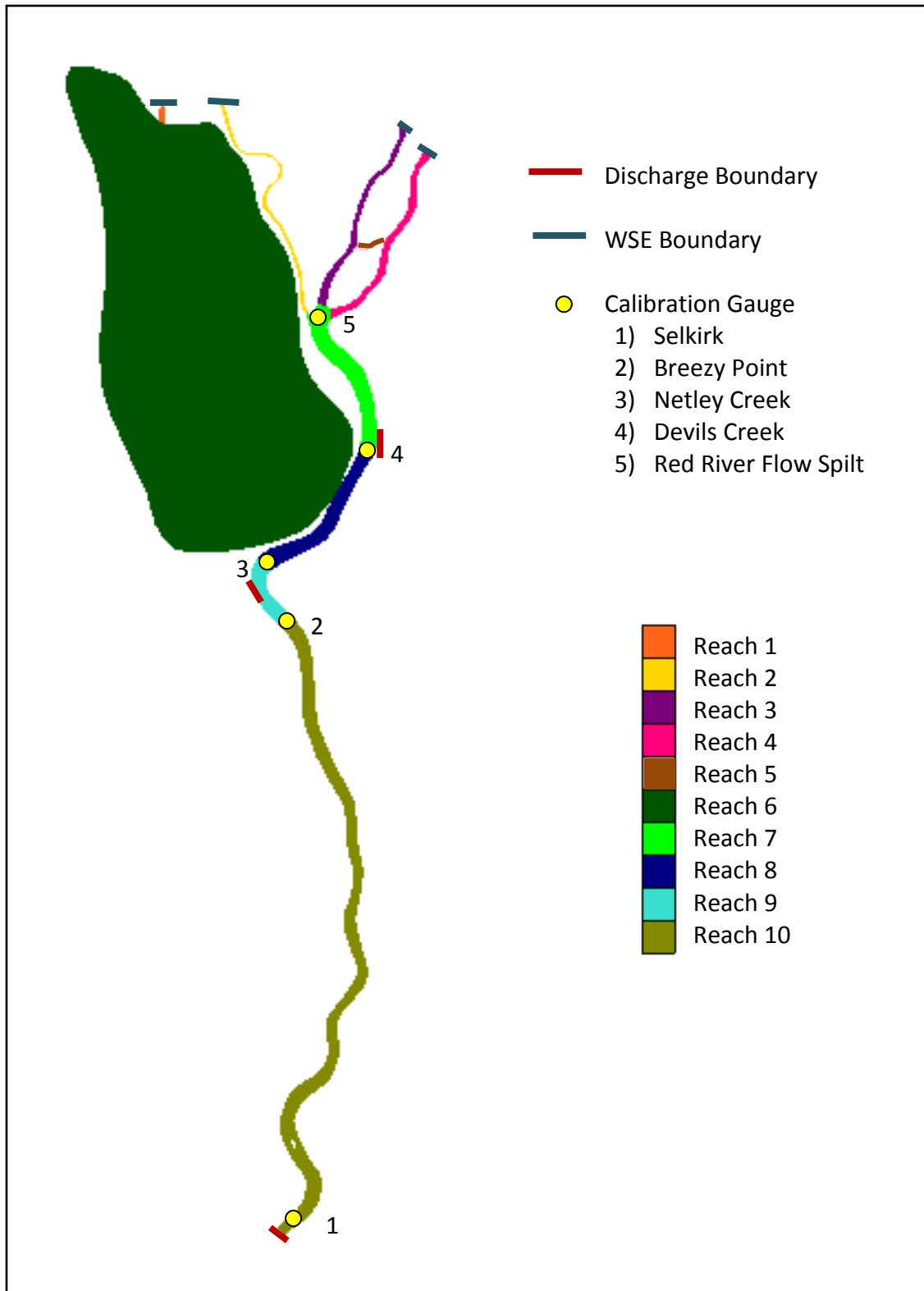


Figure 6.1: Reach boundaries and locations of calibration gauges.

The roughness coefficient for reach 9 (between Selkirk and Breezy Point) is noticeably lower than those of the other reaches within the model domain. Higher roughness coefficients caused the model to consistently overestimate the measured water surface elevations at the Selkirk gauge. This can likely be attributed to the age and uncertainty of the model bathymetry within this reach. As a result, in addition to substantially lowering the roughness coefficient, the bathymetry within the reach had to be altered minimally in order to achieve acceptable calibration results. This alteration consisted of widening the channel by 5-10 m on each river bank (approximately 5% increase in width), a change which has likely occurred naturally over the past 50 years through erosion or bank failure. Ultimately, the alteration of the geometry within this reach resulted in a minimal change in water velocity. Consequently, the alteration will produce little effect on the formation of ice within the reach, which is the primary interest of this study.

Comparisons between simulated and measured water surface elevations are shown in Figures 6.2-6.6. From these figures it is evident that the model is able to accurately simulate the water surface elevations at each of the five calibration gauges, usually within several centimetres. The maximum difference between the measured and simulated values is less than 15 cm. This is deemed acceptable, considering the level of uncertainty associated with all measured data. Additionally, the model is capable of capturing both the peaks and troughs in the measured data in both magnitude and timing.



It is evident from the calibration figures that model performance at a particular station is directly correlated to its proximity to the downstream water surface elevation boundary condition. The downstream boundary condition largely drives the water level in the entire model. As a result, as stations move further away from this dominant boundary condition, the simulations become increasingly inaccurate.

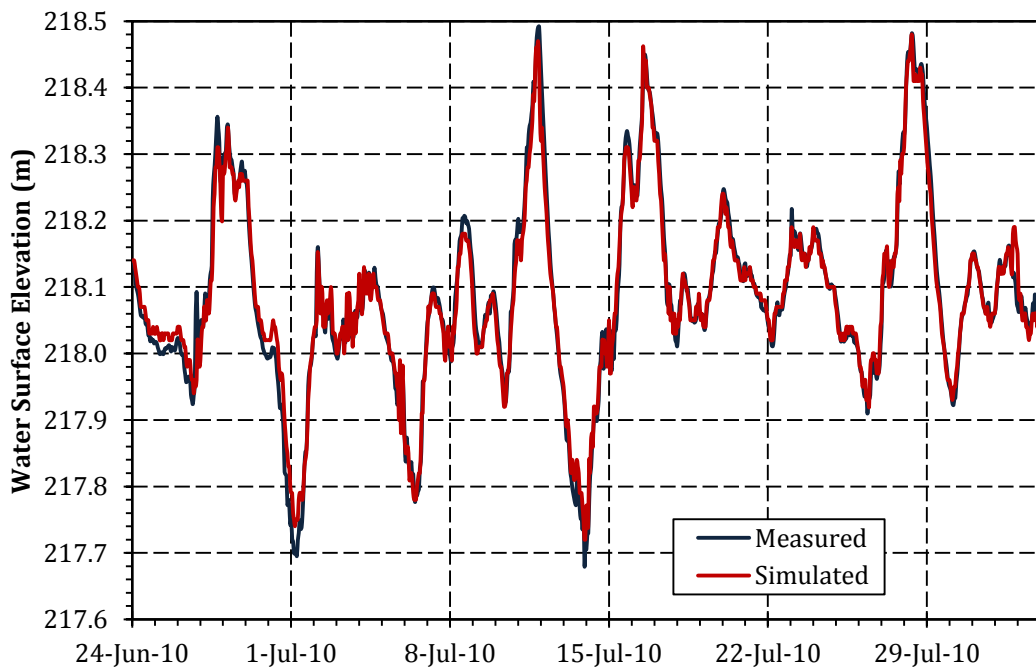


**Figure 6.2: Hydrodynamic calibration at Red River flow split.**

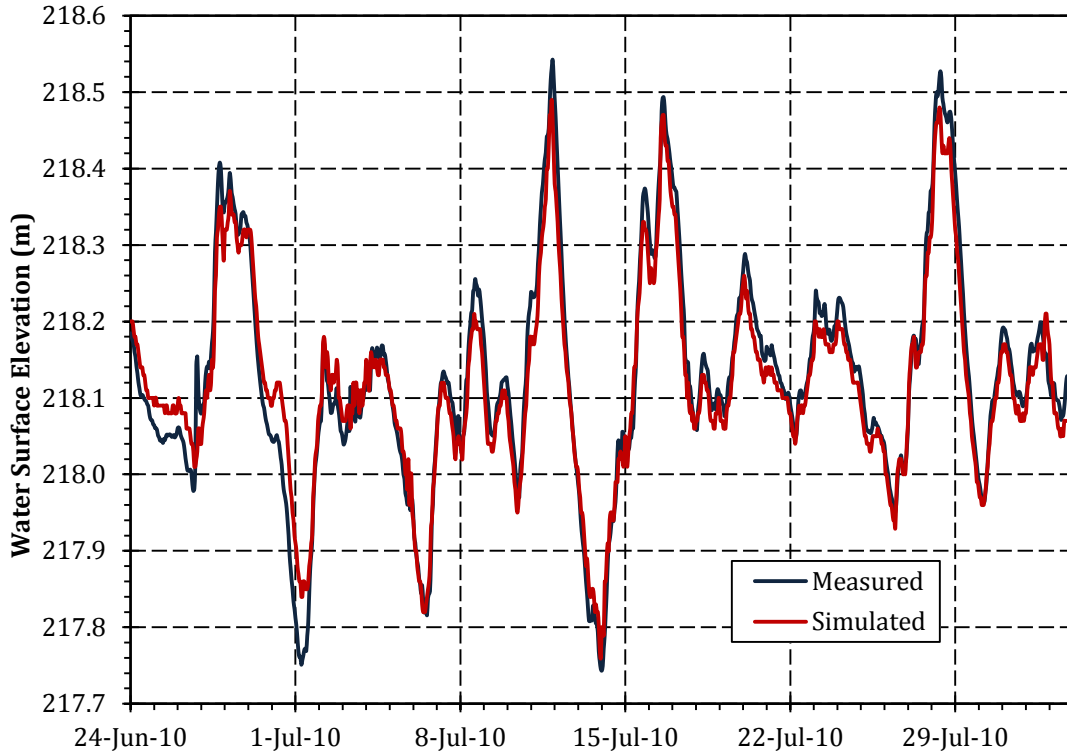


Figure 6.3: Hydrodynamic calibration at Devils Creek.

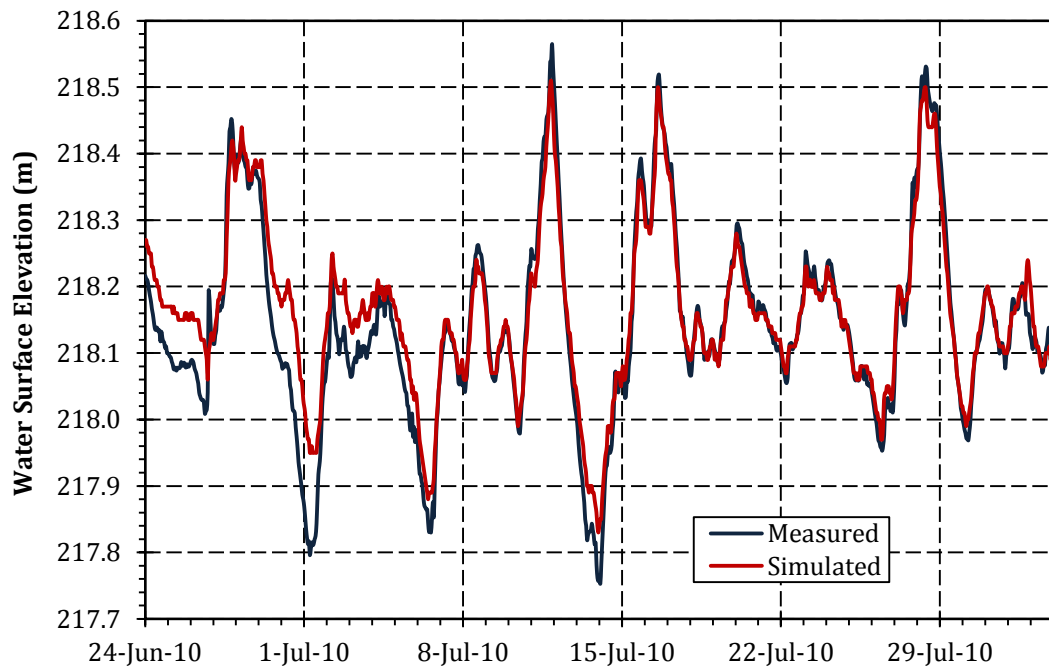


Figure 6.4: Hydrodynamic calibration at Netley Creek.

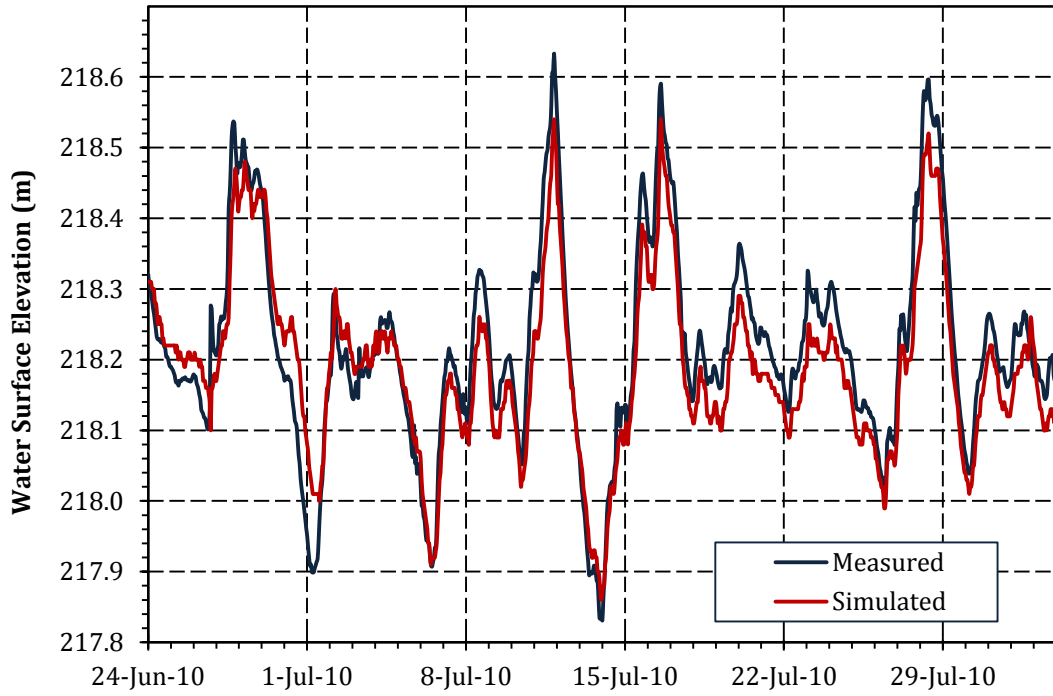


Figure 6.5: Hydrodynamic Calibration at Breezy Point

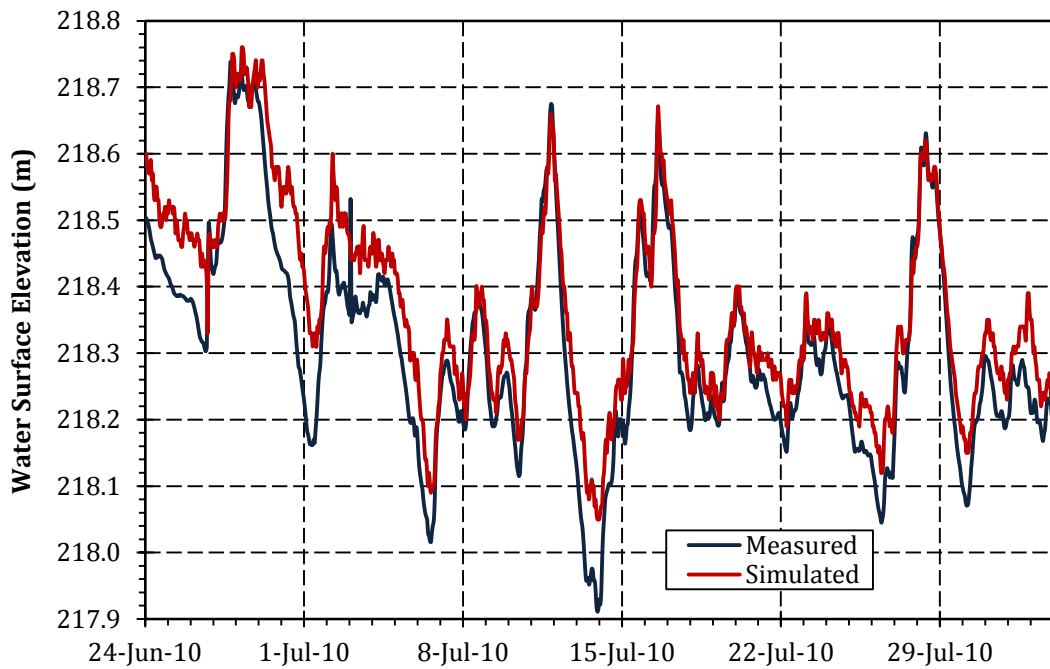


Figure 6.6: Hydrodynamic calibration at Selkirk.

Once the roughness coefficients were set, the model was subsequently used to verify that the proportion of the flow discharging through Netley Cut and each of the three branches of the Red River reflect the measurements taken in the field. In order to compare the simulated flows to the measured ones, the percentage of the total flow discharging through Netley Cut, the East Channel, the Main Channel, and the West Channel was averaged over every time step within the calibration. The average flow proportions from the model were compared to the average flow proportions that were measured in the 2009 open water season. The results of this comparison are reported in Table 6.3, showing very good agreement between the measured and simulated proportions, with a maximum difference of 5.4%.

**Table 6.3: Comparison of simulated and measured flow split for hydrodynamic calibration.**

<b>Location</b>	<b>Measured Flow Proportion (%)</b>	<b>Simulated Flow Proportion (%)</b>
Red River upstream of Netley Cut	100	100
Netley Cut	37.1	31.7
Red River West Channel	0.7	1.5
Red River Main Channel	27.4	28.5
Red River East Channel	28.3	29.5
Error	6.5	8.8

## 6.2 HYDRODYNAMIC VERIFICATION

In order to verify that the model parameters chosen during the calibration phase were adequate, a hydrodynamic verification was performed using the roughness coefficients selected during the calibration phase. A similar procedure was followed as in the calibration, using the same types of boundary conditions and hot-starting the simulation with the appropriate values for the beginning of the simulation. The verification simulation was run between August 5, 2010 and September 12, 2011. Again, this time period was chosen to ensure that the model could sufficiently simulate the peaks and troughs in water surface elevation that are characteristic of the study area. The same five calibration gauges were used and the simulated and measured water surface elevations at each of these gauges are compared in Figures 6.7-6.11.

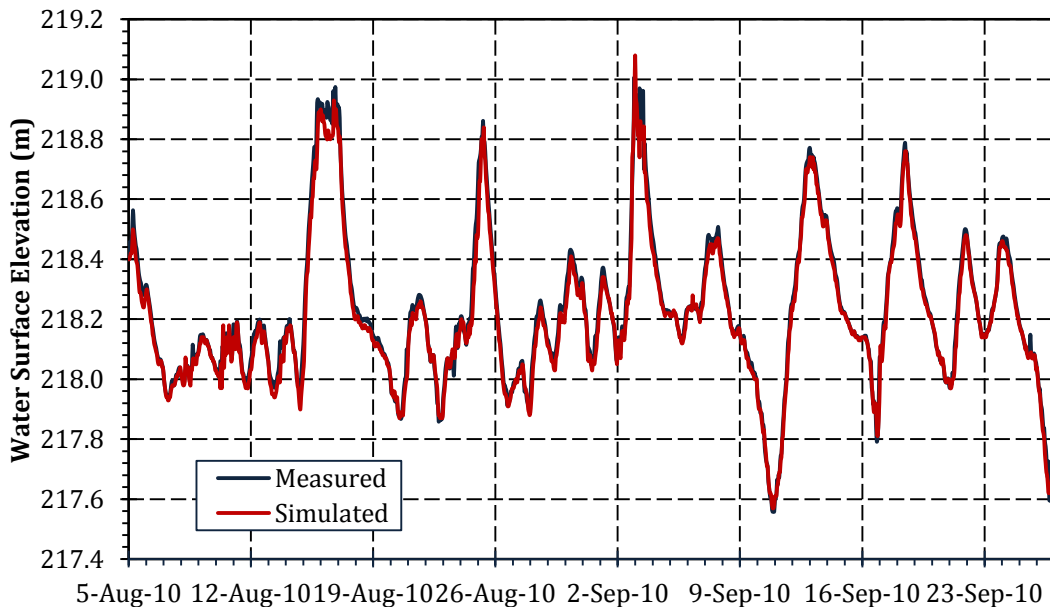


**Figure 6.7: Hydrodynamic verification at Red River flow split.**

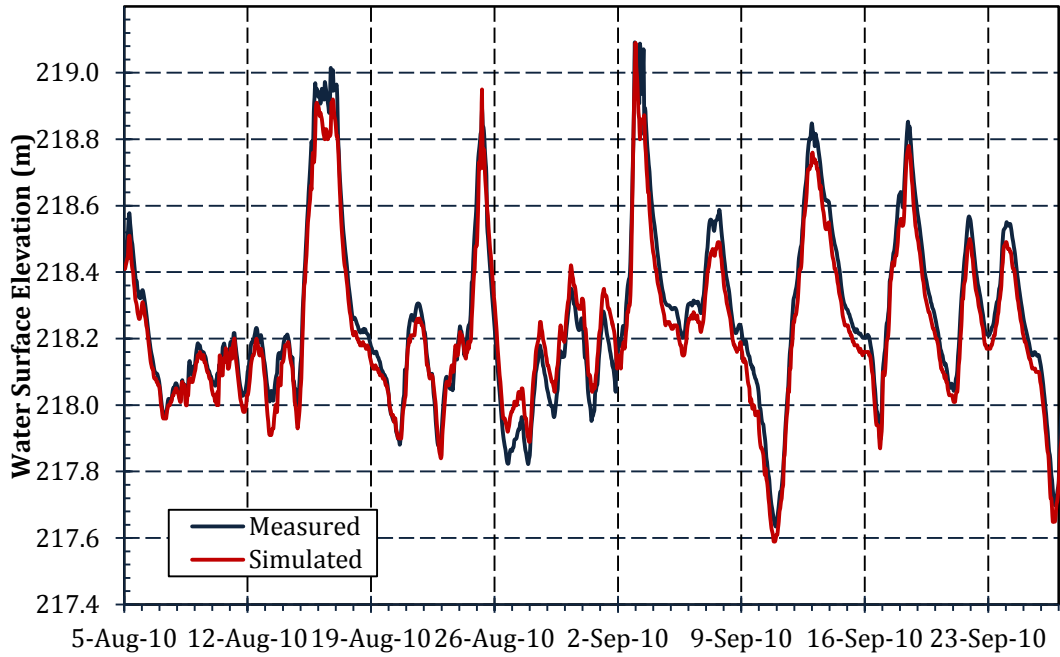


Figure 6.8: Hydrodynamic verification at Devils Creek.

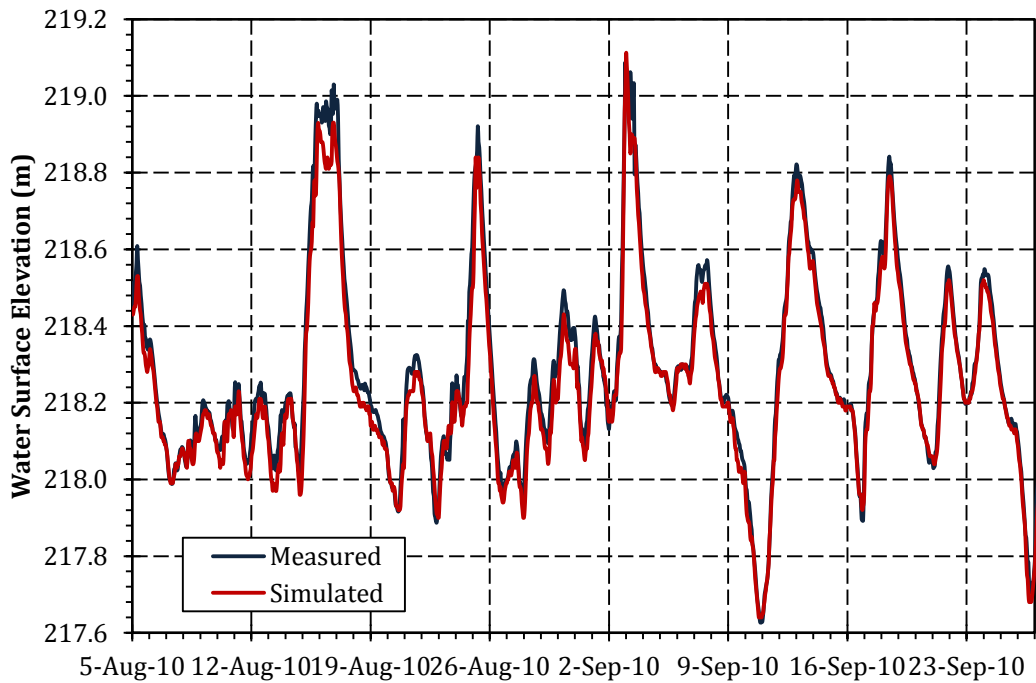


Figure 6.9: Hydrodynamic verification at Netley Creek.

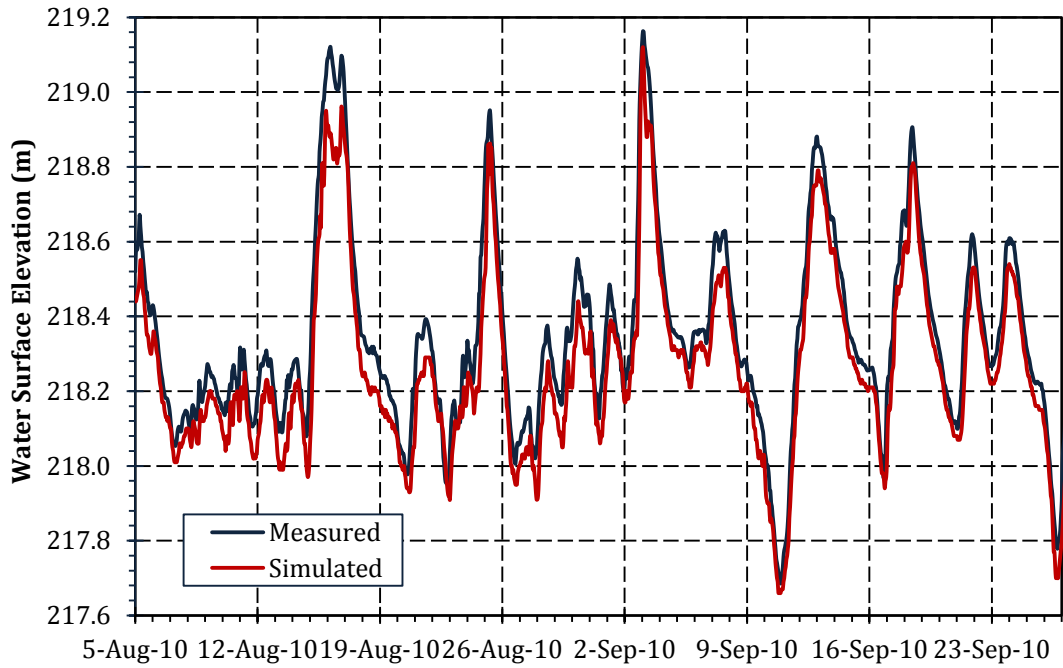


Figure 6.10: Hydrodynamic verification at Breezy Point.

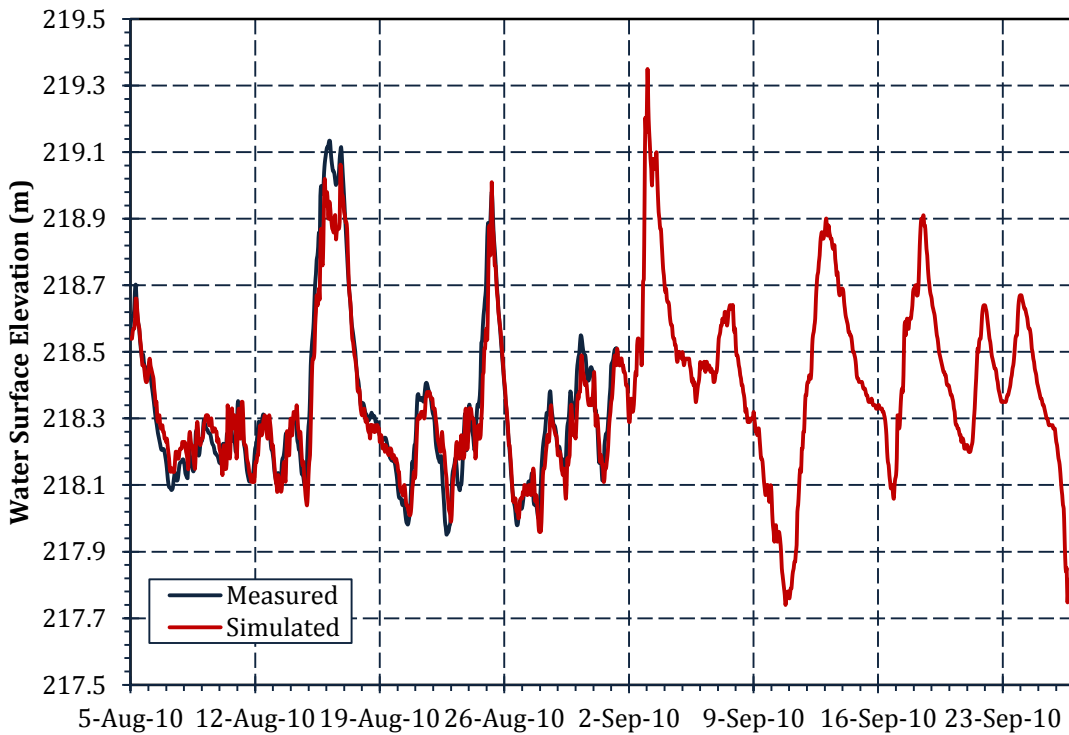


Figure 6.11: Hydrodynamic verification at Selkirk.

The above figures indicate that the model performed very well during the verification simulation. Similarly to the calibration run, the model is able to match the measured data within several centimetres as well as capture the magnitude and timing of the rapid changes in water surface elevations in the measured data. The flow proportions were also compared for the verification simulation. The results of this analysis, shown in Table 6.4, indicate that there is very good agreement between the measured and simulated flow splits, with a maximum error of 1.9%.

**Table 6.4: Comparison of simulated and measured flow split for hydrodynamic verification.**

<b>Location</b>	<b>Measured Flow Proportion (%)</b>	<b>Simulated Flow Proportion (%)</b>
Red River upstream of Netley Cut	100	100
Netley Cut	37.1	39.0
Red River West Channel	0.7	0.5
Red River Main Channel	27.4	27.0
Red River East Channel	28.3	29.7
Error	6.5	3.8

Overall, the results of the verification simulation were deemed more than adequate, indicating that the roughness coefficients chosen during the calibration phase are appropriate for this model. As a result, the calibrated hydrodynamic model will be used as an input for the dynamic ice model.



---

**7.1 INTRODUCTION**

Upon successful calibration of the hydrodynamic model, the thermodynamic and ice dynamic modules of CRISSP2D were used to simulate the thermodynamics and freeze-up process on the Red River near the Netley-Libau Marsh over three winter seasons. CRISSP2D has the capability to simulate a variety of ice processes, including skim ice runs, dynamic and static border ice growth, water supercooling, and frazil ice production. Although each of these ice processes has been observed within the study area, the main focus of this research was calibrating a model that could predict the thickness of the ice cover over the winter. This type of model would be most beneficial to Manitoba Water Stewardship as ice cover thickness is an important parameter used in determining the spatial extents of their ice jam mitigation program.

## **7.2 CALIBRATION OF WATER-AIR HEAT TRANSFER COEFFICIENT**

Prior to the calibration of the dynamic ice model, it was necessary to determine the heat transfer coefficient between the water and the air so that the model was able to accurately simulate water temperature prior to freeze-up. This will aid with both determining the correct processes that occur at freeze-up as well as simulating the onset of freeze-up at the appropriate time.

In order to calibrate the water-air heat transfer coefficient, water temperature data was collected at several locations throughout the study area, including Selkirk, Devils Creek, and the Red River flow split immediately prior to the onset of the 2011 freeze-up. The thermodynamic module of CRISSP2D was used to model the cooling of the water as winter approached. Upstream and downstream hydrodynamic boundary conditions similar to those described in Section 5.2 were used to force the model. In addition, the measured water temperature at Selkirk was input into the model as a boundary condition to force the thermodynamic conditions at the upstream end.

The thermodynamic module also requires the input of certain meteorologic parameters, particularly air temperature, to use in the model's governing heat transfer equations. This data was obtained from Environment Canada's weather station at the Winnipeg airport. After creating appropriate hydrodynamic hot-start files, (discussed in Section 5.3) the initial thermodynamic conditions were set. The water temperatures of each node were set to correspond with the first water temperature value in the upstream

temperature boundary time series. The model was simulated between September 16, 2011 and November 8, 2011 with the objective of choosing a heat transfer coefficient that would allow the model to simulate the measured water temperatures at Devils Creek and the Red River flow split. In order to meet this objective, a sensitivity analysis was performed on the water-air heat transfer coefficient,  $h_{wa}$ . The model was tested using several values of  $h_{wa}$  within the accepted range of 10 to 30  $W/m^2\text{°C}$ . Model results at both Devils Creek and the Red River flow split are shown in Figure 7.1 and Figure 7.2.

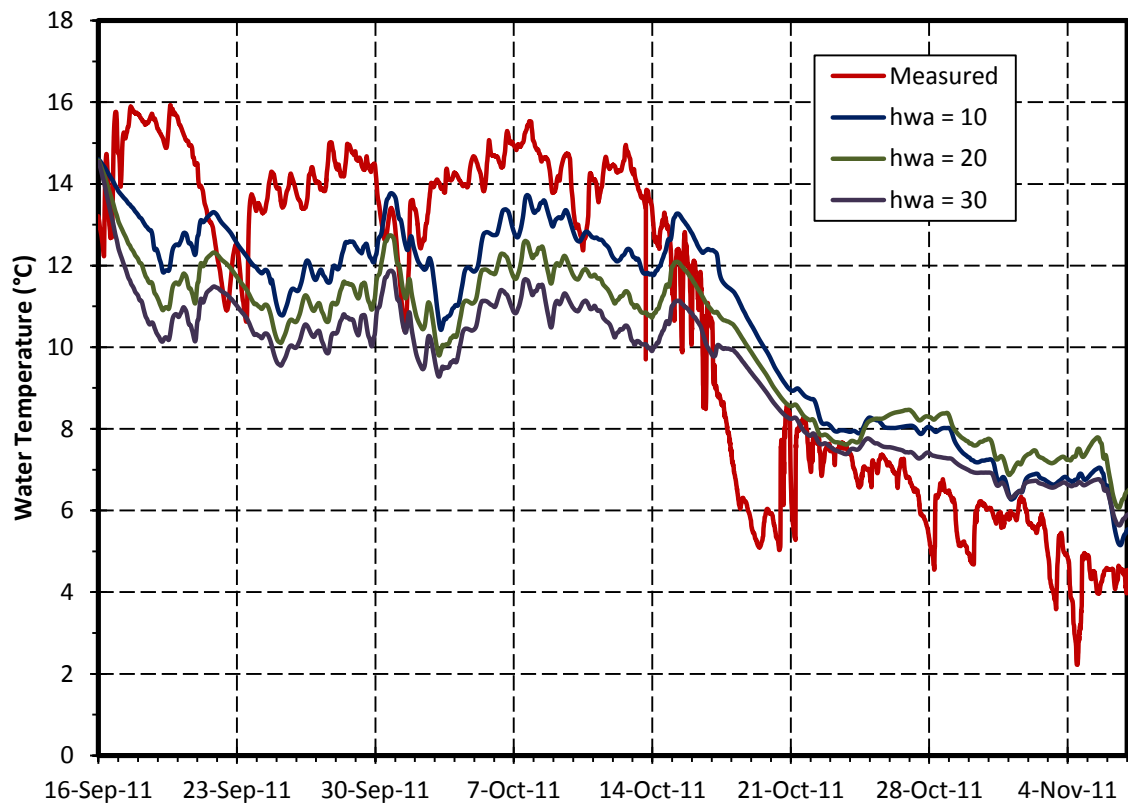


**Figure 7.1: Thermodynamic calibration of the water-air heat transfer coefficient at Devils Creek.**

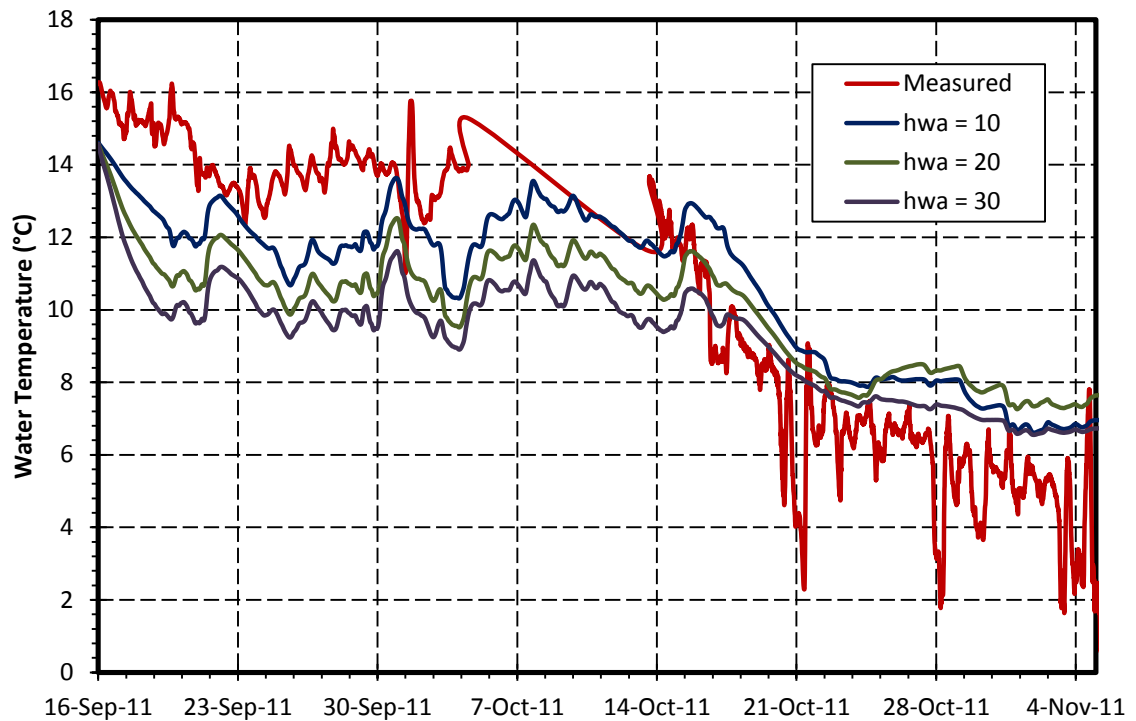


**Figure 7.2: Thermodynamic calibration of water-air heat transfer coefficient at Red River flow split.**

Although these figures indicate that the model is unable to accurately match the measured downstream water temperatures, it is able to follow the general cooling trends of the water between September 16, 2011 and November 8, 2011. At the end of the simulation, the simulated water temperature was within approximately 2°C of the measured data and for the purposes of this research, this was deemed acceptable. In addition, the model was able to simulate upward and downward temperature trends contained within the measured data, but not always at the correct magnitude or exactly the right time.

The accuracy of the model is likely limited by the fact that there are several heat sources and sinks that are not accounted for within the model. The water temperature downstream, particularly at Devils Creeks, is influenced by flows from smaller tributaries and lakes in the Netley-Libau marsh area. For simplicity, these flows were excluded from the model (including Devils Creek itself) but would have the ability to noticeably warm or cool the water within their vicinities.

The meteorological data was an important input to force the governing heat transfer equations. However, wind speed and direction are not accounted for within the model and is an important heat flux in the physical world. In addition, the air temperatures used to force the model were measured in Winnipeg, a considerable distance from the study area, particularly the downstream end.

In order to determine the value of  $h_{wa}$  that best represents the measured data, the root mean square error was calculated for each value of  $h_{wa}$  at both Devils Creek and the Red River flow split and averaged over the two locations. From this analysis it was determined that setting  $h_{wa} = 20 \text{ W/m}^2\text{°C}$  in the model produces results that best match the measured data at both Devils Creek and the Red River flow split. As a result, it was chosen as an appropriate value for the air-water heat transfer coefficient to use in the dynamic ice model calibration.

### **7.3 DYNAMIC ICE MODEL CALIBRATION**

As previously mentioned, the main purpose of this research is to aid Manitoba Water Stewardship with their ice jamming and flood mitigation strategies. Currently, the Province has a three step plan that is typically followed each winter season. First, ice thickness on the Red River is measured either manually or via ground penetrating radar (GPR) surveys. Once the survey is complete, Bobcats mounted with large circular saws, known as Wolverines (shown in Figure 7.3), are dispatched to the portions of the river that have been identified as potential problem areas. These are typically areas where the ice thickness exceeds approximately 50 cm. The Wolverines score the ice with the saws, but do not cut all of the way through, as this would cause water to leak through and freeze, resealing the cut. The final step is to deploy the Amphibex ice breakers. These units are large excavators that may operate on both land and water (shown in Figure 7.4) and are used to break up the ice sheets already weakened by the Wolverines before natural break up occurs. This process is typically carried out between Netley Cut and Selkirk.

To complement the ice jamming mitigation strategies that are already in place, it would be beneficial for Manitoba Water Stewardship to be able to utilize a computer model that is capable of simulating ice thickness within the river over the winter season, in order to minimize manual measurements and costly GPR surveys. Thus, while there were many aspects of ice dynamics that were considered during the calibration of the

dynamic ice model, the primary focus of the calibration was to obtain a model that is able to accurately predict ice growth with time in the Red River.



**Figure 7.3: The Wolverine used to pre-cut ice covers prior to natural break-up.**



**Figure 7.4: Amphibex ice breaker unit.**

The dynamic ice model was calibrated to the 2009-2010 winter season. The calibration data primarily consisted of ice thickness measurements taken periodically throughout the winter at several locations along the Red River. Various other measurements were collected during the season, including under ice discharge and velocity measurements, and snow thickness measurements. Furthermore, data required to calibrate the model's ability to simulate frazil ice formation including, water temperature and ice concentration, was not collected, causing the calibration of any frazil ice or supercooling parameters to be unfeasible.

### **7.3.1 BOUNDARY CONDITIONS**

The dynamic ice model had similar boundary conditions to the hydrodynamic and thermodynamic models. At the downstream extent of the model, a water surface elevation boundary condition was used to force the model at each of the four outlets. Hourly water level data from Water Survey of Canada gauge 05SB006 (Lake Winnipeg at Gimli) was transformed using Equation 5.1 to achieve an accurate representation of the water surface elevation at the outlets throughout the winter.

At the upstream extent of the model domain, two boundary conditions were required: a discharge boundary condition and a water temperature boundary condition. The discharge boundary condition data was obtained from the hourly flow data at Water Survey of Canada gauge 05OJ005 (Red River at Selkirk). The combined flow contribution of Netley Creek and Devils Creek, which could carry considerable flow during the



summer months, was typically less than 10 cms through the winter season. As a result, the flow contribution from these tributaries was assumed to be negligible over the winter and they were excluded from the dynamic ice model. Since no water temperature data was available, the water temperature boundary at Selkirk was assumed to remain constant throughout the winter at 0.01°C, a number which is consistent with measurements taken in subsequent winter seasons.

### **7.3.2 INITIAL CONDITIONS**

Hot-start simulations were required to set both appropriate hydrodynamic and thermodynamic initial conditions. First, the hydrodynamic module of CRISSP2D was used to set the initial water surface profile, water velocities, and depths to the conditions that match the first time step of the calibration simulation. Second, the thermodynamic module of CRISSP2D was used to set an appropriate water temperature gradient throughout the model domain. To set this gradient, the air temperature was set to correspond with that of the first hour of the simulation and the incoming water temperature at Selkirk was set to a constant 0.01°C. The model was run until steady-state thermodynamic conditions had been reached.

The initial thermodynamic conditions had the ability to significantly influence both the time of freeze-up and the types of freeze-up processes that took place. Several different initial thermodynamic conditions were tested and model results varied considerably depending on the initial conditions chosen. These conditions varied between ramping

the incoming water temperature down, starting with different initial water temperatures within the model, and varying the incoming temperature boundary between 0.01°C and 0.1°C.

In particular, the initial water temperature conditions largely dictated whether or not frazil ice would form within the reach. For simplicity, it was assumed that freeze-up would occur thermally in the calibration simulations, absent of any frazil ice growth, despite field observations that indicated otherwise. This is attributed to the fact that without accurate water temperature and frazil concentration data, accurately simulating the formation of frazil ice in such large model domain would not be feasible. As a result, initial thermodynamic conditions were estimated such that no frazil ice could form.

### **7.3.3 INITIAL FREEZE-UP PERIOD**

Although no detailed observations of the initial freeze-up period of the 2009-2010 season were made, it was noted that river began to freeze over near December 1, 2009. Thus the dynamic ice simulations were started on November 28, 2009 in order to capture the entire freeze-up period. Overall, the model did a fair job of predicting the onset of freeze-up, simulating the onset of lake ice growth on November 29, 2009 and river ice becoming present on November 30, 2009. However the timing of the formation of ice in the model is largely dependent on the initial water temperature conditions throughout the model, which had to be roughly assumed. The collection of water

temperature measurements throughout the model would be necessary to properly assess the model's performance in this area.

The freeze-up processes within the model domain are fairly consistent from year to year, but can vary based on water temperature and meteorological conditions. Typically, the less turbulent water in Netley Lake is the first to cool to the freezing point and form skim ice. Following this, skim ice and/or border ice begin to form along the banks of the river. As air temperatures continue to decrease, border ice will cover over the lake and start growing thermally downwards. The border ice on the river will eventually bridge and form a competent ice cover. Depending on the temperature conditions, frazil crystals or frazil pans may form if portions of the river are left open and the cool air is allowed to supercool the water.

The processes described above were able to be well approximated by the model. The ice cover type at several time steps during the initial freeze up is shown in Figure 7.5. Figure 7.5a shows that model begins the freeze-up process by covering Netley Lake in skim ice. Following this, border ice begins to grow around the edges of the lake and skim ice begin to form over the channels, as shown in Figure 7.5b. The border ice continues to grow over the lake until it is completely covered and it also begins to grow along the banks of the river, starting in the smaller branches in the downstream portion of the model (Figure 7.5c). As time continues, the border ice continues to grow in the channel and eventually bridging occurs and a competent ice cover is formed.

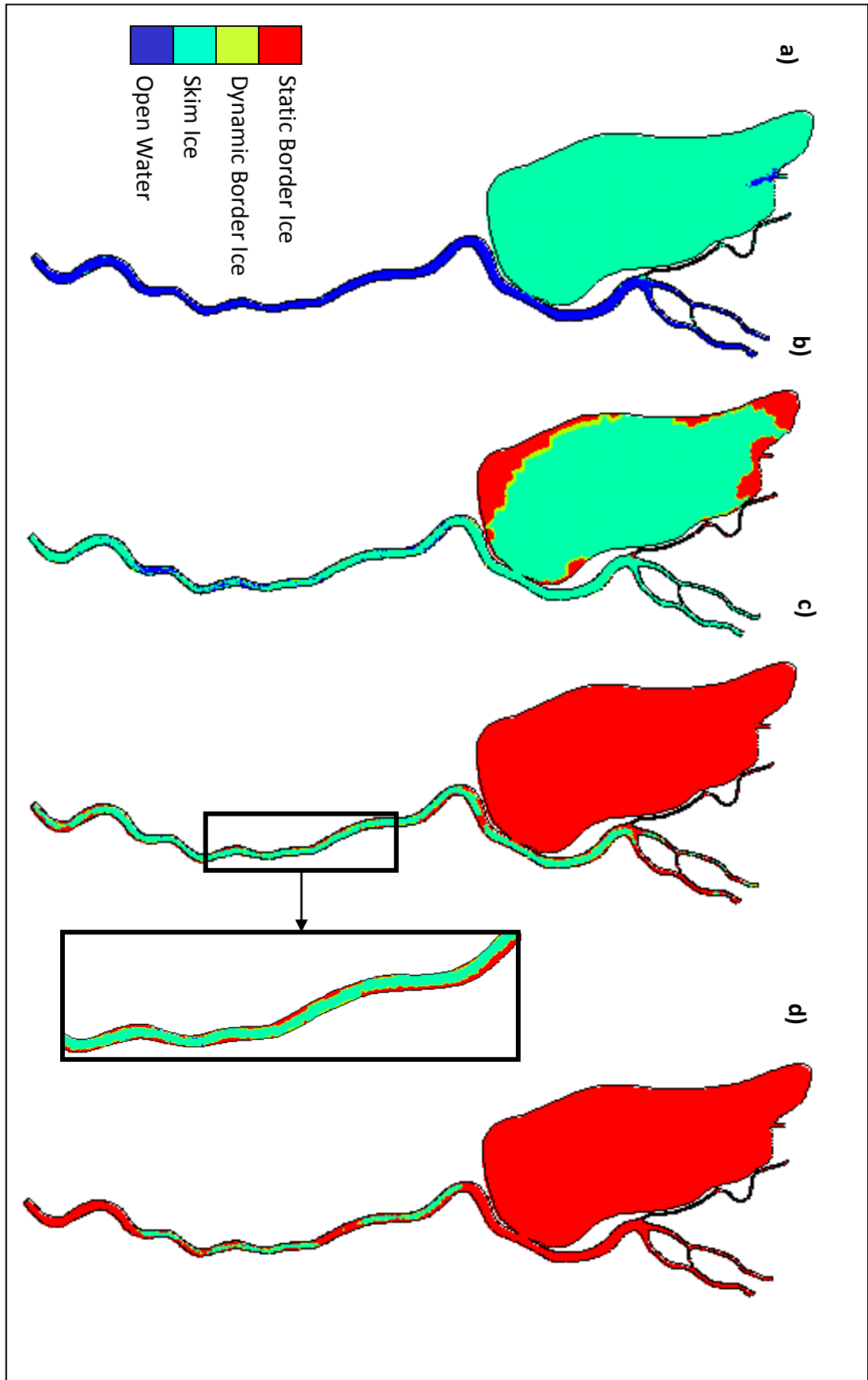


Figure 7.5: Simulated ice type during the initial freeze-up period of 2009 at a) hour 10, b) hour 20, c) hour 30, d) hour 40.

### 7.3.4 CALIBRATION OF ICE GROWTH

As previously mentioned, in addition to ensuring that the model simulated the appropriate ice processes during the initial freeze-up period, the model's ability to predict ice growth with time was the primary focus of this calibration. As such, the main calibration data that was taken were ice thickness measurements at representative locations throughout the model domain. These measurements were taken over width of the river and averaged to produce a single measurement for each cross section. The location of each cross section is shown in Figure 4.6

In CRISSP2D, the rate of ice growth within the model is largely governed by Equation 7.1

$$\frac{dh_i}{dt} = \frac{-\varphi_R + \alpha + \beta(T_m - T_a)}{\rho_i L \beta \left( \frac{h_i}{k_i} + \frac{1}{\beta} \right)} - \frac{h_{wi}}{\rho_i L} (T_w - T_m) \quad (7.1)$$

A sensitivity analysis was carried out on several of the variables directly included in or related to Equation 7.1, including several heat transfer coefficients and constants, the conductivity of the ice, and the density of the ice. This analysis determined that the heat transfer coefficient between the ice and air,  $\beta$ , had a significant effect on the rate of ice growth. Depending on the value of  $\beta$  chosen, simulated ice thickness could vary by over 1 m. The other variables did not have a significant effect on the rate of ice growth within their accepted range of values.

In order to calibrate the model using the air-ice heat transfer coefficient, the dynamic ice model was simulated for a range of  $\beta$  values between 1.5 W/m<sup>2</sup>°C and 4.5 W/m<sup>2</sup>°C. The model results are compared to the measured ice thickness data at Peguis Church and downstream of Netley Cut in Figures 7.6 and 7.7, respectively. Similar comparisons for all additional stations can be found in Appendix A in Figures A.1-A.3. These plots reveal that using this envelope of  $\beta$  values, the model is able to approximate ice growth over the winter quite well. An error analysis (shown in Table 7.1) was completed to determine the value of  $\beta$  that would minimize model error over all stations and provide the best representation of the measured data. The root mean square error (RMSE) was calculated at each station for every value of  $\beta$ . This analysis determined that using  $\beta = 2.5$  resulted in the best representation of all the collected data, having a maximum error of 10 cm, as shown in Figures 7.6, 7.7 and A.1-A.3.

**Table 7.1: RMSE analysis for dynamic ice calibration simulations.**

Location	$\beta = 1.5$	$\beta = 2.0$	$\beta = 2.5$	$\beta = 3.0$	$\beta = 3.5$	$\beta = 4.0$	$\beta = 4.5$
Upstream Peguis Church	0.130	0.134	0.083	0.120	0.160	0.196	0.228
Peguis Church	0.136	0.071	0.059	0.095	0.174	0.174	0.206
Breezy Point	0.097	0.034	0.063	0.115	0.200	0.200	0.233
Netley Cut	0.332	0.249	0.177	0.122	0.031	0.031	0.003
Downstream Netley Cut	0.200	0.117	0.044	0.015	0.109	0.109	0.144
Average RMSE	0.179	0.121	0.085	0.094	0.142	0.142	0.163

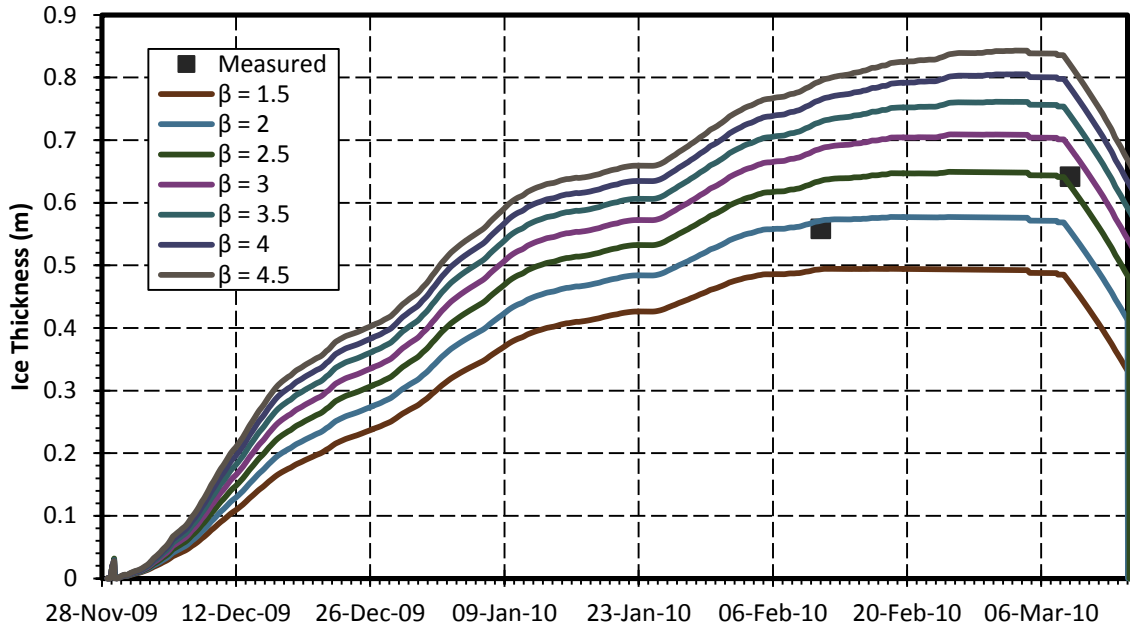


Figure 7.6: Calibration simulation at Peguis Church in winter 2009-2010.

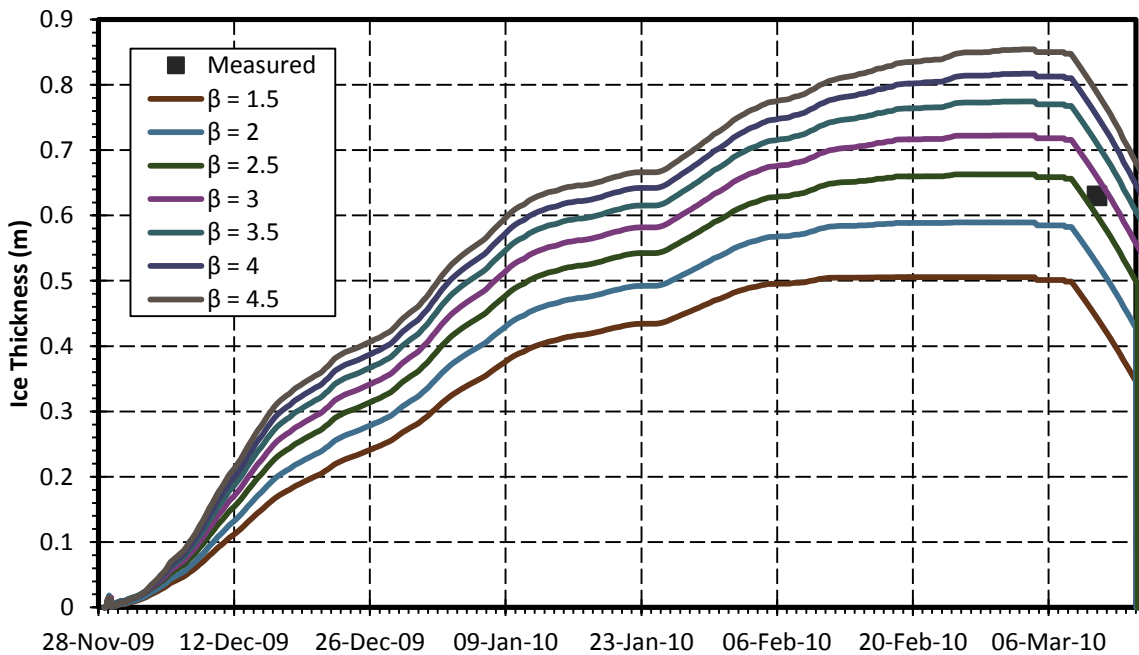


Figure 7.7: Calibration Simulation downstream of Netley Cut in winter 2009-2010.

### **7.3.5 DISCHARGE AND WATER SURFACE ELEVATION MEASUREMENTS**

In addition to the ice thickness data, other hydrodynamic properties of the dynamic ice model were monitored to ensure that the model was performing realistically. Between 2009 and 2012, under ice discharge measurements were taken throughout the study area to determine the proportion of the total flow that discharges through each branch of the Red River, as well as through Netley Cut, during the winter season. The measurements taken were distributed among the three winter seasons, but flow proportions were assumed to be relatively constant over all seasons. No measurements were made in the west branch of the Red River. However, due to the very low velocities in open water season and the very small cross sectional area of the channel, it was assumed that the channel carries no flow during the winter season. Furthermore, the proportion of flow discharging through the main channel was also not directly measured. Rather, it was calculated by summing the proportions passing through the Netley Cut and the east channel assuming the difference between that total and the total incoming flow was directed through the main channel.

The measurements described above were subsequently compared to the simulated flow proportions produced by the dynamic ice model and are shown in Table 7.2. This data indicates that there is good agreement between modeled and measured flow proportions throughout the model domain. Additionally, it is evident that, although the hydrodynamic properties of the model were primarily calibrated during the open water season, these properties are still valid once an ice cover has formed.



**Table 7.2: Comparison of modelled and measured discharge proportions for 2009-2010 winter season.**

Location	Measured (%)	Simulated (%)
Red River Upstream of Netley Cut	100	100
Netley Cut	15	19
East Channel	38	36
Main Channel	47	42
West Channel	≈0	1
Error	N/A	2

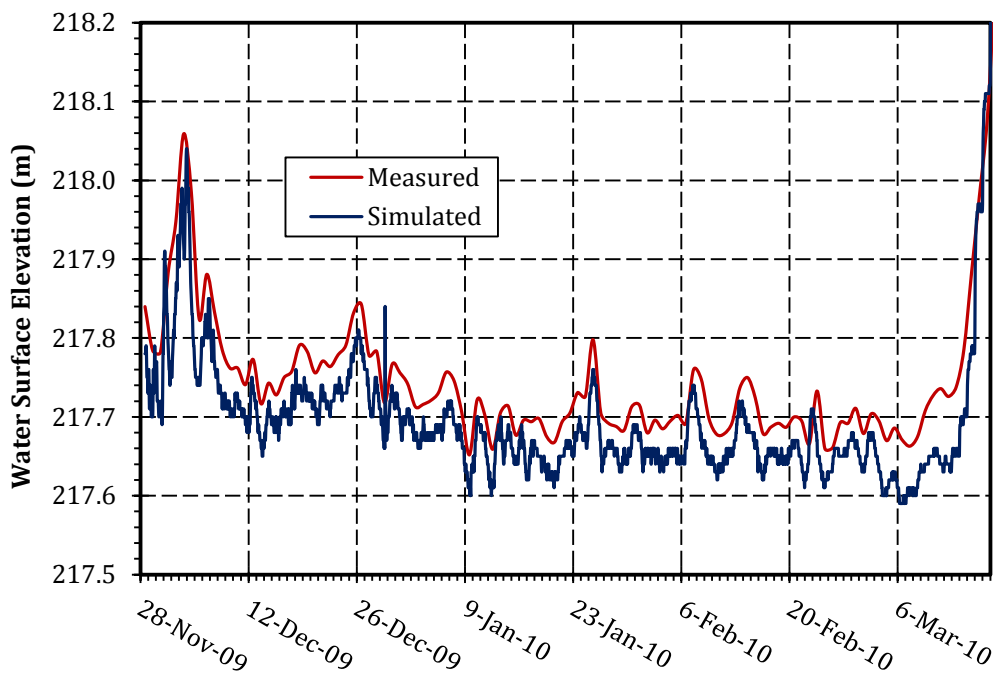


**Figure 7.8: Comparison of modelled and measured WSE at Selkirk in winter 2009-2010.**

To further verify that the hydrodynamic properties of the dynamic ice model were performing adequately, measured and simulated water surface elevations within the model were also compared. The only water level gauge available during this time period was located at Selkirk. A comparison between the modeled and measured water surface

elevation at this gauge is shown in Figure 7.8. From this figure it is evident that the model consistently underestimates the water level at Selkirk by approximately 5 cm. This small discrepancy can likely be attributed to bathymetry and measurement error, as discussed in Section 6.1. It is unlikely that this small discrepancy has any significant impact on ice formation within the model.

## **7.4 DYNAMIC ICE VERIFICATION**

Upon successful calibration of the dynamic ice model with the 2009-2010 winter season, data collected from the two subsequent winter seasons was used to verify that the parameters chosen for the model would yield an accurate representation for the following years.

### **7.4.1 2010-2011 WINTER SEASON**

Observations from the 2010-2011 winter season indicate that the onset of freeze-up occurred near November 18, 2010. This estimate is supported by observations made from a flight over the study area taken on November 20, 2010. Observations from this flight indicated that nearly all of the study area had covered in ice by this date, with very few open water spots along the upstream portion of the Red River channel. Simulated ice concentration predictions from the dynamic ice model during this time period are shown in Figure 7.9.

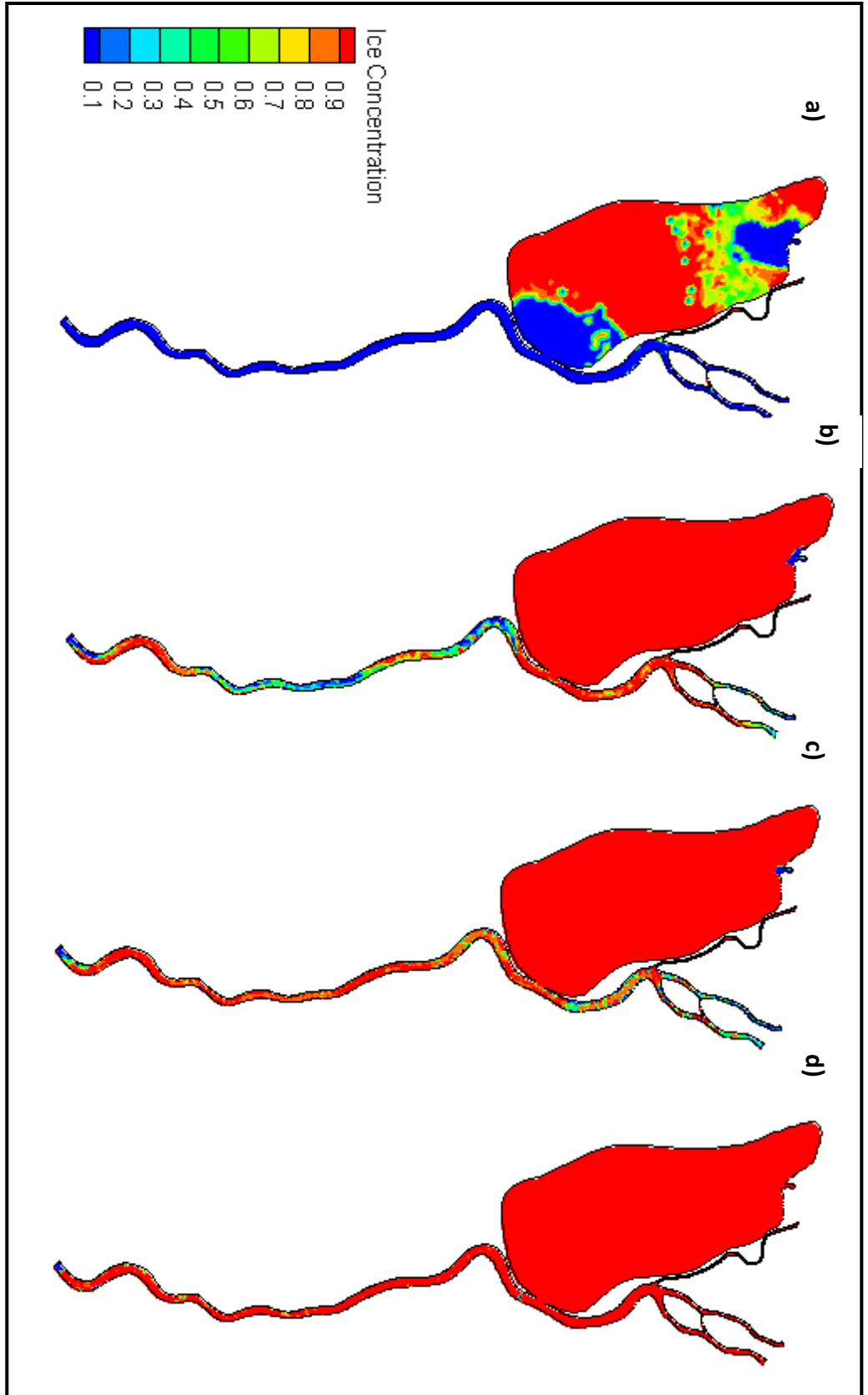


Figure 7.9: Ice concentration during freeze-up period, a) November 17, 2010 b) November 18, 2010 c) November 19, 2010 d) November 20, 2010.

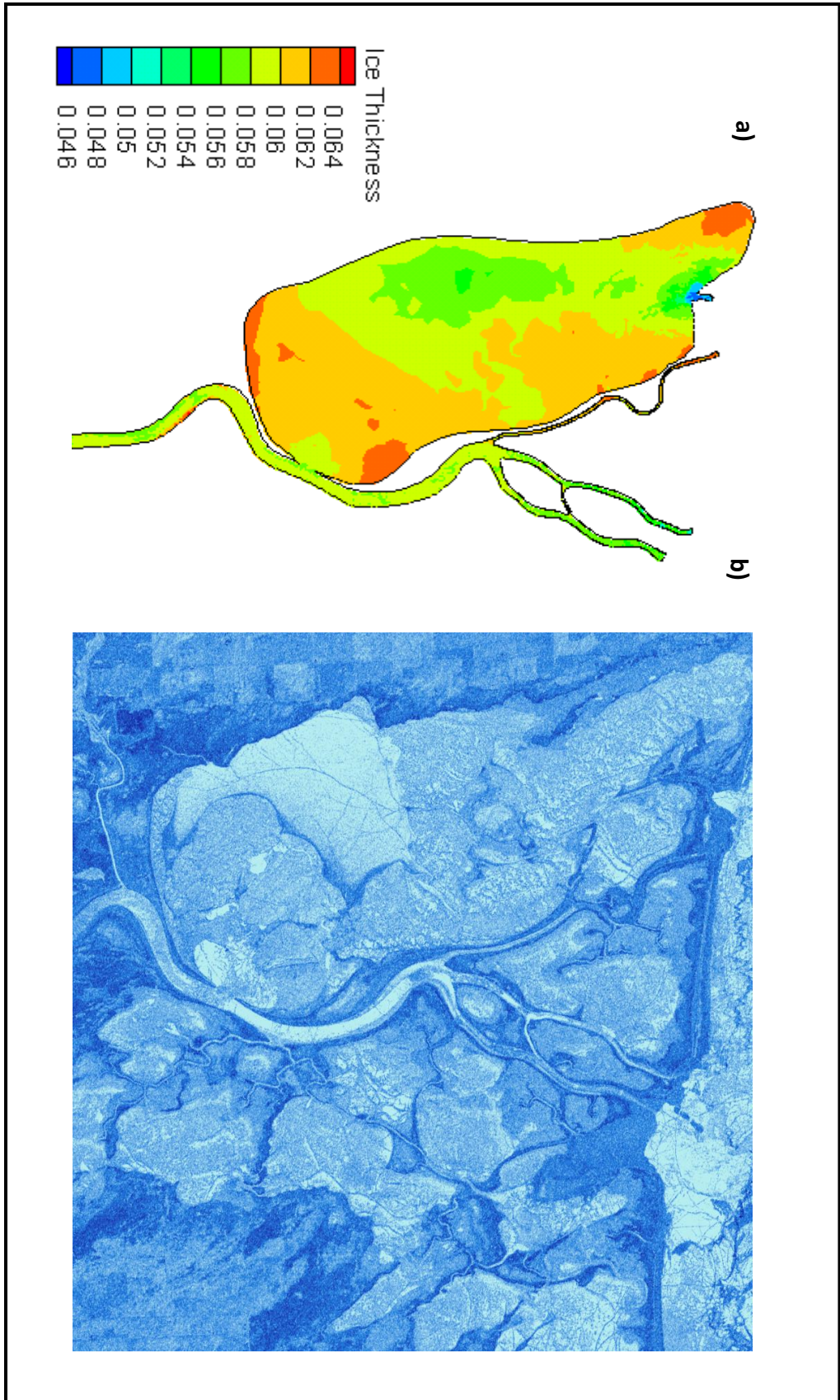


Figure 7.10: Comparison between a) modelled results and b) a RADARSAT image from November 29, 2010.

It is evident from Figure 7.9 that the model is able to simulate the freeze-up timeline described above quite well. It simulated the onset of freeze-up to be on November 17, 2010 (Figure 7.9a), with the initial ice particles forming in Netley Lake. By November 20, 2010, nearly the whole model domain has reached 100% ice concentration, as noted during the November 20<sup>th</sup> flight. However, it should be noted that the assumed initial temperature conditions in the model can considerably affect this timeline, as discussed in Section 7.3.2.

To further verify this timeline, a radar-sat image of the study area was obtained from Manitoba Water Stewardship that was taken on November 28, 2010, which is shown in Figure 7.10b. The RADARSAT image shows that a competent ice cover has formed over all water in the study area by November 28, 2010. This is in good agreement with the simulated ice cover at this time. Model results from November 28, 2010 (Figure 7.10a) indicate the formation of a competent ice cover with a thickness of approximately 6 cm.

Ice thickness measurements were taken at various locations along the Red River. The locations of these measurements are shown in Figure 4.8. The model was run through the winter season using the previously calibrated air-ice heat transfer coefficient ( $\beta = 2.5$ ) and an assumed incoming water temperature boundary of 0.01°C. The results of this simulation are compared to field measurements at Sugar Island and Netley Cut in Figures 7-11 and 7-12 and for all remaining stations in Figures A.4-A.13 in Appendix A.

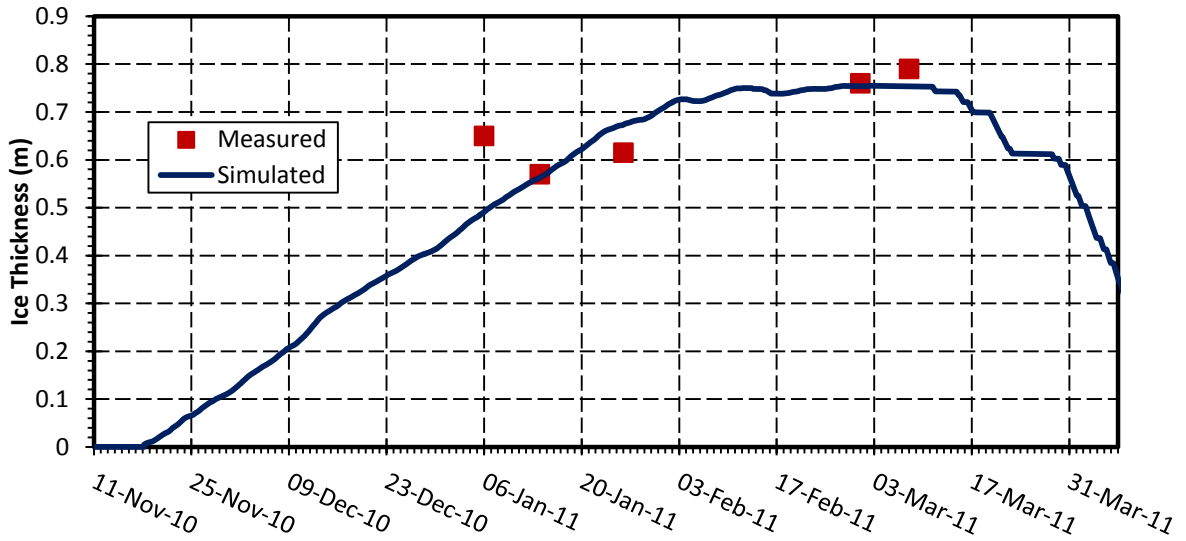


Figure 7.11: Dynamic ice model verification at Sugar Island during 2010-2011 winter season.

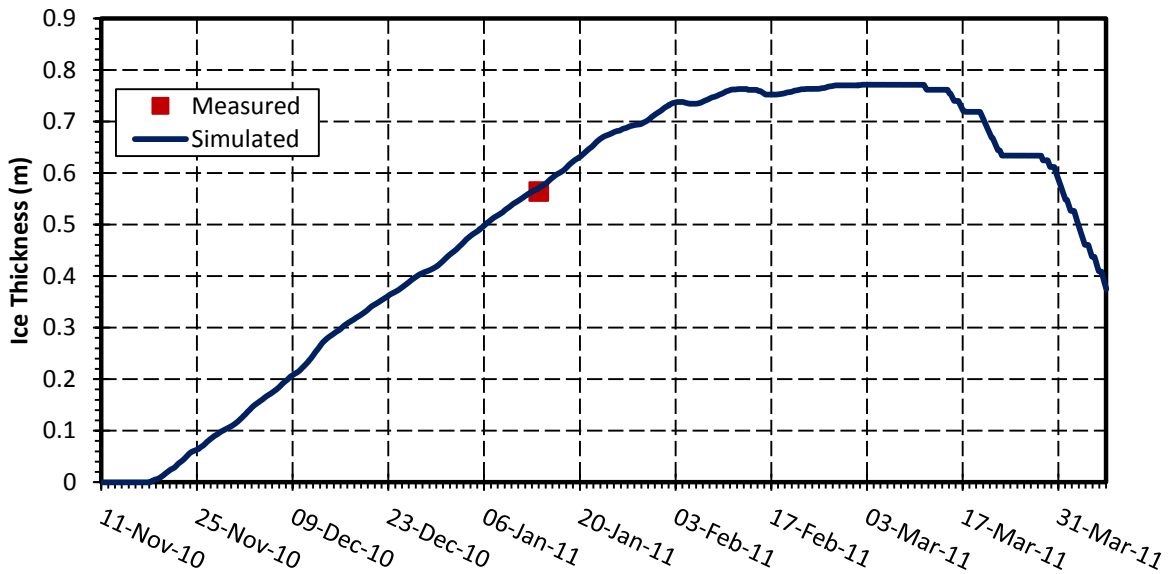


Figure 7.12: Dynamic ice model verification at Netley Cut during 2010-2011 winter season.

Overall, the model was able to represent the measured data collected for most locations within the model. However, for some stations, only one measurement of ice thickness was taken over the entire winter. This makes it extremely difficult to objectively evaluate the model's ability to simulate ice growth over the season. Ideally, measurements would span the entire winter so that ice growth during the beginning, middle, and end of the season could be evaluated.

In addition to ice growth over the winter season, the simulated flow proportions and water surface elevations within the model were also compared to measured values to further verify the validity of the dynamic ice model. Table 7.3 shows a comparison between the modeled and measured flow distribution. From this table, it is evident that the hydrodynamic conditions under the ice are being modelled appropriately in the verification simulation, as the maximum difference between modelled and measured flow proportions is 8%.

**Table 7.3: Comparison of modelled and simulated discharge proportions for the 2010-2011 winter season.**

<b>Location</b>	<b>Measured (%)</b>	<b>Simulated (%)</b>
Red River Upstream of Netley Cut	100	100
Netley Cut	15	23
East Channel	38	33
Main Channel	47	39
West Channel	≈0	1
Error	N/A	4

The measured water surface elevations at the Red River flow split, Devils Creek, Breezy Point and Selkirk were compared to those simulated by the model. These comparisons are shown in Figures 7-13 – 7.16. These figures indicate that very good agreement exists between the measured and modelled data, as all the trends in the data are captured by the model with little error. However, it is evident that the stations closest to the downstream boundary condition are better able to reproduce the measured data. This is directly related to the fact that the downstream water surface elevation boundary condition largely controls the water level in the entire model. As a result, the stations closest to this boundary often show the least error between modelled and measured data.

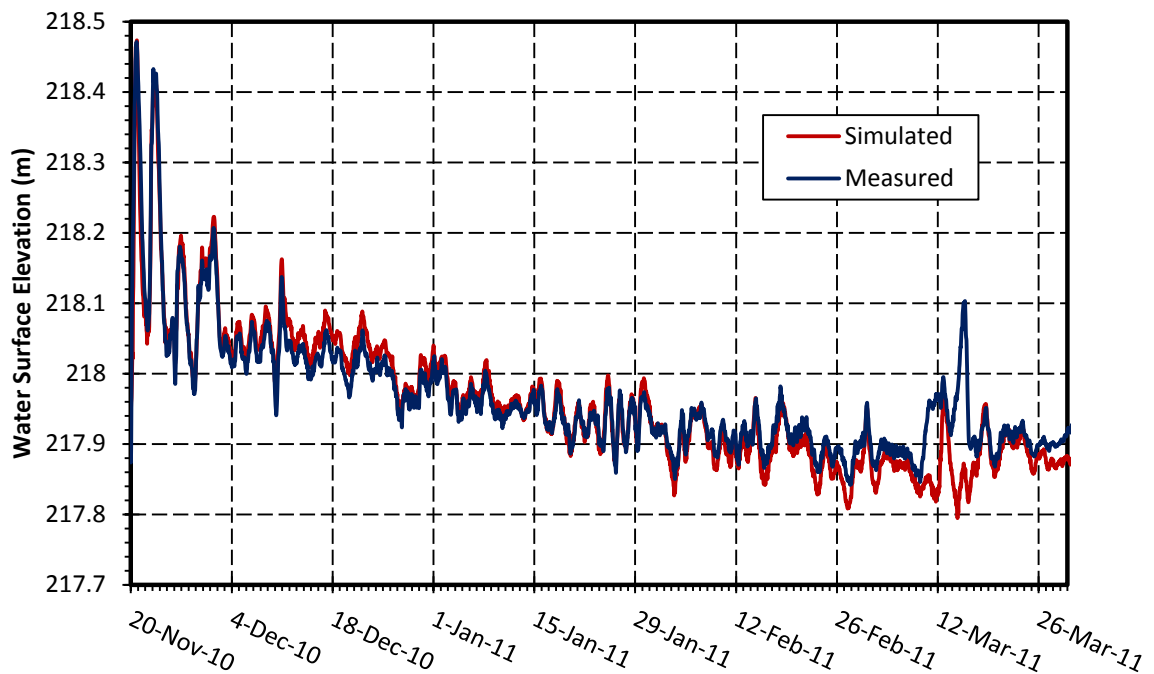


**Figure 7.13: Verification simulation of WSE at Red River flow split in 2010-2011 winter season.**



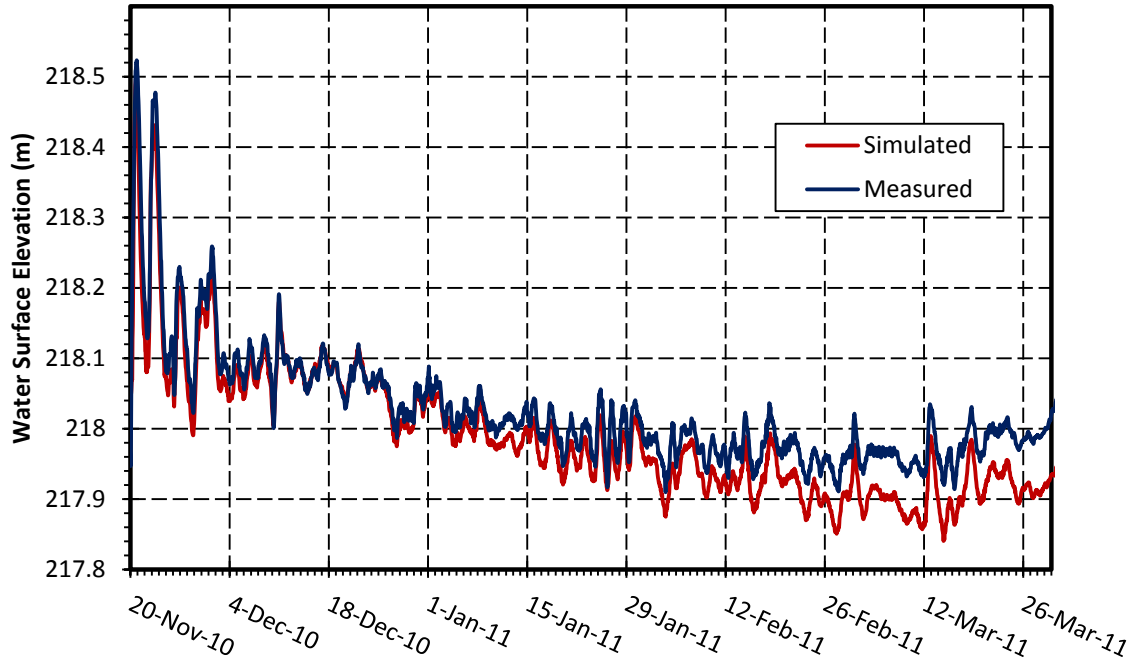


Figure 7.14: Verification simulation of WSE at Devils Creek in 2010-2011 winter season.

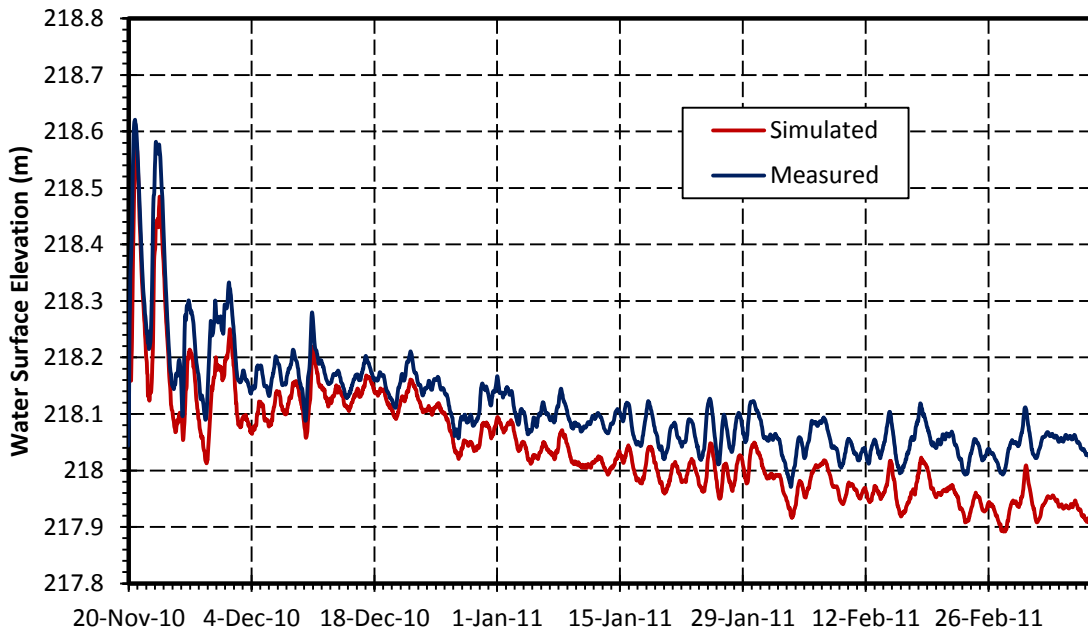
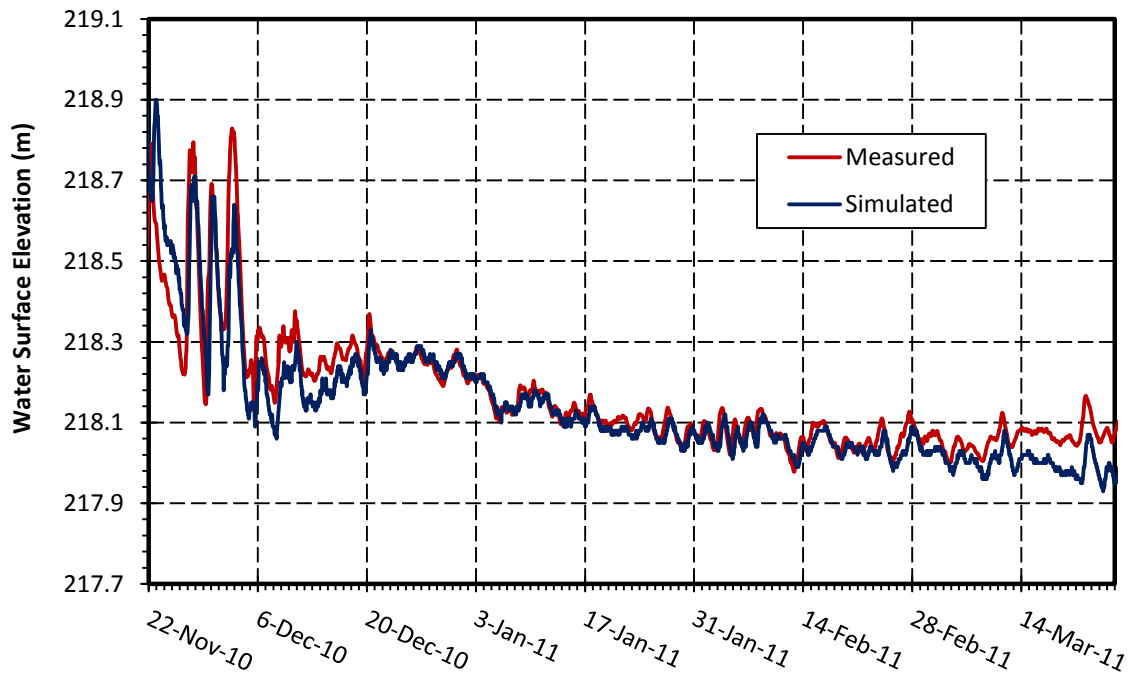


Figure 7.15: Verification simulation of WSE at Breezy Point in 2010-2011 winter season.



**Figure 7.16: Verification simulation of WSE at Selkirk in 2010-2011 winter season.**

#### 7.4.2 2011-2012 WINTER SEASON

In terms of data collection, the 2011-2012 winter season had the most comprehensive data collection. During this winter, ice thickness, water temperature, snow thickness, discharge, and water depth measurements were made throughout the study area. Each of these data sets had a role in verifying the model.

The primary difference between this simulation and those discussed previously was that the boundary temperature at Selkirk was measured during the freeze-up period and did not have to be estimated. As a result, setting realistic thermodynamic initial conditions

was much more straightforward and likely more representative of the actual physical conditions. The simulation was initiated several weeks before the known onset of freeze-up and the water was allowed to cool naturally via the measured boundary temperature and the heat transfer to the air. As a result, the model predicted a thermal freeze-up, quite similar to the one that occurred in reality.

During the freeze-up period, thorough observations were made and documented. Photos from November 16, 2011 indicate that the onset of freeze up in the river channel occurred very close to this date, most likely during the previous night. Figure 7.17 shows a comparison between the modelled results at the onset of freeze-up and the observations made in the field on November 16. It is evident from the figure that the model is able to predict both the timing and ice processes occurring at freeze-up.

In addition to the photos taken at the onset of freeze-up, aerial photos from an air plane were taken on December 1, 2011. From the observations made on December 1, it was evident that the entire study area had frozen over by this date. Model results on December 1 are compared to an aerial photo of Netley Cut in Figure 7.18. It is clear from this figure that the model is also predicting a full ice cover by this time.

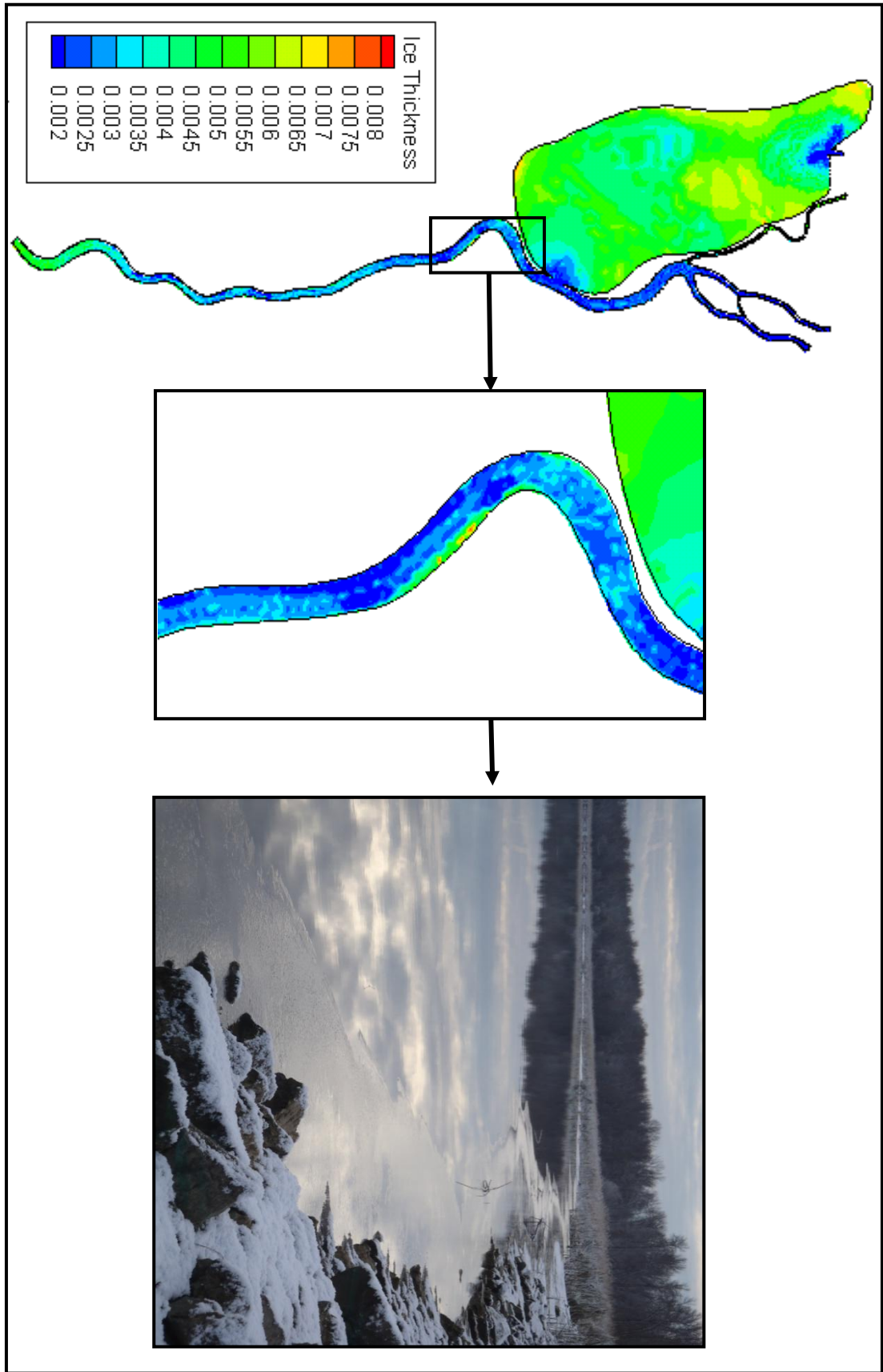


Figure 7.17: Comparison between the modelled results at the onset of freeze-up and the observations made in the field on November 16, 2011.

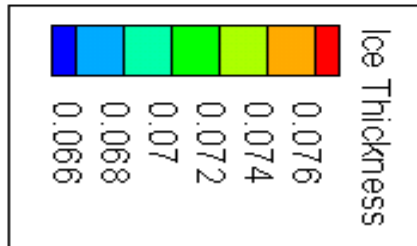
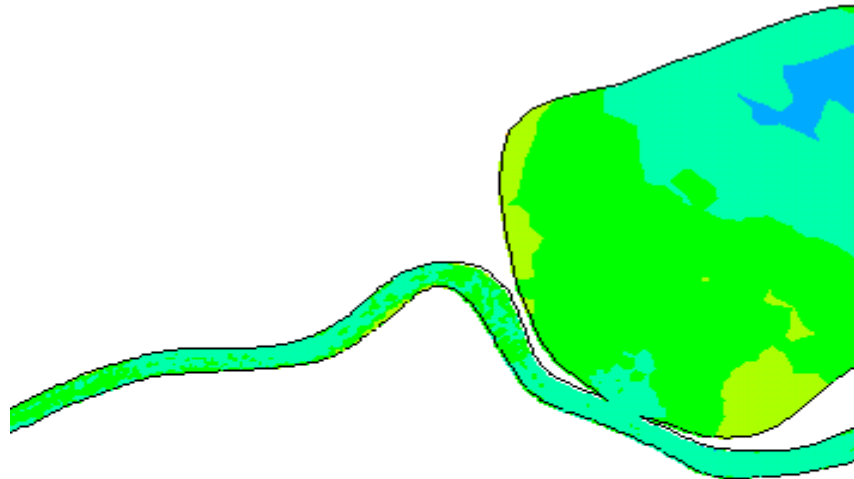
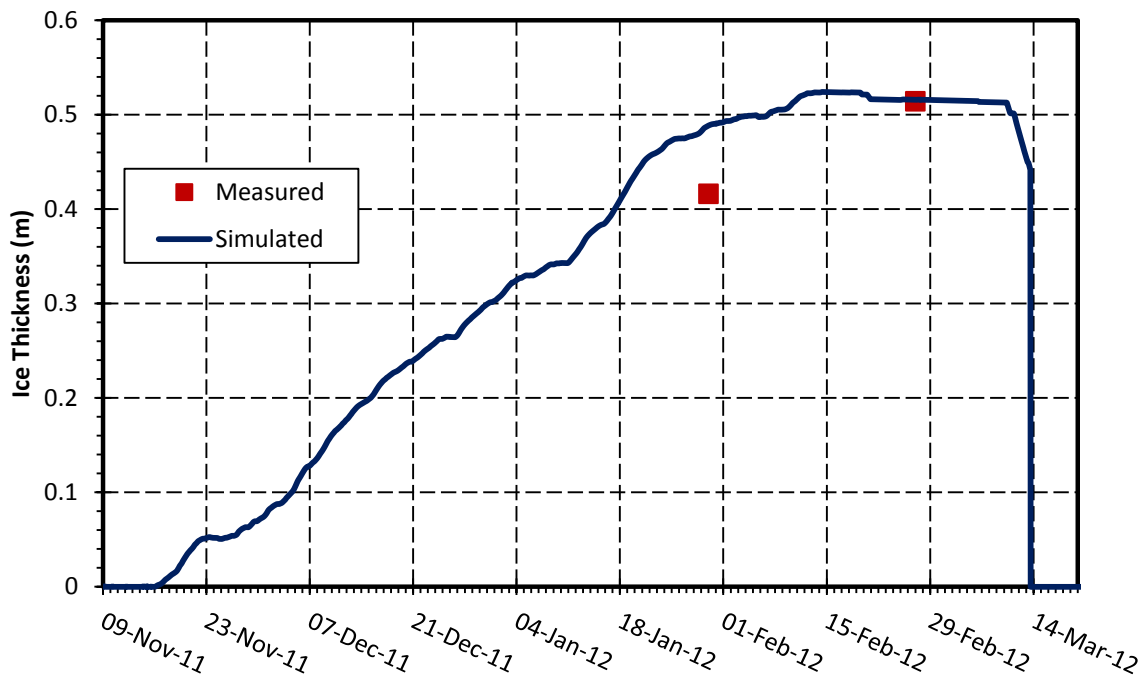


Figure 7.18: Comparison between model results and aerial photo on December 1, 2011.

Similar to the previous winter seasons, an assortment of ice thickness measurements were taken throughout the winter. These measurements were taken at several locations along the river, shown in Figure 4.9. At each cross section, between 10 and 20 holes were drilled and both water depth and ice thickness was measured. The ice thickness measurements were averaged to obtain a mean ice thickness at each location. Similar to the previous winter seasons, the model was run over the winter period using the established  $\beta$  value from the calibration. Comparisons between modelled and measured data at Selkirk, Hwy 4, and upstream of Netley Cut are shown in Figures 7.19-7.21 and all other stations are shown in Figures A.14-A.18 in Appendix A. Once again, these figures indicate that the model is performing adequately for most of the stations where data was collected.



**Figure 7.19: Dynamic ice model verification at Selkirk during 2011-2012 winter season.**

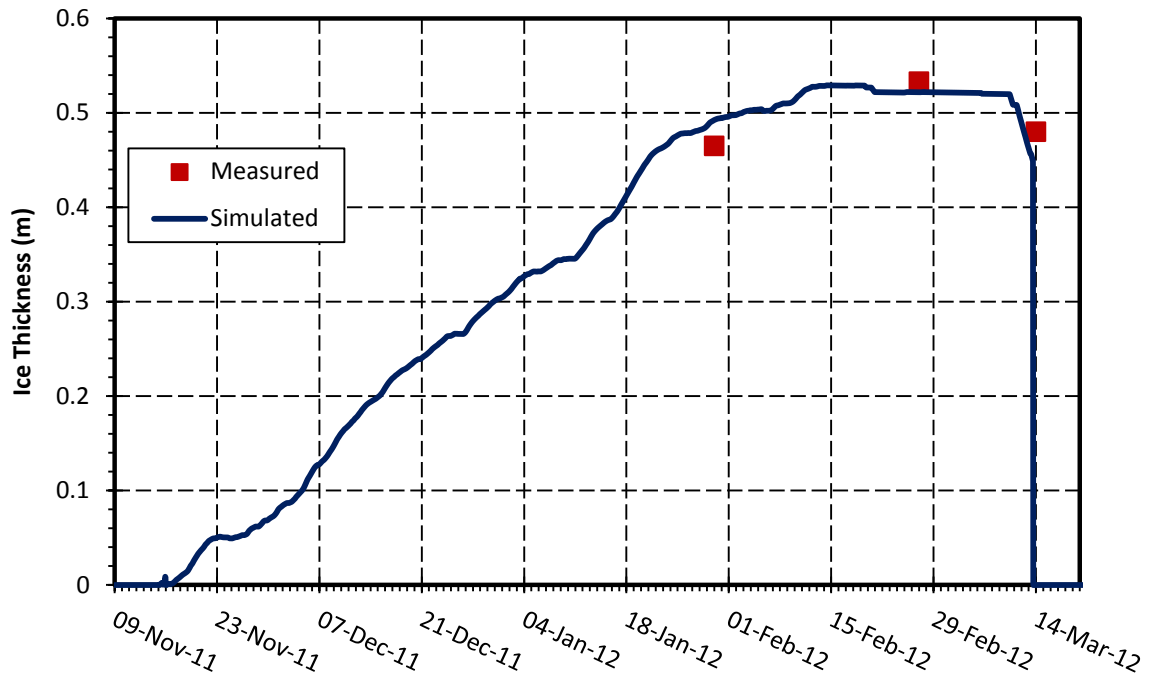


Figure 7.20: Dynamic ice model verification at Hwy. 4 during 2011-2012 winter season.

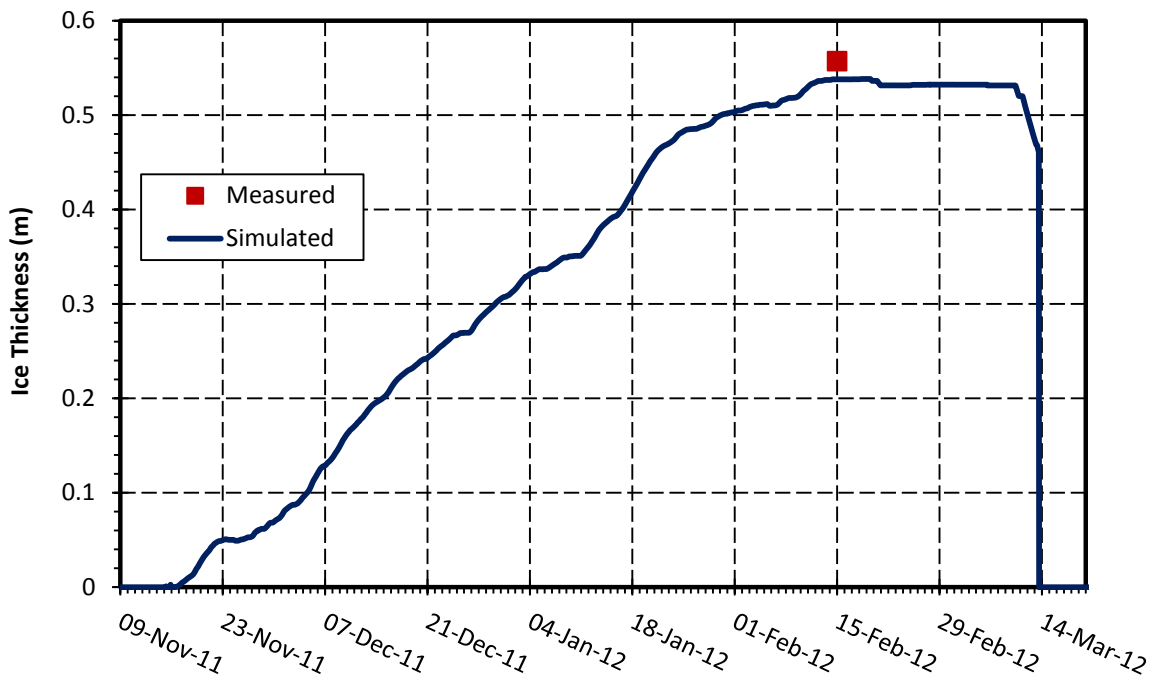


Figure 7.21: Dynamic ice model verification upstream of Netley Cut during 2011-2012 winter season.

The flow proportions were also verified for the 2011-2012 winter season and are compared in Table 7.4. Similar to the previous winter seasons, the 2011-2012 simulation indicates that there is very good agreement between the modelled and measured values of flow proportions, with a maximum difference of 8% between the modelled and measured values.

**Table 7.4: Comparison of modelled and measured discharge proportions for 2011-2012 winter season.**

<b>Location</b>	<b>Measured (%)</b>	<b>Simulated (%)</b>
Red River Upstream of Netley Cut	100	100
Netley Cut	15	22
East Channel	38	33
Main Channel	47	39
West Channel	≈ 0	1
Error	N/A	5

Finally, two water level gauges were used to verify the water surface elevations predicted by the model. Over the winter, water level data was collected at Selkirk, Devils Creek. These measurement are compared to modelled predictions in Figure 7.22 and Figure 7.23. As noted in the results for the previous two winters, the water surface elevations are well matched at both gauge locations.



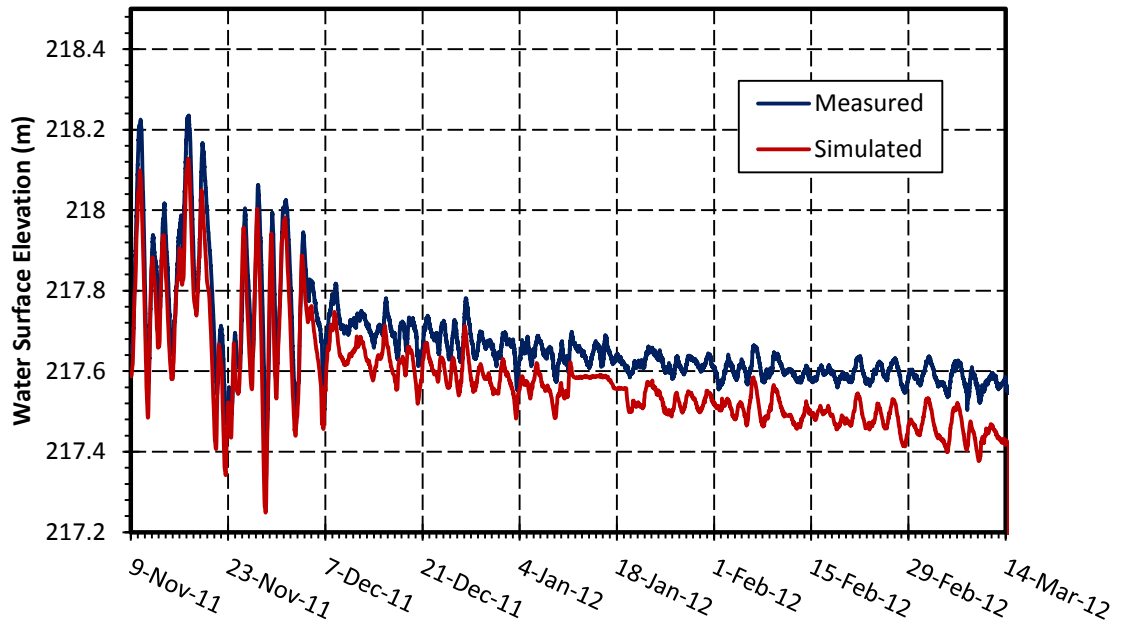


Figure 7.22: Comparison of measured and simulated water surface elevation at Devils Creek during the 2011-2012 winter season.

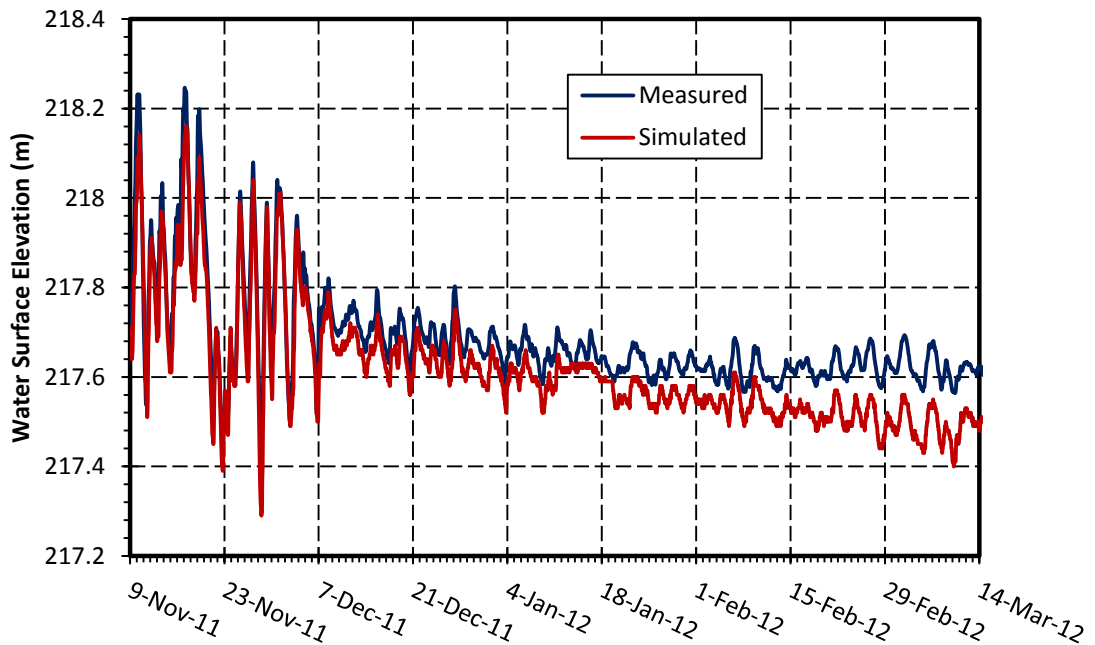


Figure 7.23: Comparison of measured and simulated water surface elevation at Selkirk during the 2011-2012 winter season.

## **7.5 DISCUSSION OF DYNAMIC ICE MODEL**

From the results presented in this chapter, it is evident that the dynamic ice model was able to predict ice thickness within the study reasonably well. However, there are several limitations of the study and of the model itself that hindered the model's ability to perform more accurately. These limitations are discussed in detail in the following sections.

### **7.5.1 THE INFLUENCE OF WATER VELOCITY ON ICE THICKNESS**

It has been well documented in the literature (Ashton and Kennedy, 1972, Hausser and Parkinson, 1991, and Matousek and Havlik, 1988) that water velocity plays an important role in river ice formation. Water that travels at higher velocities tends to be more turbulent and thus, more heat is transferred between the warmer water and the ice cover, impeding its growth.

In CRISSP2D, this heat flux is calculated as

$$\varphi_{wi} = h_{wi}(T_w - T_m) \quad (7.2)$$

where  $h_{wi}$  is the heat transfer coefficient between the water and ice [ $\text{W}/\text{m}^2\text{°C}$ ],  $T_w$  is the water temperature [ $^{\circ}\text{C}$ ], and  $T_m$  is the melting temperature of water ( $0^{\circ}\text{C}$ ). The heat transfer coefficient is a function of water velocity and depth and can be calculated as

$$h_{wi} = C_{wi}U^{0.8}D^{-0.2} \quad (7.3)$$

where  $C_{wi}$  is a coefficient,  $U$  is the mean water velocity [m/s], and  $D$  is the depth of the flow [m]. In order to complete its ice growth calculations, CRISSP2D inputs Equation 7.2 into its thermal growth equation which is given as

$$\frac{dh_i}{dt} = \frac{-\varphi_R + \alpha + \beta(T_m - T_a)}{\rho_i L \beta \left( \frac{h_i}{k_i} + \frac{1}{\beta} \right)} - \frac{h_{wi}}{\rho_i L} (T_w - T_m) \quad (7.4)$$

where  $\varphi_R$  is the net shortwave radiation [ $\text{W}/\text{m}^2$ ],  $\alpha$  is a heat exchange constant [ $\text{W}/\text{m}^2$ ],  $\beta$  is the heat transfer coefficient between the ice and air [ $\text{W}/\text{m}^2\text{C}$ ],  $\rho_i$  is the density of ice,  $T_a$  is the air temperature,  $h_i$  is the ice thickness [m],  $k_i$  is the heat conductivity of ice, and  $L$  is the latent heat of fusion of ice.

However,  $0.01^\circ\text{C}$  was chosen as the upstream incoming water temperature boundary condition, as this is in accordance with data collected in the field. As water flows away from the upstream boundary it begins to lose heat. Due to the extremely long reach length, (33 km) the water has ample time to cool and eventually cools to the default minimum temperature of CRISSP2D (without the presence of supercooling) of  $1.0 \times 10^{-5}^\circ\text{C}$ . This modelled result is fairly unrealistic, as water flowing under a competent ice cover typically does not cool below  $0.001^\circ\text{C}$ . The implication of the unrealistically low water temperatures is that when they are inserted into Equation 7.4, the second term of the equation becomes negligible and effectively removes the

influence of water velocity from the ice growth equation. This phenomenon is particularly evident when water velocities and ice thickness measurements are compared in the east and main channels of the Red River. The main channel carries a larger proportion of the total flow and thus, experiences larger water velocities than the east channel. Through the winter season, the average water velocity in the main channel is approximately 20 cm/s in comparison to 15 cm/s in the east channel.

Due to this difference in velocity, there is a noticeable difference in measured ice thickness between the east and main channel. However, as discussed above, the model cannot adequately take the velocity difference into account as the simulated average water temperature in both of these channels throughout the winter is approximately 0.0007°C. Consequently, results produced by the model show no noticeable difference in ice thickness between the east and main channels, as shown in Figure 7.24. A similar phenomenon is noticed upstream and downstream of Netley Cut, as a large portion of the flow is routed through the cut, decreasing water velocities downstream. However, this is more prominent in the beginning of the winter season since, as the ice thickens, it is more difficult for water to pass through the cut and a larger portion of it continues downstream.

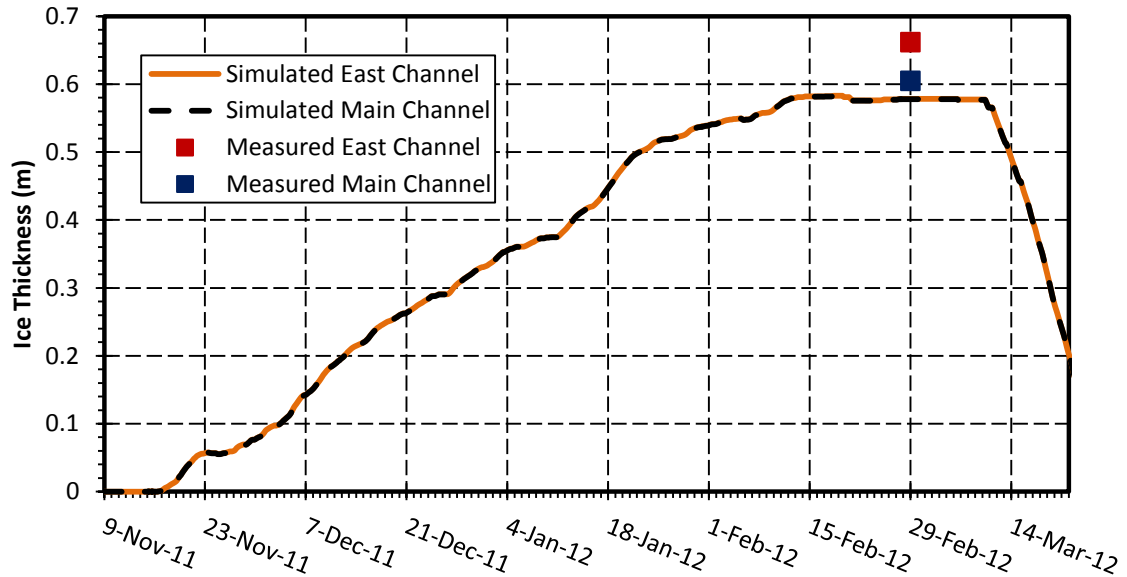


Figure 7.24: Comparison of simulated and measured ice thickness in the east and main channel.

### 7.5.2 THE INFLUENCE OF FRAZIL ICE PRODUCTION ON ICE GROWTH

CRISP2D has alternate equations that govern ice growth depending on whether or not frazil particles are present. This can be attributed to the fact that the presence of frazil ice on the underside of the ice cover typically accelerates the growth of the ice cover. The frazil ice layer insulates the ice cover from the warm water below, allowing the rate of ice growth to increase. In addition, when frazil ice is present, only the pore water in the frazil layer needs to be solidified for the downward growth of the ice cover.

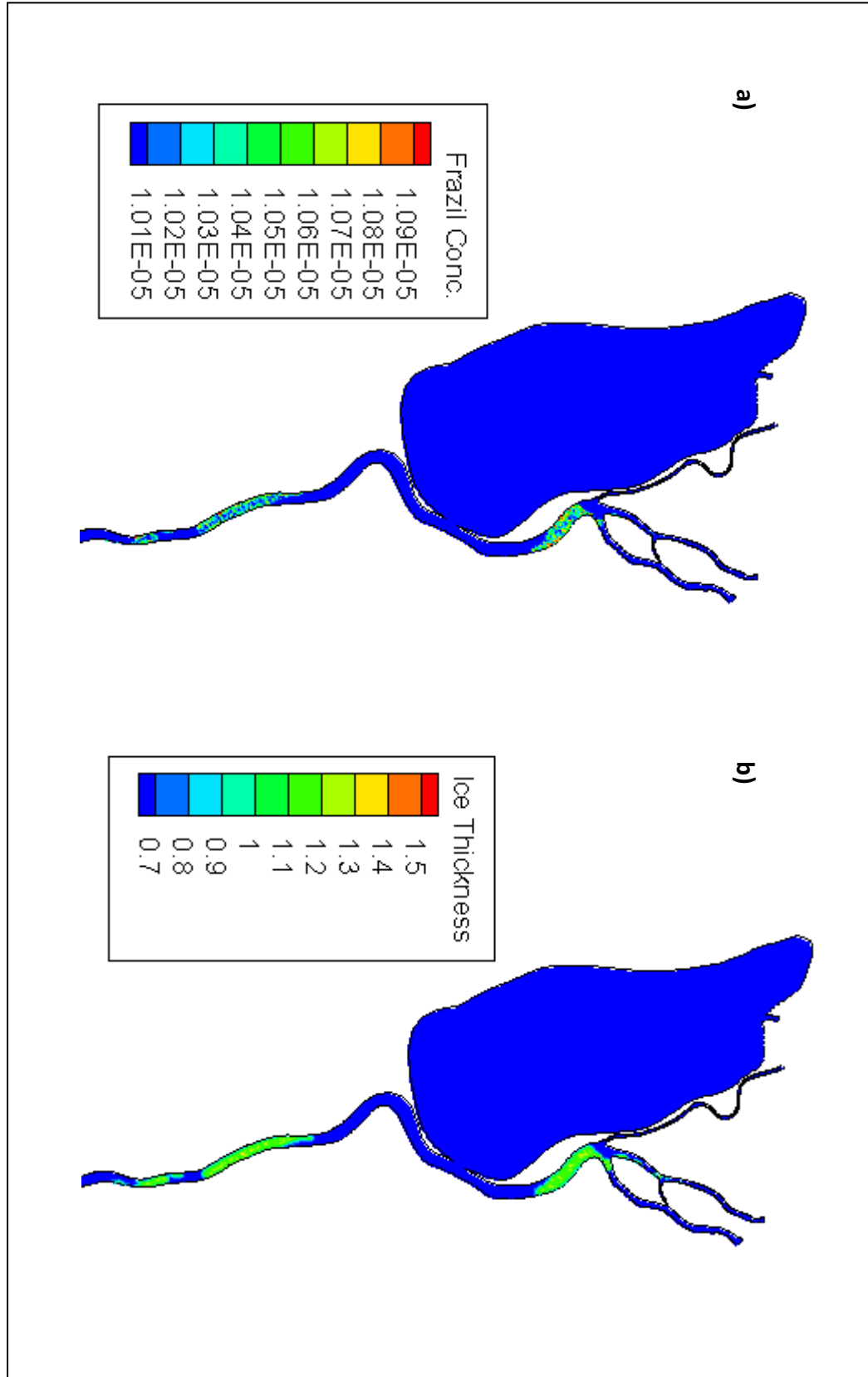


Figure 7.25: The influence of a) frazil ice on b) ice thickness in simulated results.

This phenomenon was well documented within the model results. Figure 7.25a shows the 2009-2010 simulation using initial thermodynamic conditions that allow frazil ice to form. It is clear from this figure that in the portions of the model where frazil particles are generated, the ice grows much thicker (shown in Figure 7.25b) than areas that are absent of frazil ice. In addition, the frazil affected areas grow to an unrealistic ice thickness of approximately 1.3 m, which is not representative of field conditions anywhere within the study area.

For the purposes of the research the dynamic ice model was simplified by assuming that frazil growth does not occur, as discussed in Section 7.3. However, it is not uncommon to observe supercooling and frazil production within the study area. It is clear from Figure 7.26 that the frazil ice parameters must be calibrated in order to allow the model to produce frazil particles and still be able to predict reasonable ice thicknesses. However, with such a large model domain, it would be very difficult to calibrate these parameters without extensive field observations of where, when and how much frazil forms. Additionally, it is unlikely to expect a single value of these frazil ice parameters to be valid for the entire model domain, or even a portion of the domain over the entire winter.

### **7.5.3 THE INFLUENCE OF SNOW AND WIND ON ICE THICKENING**

It is important to note that Equation 7.4 is independent of wind velocity, snow thickness, and snow density. However, these are important factors that can considerably affect the rate of ice growth on rivers and lakes. Wind is an important source of heat loss that acts to help cool the water and grow the ice cover, while snow insulates the ice from cool air above, retarding its growth.

In an attempt to compensate for not accounting for these factors, the air-ice heat transfer coefficient,  $\beta$ , was adjusted and calibrated as discussed in Section 7.3. However, the model was calibrated such that a single value of  $\beta$  was chosen for the entire model domain and remained constant over the entire length of the simulation. In reality, the value of  $\beta$  would be expected to vary over the model domain as it is a function of variables that are not always spatially or temporally constant. Over the winter, wind speed and direction can vary substantially and the snow goes through cycles of falling and compacting, impacting both depth and density of the snow cover. In addition, strong winds have the tendency to blow snow between locations, particularly on wide open lake areas. However, the complexity of these processes makes them impossible to measure and accurately input into a model of this size.



## **7.6 THE EFFECT OF SEALING NETLEY CUT**

As previously mentioned, Netley Cut is a topic of debate among many of the stakeholders involved with this project. It has been hypothesized based on the evidence presented in Chapter 1 that the growing proportion of flow discharging through Netley Cut is exacerbating the declining health of Lake Winnipeg. As a result, considerations to seal Netley Cut permanently have been made. However, some believe that during the break up season the opening allows large pieces of ice to exit the river and be deposited in Netley Lake, helping to alleviate the common ice jamming that often forms in the vicinity.

This project has examined the effect of sealing Netley Cut on the freeze-up and thermal growth processes within the model. To accomplish this, the model geometry was altered such that Netley Lake was removed and 100% of the incoming flow was forced to remain in the Red River and exit the model via the west, main, or east branch. All other hydrodynamic, thermodynamic, and ice dynamic parameters remained consistent with those discussed in previous sections of this thesis. Each of the three winter seasons were re-simulated using the altered model geometry and comparisons were made to the original simulations.

Hydrodynamically, the model responded to the geometry change as expected. Due to the cut closure there were noticeable increases in water velocity in the Red River downstream of Netley Cut, increasing by approximately 2 cm/s. Although this velocity

increase is not extremely large, it is important to note that this data was taken during the winter season when discharge is at a minimum. It is possible that effects of sealing Netley Cut on water velocity will be more pronounced in the open water season, particularly during the spring freshet. If this is the case, the downstream portion of the study may become more susceptible to erosion and associated consequences.

The altered geometry of the model also had an effect on the water surface profile within the Red River. Figure 7.27 shows a longitudinal profile of the water surface elevation along the length of the study reach. It is evident from Figure 7.27 that sealing Netley Cut will likely cause backwater effects in the channel of approximately 3 cm as far upstream as Selkirk. Again, this difference is small, but may increase the severity of flood consequences should a jam occur within the study area.

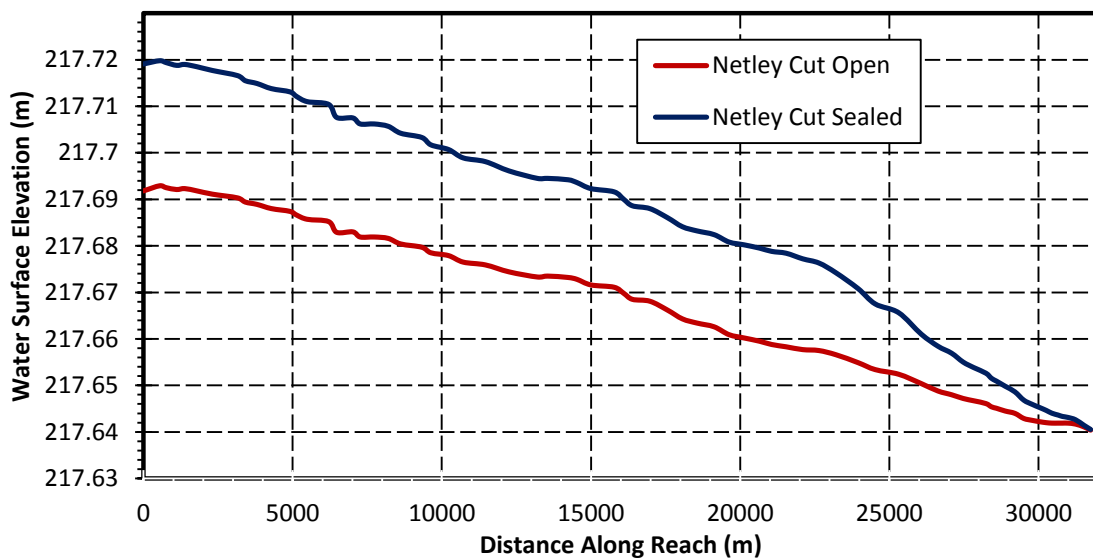


**Figure 7.26: Comparison of modelled water surface elevation with Netley Cut open and sealed.**

The dynamic ice model showed no noticeable change in ice cover thickness anywhere within the model domain after sealing Netley Cut. This was not surprising considering the fact that the model has severe limitations with respect to accounting for water velocity within its governing ice growth equations (discussed at length in Section 7.5.1).

Further work needs to be completed to determine the effects of sealing Netley Cut both during the ice-on and break-up seasons. In particular, this work would benefit substantially by a detailed field observation program to determine the ice dynamics near Netley Cut during an ice jam. Although it is believed that the cut helps alleviate ice jams by allowing some ice to flow into Netley Lake, it has been shown in this study that the ice formed over Netley Lake may be sufficiently thick, preventing ice flows from the Red River from entering the lake.

Furthermore, the natural geometry of the Red River (a mild, meandering Prairie river) makes it particularly susceptible to ice jamming. As a result, it is plausible that even if a jam is prevented from forming near Netley Cut by allowing some ice flows to enter Netley Lake, it is likely that a jam will still occur further downstream. The latter situation may be more desirable due to the fact that flooding consequences in larger upstream communities such as Selkirk and St. Andrews would be reduced.

---

**CHAPTER 8****CONCLUSION**

---

**8.1 PROJECT SUMMARY**

In recent decades, the health of Manitoba's largest lake, Lake Winnipeg, and its neighbouring wetland, the Netley-Libau Marsh, has declined significantly. Although their declining health has been linked to a number of processes, it is widely accepted that changing flow patterns in the Netley-Libau Marsh area have contributed significantly (Grosshans et al., 2004). In particular, the increasing size of Netley Cut, an opening in the western bank of the Red River, has significantly altered the portion of flow that enters Netley Lake. This cut has grown in size from approximately 5 m to 450 m since it was originally excavated in the early 1900's. In order to restore flow conditions to what they once were and possibly revitalize the health of Lake Winnipeg and the Netley-Libau Marsh, the various stakeholders have considered sealing Netley Cut. However, ice jamming and associated flooding has been a longstanding problem for Manitobans and

---

## CONCLUSION

---

this area is particularly susceptible to ice jams during the winter ice break-up season. Some speculate that the cut allows some relief to ice flows in the Red River, allowing large ice chunks to flow into Netley Lake. If this is indeed the case, it is possible that the ice jams and their consequences will become even more severe upon closure of the cut.

In order to obtain a better understanding of the hydraulic processes occurring in the vicinity of Netley Cut and determine the implications of sealing it, a comprehensive hydrodynamic and ice dynamic study was completed on the Red River between Selkirk and Lake Winnipeg. This study examined the open water hydrodynamic conditions, thermodynamic conditions prior to freeze-up, and three seasons of ice growth. There have not been modelling attempts of the study in the past and as such, existing data was scarce. An extensive field program was undertaken that included both open water and ice covered data collection. This program was carried out between June 2009 and May 2012 and various data sets were collected, including open water and ice covered discharge and velocity measurements, water depths, ice thicknesses and water temperatures. These data sets were used to calibrate and verify many of the parameters in the numerical model.

CRISP2D, a two-dimensional finite element model, was used to simulate the hydrodynamics, thermodynamics, and ice dynamics within the study area. The finite element mesh was developed using bathymetry from a variety of sources, and consisted of linear triangular elements. Element size varied depending on channel width and the

---

## CONCLUSION

---

hydraulic importance of the area. A sensitivity analysis determined that having six elements across each channel optimized computational time and model stability.

The model was first calibrated for open water conditions. The Manning's  $n$  of various portions of the mesh were adjusted iteratively until good agreement was found between modelled and measured water surface elevations. The model was subsequently verified using a second time period during the open water season. Overall, the hydrodynamic model performed very well and was typically able to match water surface elevation measurements within 5 cm. It also succeeded in capturing the characteristic rapid fluctuations in water surface elevation in both timing and magnitude. Furthermore, the model was able to adequately replicate the proportion of the total flow that discharges through Netley Cut and each branch of the Red River downstream.

As a precursor to the dynamic ice simulations, thermodynamic simulations were completed in order to calibrate the heat transfer coefficient between the water and air. This calibration helped to ensure that water cools at an appropriate rate just prior to the onset of freeze-up. The heat transfer coefficient was altered iteratively until the model was able to simulate the water temperature measured at Devils Creek and the Red River flow split. The heat transfer coefficient was found to be  $20 \text{ W/m}^2\text{C}$ .

---

## CONCLUSION

---

The calibrated hydrodynamic and thermodynamic models were used as inputs to the dynamic ice model. The primary objective of this model was to predict ice growth with time throughout the model domain. The model was calibrated using the data collected in the 2009-2010 season and verified with data from the subsequent two winter seasons. A sensitivity analysis was carried out on a variety of dynamic ice parameters and it was determined that the heat transfer coefficient between the ice and air had the most significant effect on rate of ice growth. The model was run using a range of values for the heat transfer coefficients and an RMSE error analysis was completed in order to choose the coefficient that best fit the data. Overall, the dynamic ice model was able to approximate the ice thickness in the study area well at most locations. However, there were limitations of the model that prevented better model results from being attained in some portions of the model, including the inability of the model to properly account for water velocity in its ice growth calculation.

Upon successful calibration of the dynamic ice model, it was subsequently used to determine the effects of sealing Netley Cut. An alternate mesh was created that excluded the Netley Lake (effectively sealing the cut) from the model domain. All winter seasons were re-simulated and model results were compared to the results from the original geometry. Sealing the cut increased water velocity and water surface elevation in the Red River, but did not have a noticeable effect on the rate of ice growth anywhere within the model. This was attributed to the fact that the model is not able to adequately incorporate the influence of water velocity on ice thickness in the model.

This project has provided good knowledge base of the hydraulic processes that occur within the study area, where none previously existed. It is a solid basis for future studies that may include ice break up as well as good information for Manitoba Water Stewardship and their ice cutting program.

## 8.2 CONCLUSIONS

The following conclusions and contributions can be drawn from the results of this research:

- 1) CRISSP2D can be successfully applied to large model domains with reasonably complex geometry.
- 2) A minimum of six elements is required across each channel in order to optimize model continuity and computational time.
- 3) The model is able to replicate the hydrodynamic conditions, including flow splits (within 5.4%) and water surface elevations (within approximately 10 cm).
- 4) An appropriate value of the water-air heat transfer coefficient is  $20 \frac{W}{m^2 \cdot ^\circ C}$ .
- 5) Ice thickness throughout the model domain can be reasonably predicted using the CRISSP2D model and the calibrated ice-air heat transfer coefficient  $\beta = 2.5 \frac{W}{m^2 \cdot ^\circ C}$ .
- 6) The initial thermodynamic conditions assumed can significantly affect the timing and types of freeze-up processes that occur.



- 7) The effects of water velocity on ice growth are not adequately taken into account in this model.
- 8) Sealing Netley Cut will have noticeable but not major impacts on the water velocity and water surface elevation within the study area (an increase of approximately 3 cm).
- 9) The dynamic ice model was not capable of simulating differences between model geometries with Netley Cut open and Netley Cut sealed.

### **8.3 RECOMMENDATIONS & FUTURE WORK**

There have not been any recent numerical ice modelling attempts carried out on the Red River near Netley Cut. As a result, this study has provided valuable information regarding the hydrodynamics and ice dynamics of this area and has provided a solid foundation for many related studies in the future. In addition, several important limitations of the numerical model were identified that could be adjusted to help ensure the success of future endeavors with CRISSP2D. Overall, this study was a success, but there are several recommendations that can be made to make future similar endeavors even more successful.

The availability of quality data often dictates the success of any numerical modelling endeavor. However, data collection during the winter months is particularly challenging

---

## CONCLUSION

---

for numerous reasons. Safety considerations, daylight hours, and transportation options to remote areas all influence the quality and quantity of data that can be collected.

Although data was collected over three seasons throughout the study area, this project could have greatly benefited from further data collection. In particular, there was a noticeable lack of ice thickness data collected during the beginning of the freeze-up period. This period is arguably the most important portion of the winter season, as ice typically grows more rapidly during this portion. However, this is also the most dangerous time of the season to collect data, as there have been numerous cases of people and equipment falling through thin ice resulting in serious injury or death. It is also evident from this study that the collection of water temperature data during the period immediately prior to freeze-up as well as during the winter is an important data set to collect when trying to calibrate a dynamic ice model. It is evident from the results of this study that model results can vary significantly depending on the assumed temperature conditions. If this data was collected, it would eliminate the need to make temperature assumptions. It is recommended that Manitoba Water Stewardship measure water temperature at its existing gauges and make that data available for future research projects.

This application of CRISP2D was unique in the fact that model domain was quite large and complex. It included a lake, several flow splits, and a river reach of over 32 km. Previous to this study, CRISP2D modelling efforts have been concentrated primarily on

---

## CONCLUSION

---

smaller, very specific portions of rivers. This difference in applications highlighted some of the shortcomings of the model that likely had not been issues in previous projects. In particular, it has been well documented throughout this thesis that a model of this size requires spatially varying parameters in order to be calibrated properly. This feature is already available with the hydrodynamic module with the capability of adjusting roughness coefficients by reach, but has not yet been incorporated into the thermodynamic and ice dynamic modules. It is unrealistic to assume that a lake would have the same freeze-up parameters as a river or even that every branch of a river has identical properties.

Furthermore, when modelling larger model domains, it would be beneficial to have the ability to set a minimum water temperature value that cannot be exceeded. This study showed that in using such large river reach, the water cools to unrealistically low temperatures by the time it flows to the downstream end of the model. As a result, certain processes, specifically the effect of velocity on ice thickness, are not modelled correctly.

There are several important factors that have substantial effects on the rate of ice growth. In particular, snow depth and density both have the ability to influence the rate at which ice will grow. However, currently CRISSP2D does not take either parameter into account and as a result, their effects have to be estimated via altering the ice-air heat transfer coefficient. For smaller model domains, it may be beneficial to directly model

---

## CONCLUSION

---

the cycle of snow fall and snow packing. However, in larger model domains this process would be extremely difficult to carry out accurately without extremely detailed field measurements.

Overall, the modelling work completed in this study was relatively successful. However, it can be followed up with a variety of different studies and modelling efforts that would contribute greatly to the understanding of the hydraulic processes in the vicinity of Netley Cut. An ice break-up study in the same region would be both relevant and practical. It should also be determined as to whether it is possible to incorporate Manitoba Water Stewardship's ice cutting program into the numerical model. This would provide a better idea of how effective the months of work are that is required to carry out this program each year.

Finally, given the complex geometry of the study area, it may be beneficial to develop a physical model of the Netley Cut region. The geometry in this region is reasonably complicated and some processes may be better modelled physically than numerically.

## REFERENCES

- Ager, B. (1962). Studies on the density of naturally and artificially formed fresh-water ice. *Journal of Glaciology*, 4(32), 207-214.
- Anderson, E. (1954). *Energy-budget studies. In United States Geological Survey, Water-loss investigations: Lake Hefner studies*. Washington: United States Department of the Interior.
- Andersson, A., & Andersson, L. (1992). Frazil Ice Formation and Adhesion on Trash Racks. *11th IAHR Symposium on Ice*, (pp. 671-682). Banff.
- Ashton, G. (1986). *River Lake Ice Engineering*. Highlands Ranch: Water Resources Publications, LLC.
- Ashton, G., & Kennedy, J. (1972). Ripples on underside of river ice covers. *ASCE*, (p. 1603).
- Beltaos, S. (1995). *River Ice Jams*. Colorado: Water Resources Publications, LLC.
- Bolsenga, S. (1969). Total Albedo of Great Lakes Ice. *Water Resources Res.*, 1132-1133.
- Bowen, I. (1926). The Ratio of Heat Losses by Conduction and by Evaporation from any Water Surface. *Physical Review*, 27, 779-787.
- Carper, G., & Bachmann, R. (1984). Wind Re-suspension of Sediments in a Prairie Lake. *Canadian Journal of Fisheries and Aquatic Sciences*, 41, 1763-1767.

---

## REFERENCES

---

- Clark, S. (2006). An Experimental Study of the Formation and Evolution of Frazil Ice. Winnipeg: University of Manitoba.
- Dorsey, N. E. (1940). Properties of ordinary water-substance in all its phases: water vapor, water, and all the ices. *American Chemical Society: Monograph Series*. University of Michigan.
- Fischer, H., List, E., Koh, R., Imberger, J., & Brooks, N. (1979). *Mixing in Inland and coastal Waters*. New York: Academic Press.
- Gray, M., & Prowse, T. (1993). Snow and Floating Ice. In *Handbook of Hydrology*. McGraw-Hill.
- Grosshans, R., Wrubleski, D., & Goldsborough, L. (2004). *Changes in the Emergent Plant Community of Netley-Libau Marsh between 1979 and 2001*. Winnipeg, Manitoba: Delta Marsh Field Station Occasional Publication.
- Hausser, R., & Parkinson, F. (1991). Heat Exchange at the Ice/Water Interface on Flowing Water. *International Cold Region Engineering Specialty* (pp. 348-354). West Lebanon: ASCE.
- Herdendorf, C. (1982). Large Lakes of the World. *Journal Great Lakes Res.*, 379-412.
- IISD, International Institute of Sustainable Development. (2011). *Netley-Libau Marsh Integrated Management Overview*. Retrieved from [http://www.iisd.org/pdf/2011/netleylibau\\_marsh.pdf](http://www.iisd.org/pdf/2011/netleylibau_marsh.pdf)

---

## REFERENCES

---

- International Coalition for Land/Water Stewardship in the Red River Basin. (2002). *Operational and Economic Impacts of No River and Lake Winnipeg Dredging*. Winnipeg: Unpublished Report.
- International Institute of Sustainable Development. (2011). Netley-Libau Marsh Integrated Management Overview. Retrieved from [http://www.iisd.org/pdf/2011/netleylibau\\_marsh.pdf](http://www.iisd.org/pdf/2011/netleylibau_marsh.pdf)
- Jayasundra, N. C. (2007). A Comprehensive River Ice Model. Clarkson University.
- Ji, S., She, H., Wang, X., She, H., & Yue, Q. (2004). Ice Dynamics Model with a Viscoelastic-Plastic Constitutive Law. *17th IAHR Symposium on Ice*, (pp. 274-281). St. Petersburg, Russia.
- Jones, G., & Armstrong, N. (2001). *Long-term trends in total nitrogen and total phosphorus concentrations in Manitoba streams*. Winnipeg, Manitoba: Manitoba Conservation Report.
- Kadlec, R., & Knight, R. (1996). *Treatment Wetlands*. Boca Raton: CRC Press.
- KGS Group. (2002). *Engineering Aspects of No Red River Dredging*. Winnipeg, Manitoba: International Coalition for Land/Water Stewardship in the Red River Basin.
- Lal, A., & Shen, H. (1989). *An Unsteady Flow Model for the Upper Niagara River*. Civil and Environmental Engineering Department, Clarkson University.

---

## REFERENCES

---

- Lal, A., & Shen, H. (1991). A Mathematical Model for River Ice Processes. *Journal of Hydraulic Engineering*, 117(7), 851-867.
- Lui, L., & Shen, H. (2003). *A Two Dimensional Characteristic Upwind Finite Element Method for Transitional Open Channel Flow*. Potsdam, New York: Clarkson University.
- Lui, L., & Shen, H. (2005). *CRISSP2D Version 1.0 Programmer's Manual* . Potsdam, New York: Clarkson University.
- Lui, L., Shen, H., & Tuthill, A. (1998). A Numerical Model for River Ice Jam Evolution. *Proceedings of the 14th International Symposium on Ice*. Potsdam, New York.
- Matousek, V. (1984a). Regularity of the Freezing-up of the Water Surface and Heat Exchange Between Water Body Water Body and Water Body and Water Surface. *Ice Symposium* (pp. 187-201). Hamburg: International Association of Hydro-Environment Engineering and Research.
- Matousek, V. (1984b). Types of Ice Run and Conditions for their Formation. *Ice Symposium* (pp. 315-327). Hamburg: The International Association for Hydro-Environment Engineering and Research.
- Matousek, V., & Havlik, A. (1988). Heat Transfer Between Water and Ice Cover. *IAHR Ice Symposium*, (pp. 367-377). Sapporo, Japan.



---

## REFERENCES

---

- McLeod, J., & Moir, D. (1944). *Report on an Investigation of Conditions Arising Out of the Presence of Carp in Netley Marsh*. Winnipeg, Manitoba: Manitoba Department of Mines and Natural Resources.
- Mellor, M. (1966). Some Optical Properties of Snow. *Proceedings of the International Symposium on Scientifica Aspects of Snow and Ice Avalanches*. Davos, Switzerland: AIHS.
- Mellor, M. (1977). Engineering Properties of Snow. *Journal of Glaciology*, 19(81), 15-16.
- Michel, B. (1971). Winter Regime of Rivers and Lakes. *Cold Regions Science and Engineering Monograph 3, Cold Regions Research and Engineering Laboratory*.
- Michel, B., Mascotte, N., Fonseca, F., & Rivard, G. (1982). Formation of Border Ice in the Ste. Anne River. *2nd Workshop on the Hydraulics of Ice Covered Rivers* (pp. 38-61). Edmonton, Alberta: Committee on River Ice Processes and the Environment.
- Miles, T. (1993). *A Study of Border Ice Growth on the Burntwood River*. Winnipeg: University of Manitoba.
- Newbury, R. (1968). *The Nelson River: A Study of Subarctic River Processes*. Baltimore: John Hopkins University.
- Phillips, G., Eminson, D., & Moss, B. (1978). A Mechanism to Account for Macrophyte Decline in Progressively Eutrophicated Freshwaters. *Aquatic Botany*, 4, 103-126.

---

## REFERENCES

---

- Rimsha, V., & Donchenko, R. (1957). *The Estimation of Heat Loss from Free Water Surfaces in Wintertime*. Trudy Leningrad Gosud. Hidrol. Institute.
- Salki, A. (2002). *Climate Change Connection*. Retrieved from Climate Change and Lake Winnipeg: [http://www.climatechangeconnection.org/pages/lake\\_winnipeg.html](http://www.climatechangeconnection.org/pages/lake_winnipeg.html)
- Scheffer, M. (1998). *Ecology of Shallow Lakes*. New York: Chapman and Hall.
- Shen, H., & Lui, L. (2000). SPH Simulation of River Ice Dynamics. *Journal of Computational Physics*, 165(2), 752-770.
- Shen, H., & Van Devalk, W. (1984). Field Investigation of St. Lawrence River Hanging Ice Dams. *Proceedings of the IAHR Ice Symposium*, (pp. 241-249). Hamburg.
- Shen, H., Chen, Y., Wake, A., & Crissman, R. (1993). Lagrangian Discrete Parcel Simulation of River Ice Dynamics. *International Journal of Offshore and Polar Engineering*, 3(4), 328-332.
- Stainton, M., & Salki, A. (2003). *Ecosystem Evidence for the Need to Remove Phosphorus from the City of Winnipeg's Wastewater Effluents*. Winnipeg: Submission to the Manitoba Clean Environment Commission Public Hearing on the City of Winnipeg Wastewater Collection and Treatment System.
- Venema, H., Regehr, S., Grosshans, R., Roy, M., & Pinter, L. (2005). *Letley-Libau Marsh Revitalization: Water Level Management and Habitat Enhancement with Implications for Nutrient Removal and Bioenergy Production*. Winnipeg, Manitoba: International Institute for Sustainable Development.

---

## REFERENCES

---

Verbiwski, B. (1986). *Netley-Libau Marshes Resource Development and Management Proposal*. Winnipeg: Manitoba Natural Resources.

Wetzel, R. (2001). *Limnology, 3rd edition*. New York: Academic Press.

Yapa, P., & Shen, H. (1984). Effect of Ice Cover on Hydropower Production. *Journal of Energy Engineering*, 110(3), 231-234.

---

**APPENDIX A**

---

Appendix A contains comparisons between measured and simulated ice thickness for all measured locations from the 2009-2010, 2010-2011, and 2011-2012 winter seasons.

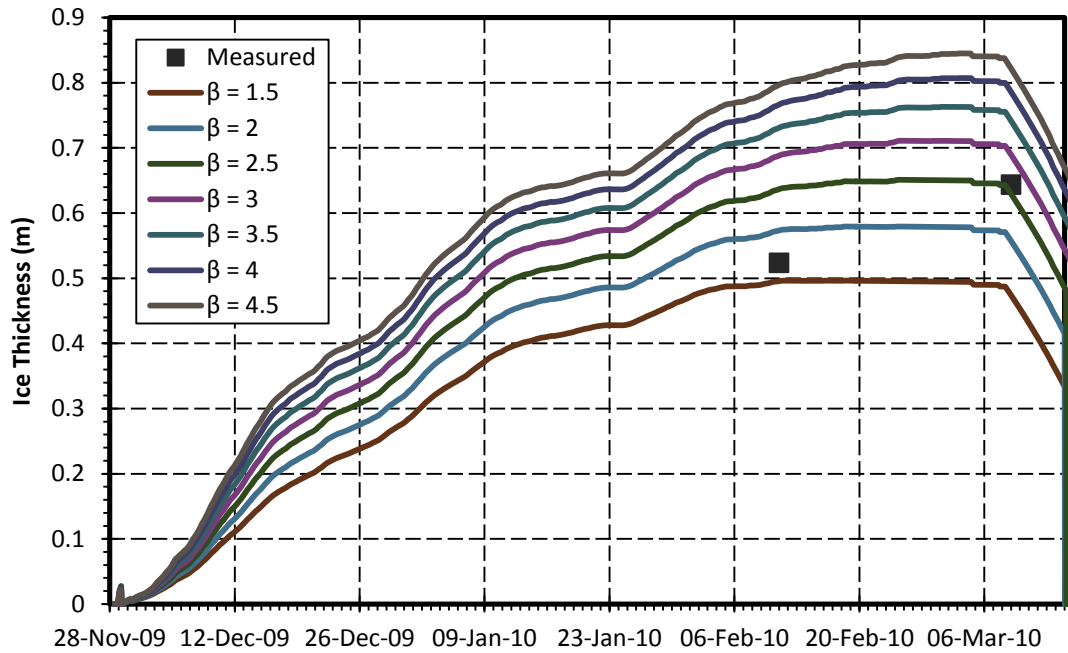


Figure A. 1: Dynamic ice calibration upstream of Peguis Church in winter 2009-2010.

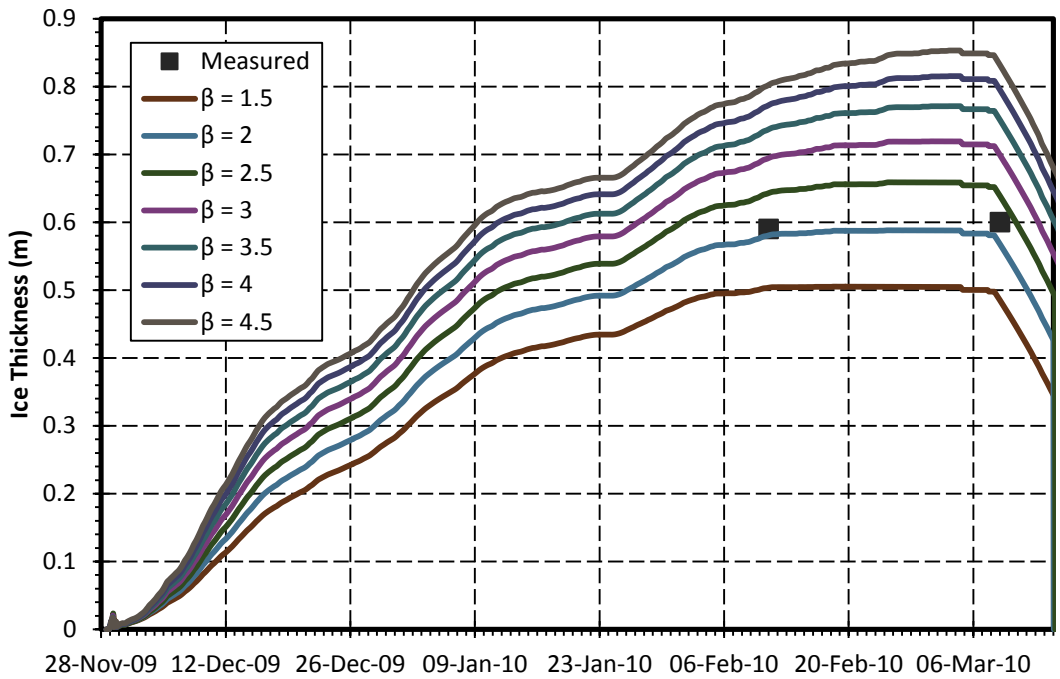


Figure A. 2: Dynamic ice calibration at Breezy Point in winter 2009-2010.

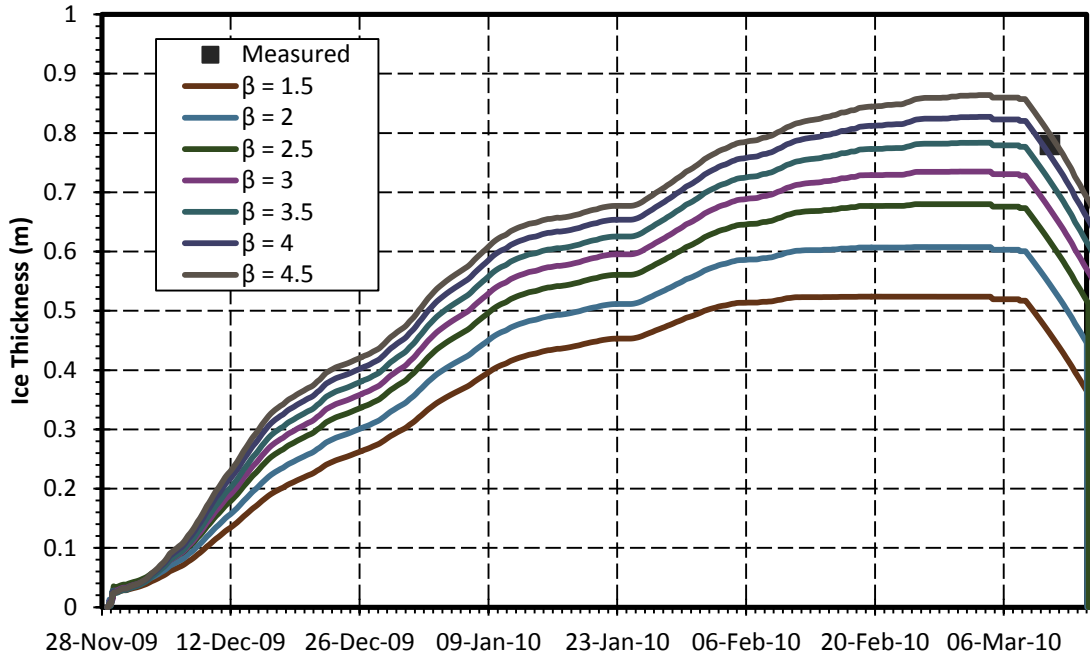


Figure A. 3: Dynamic ice calibration at Netley Cut in winter 2009-2010.

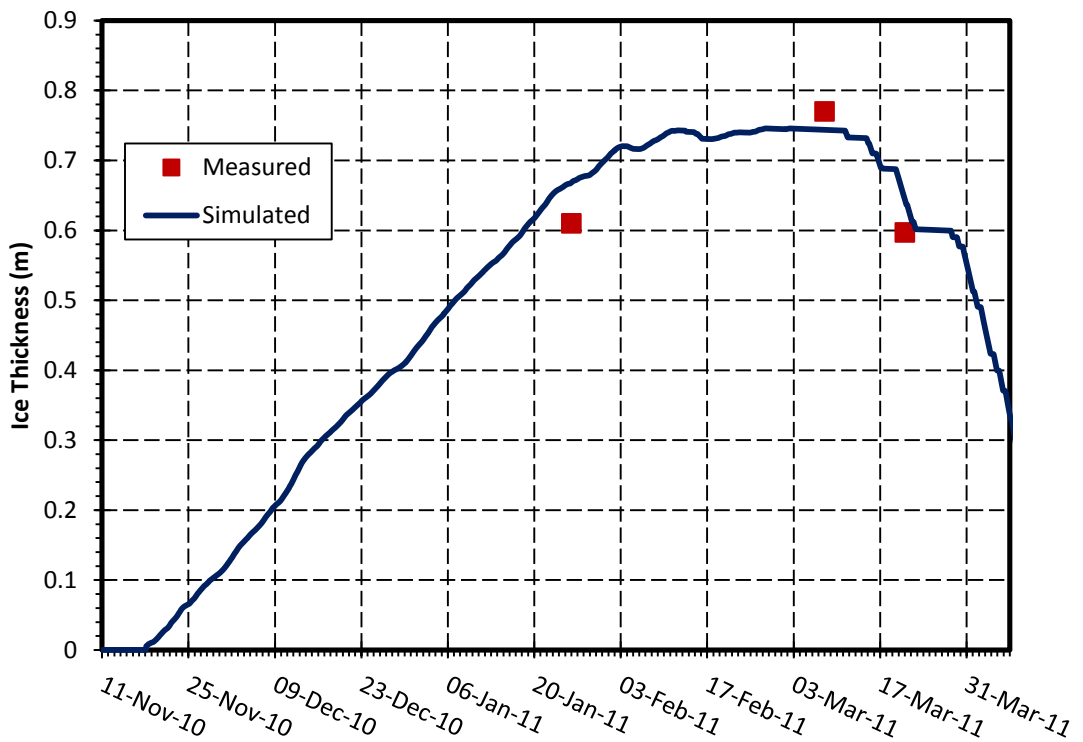


Figure A. 4: Dynamic ice verification upstream of Sugar Island in 2010-2011

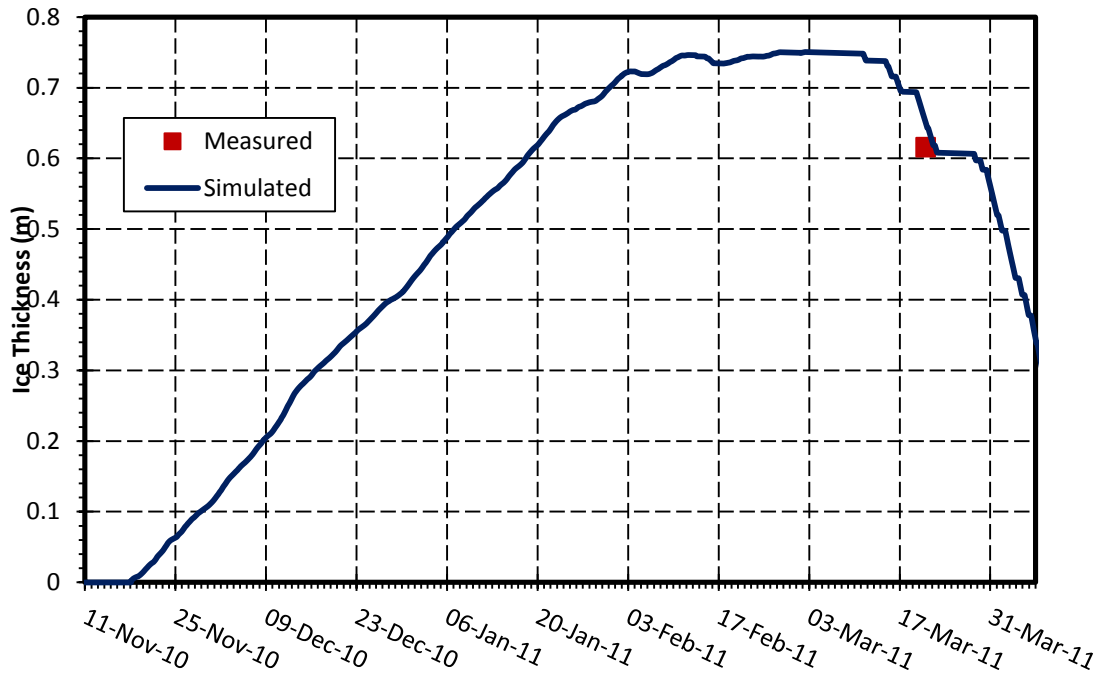


Figure A. 5: Dynamic ice verification at Hwy. 4 in 2010-2011

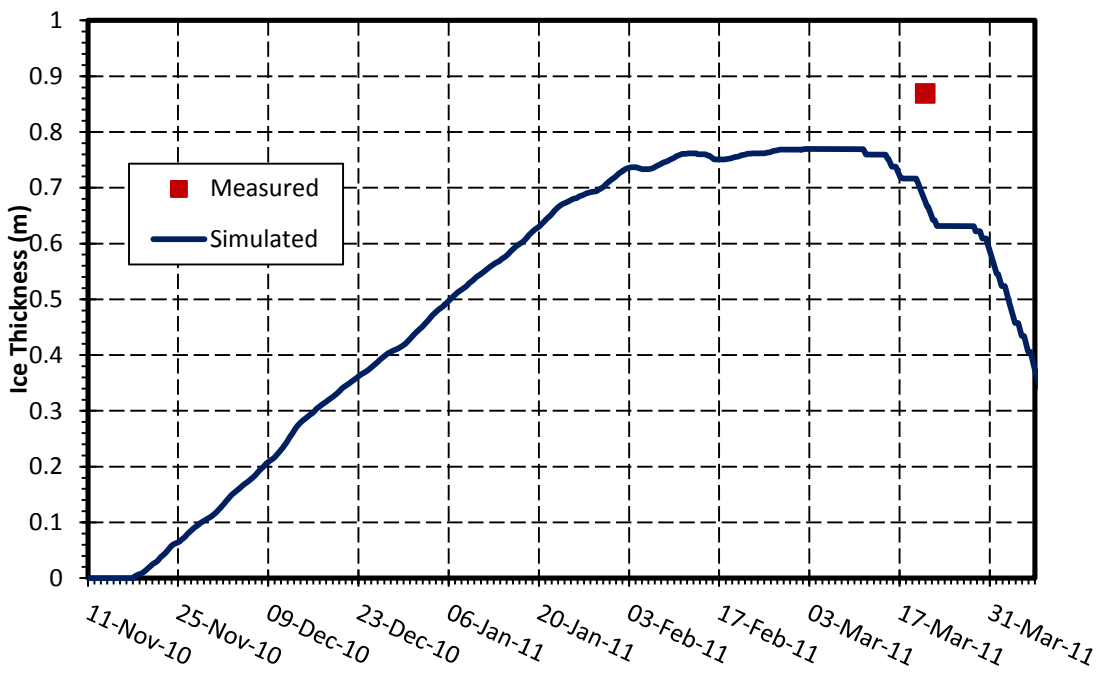


Figure A. 6: Dynamic ice verification at Breezy Point in 2010-2011

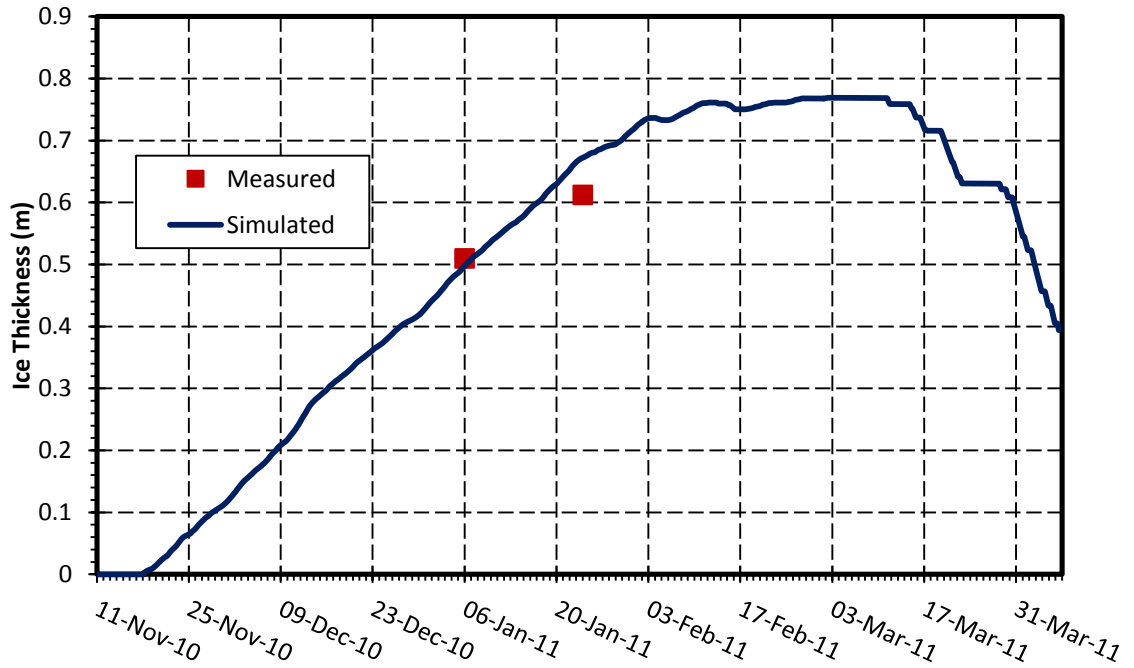


Figure A. 7: Dynamic ice verification at Goldeye Lake in 2010-2011.

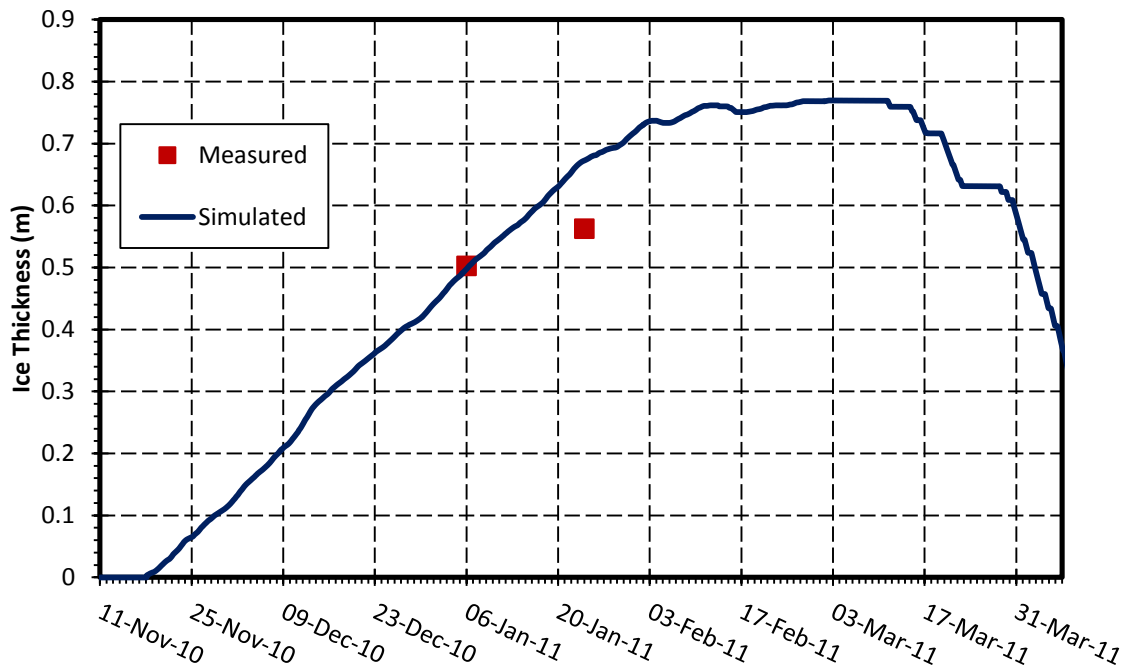


Figure A. 8: Dynamic ice verification at Goldeye Creek in 2010-2011.



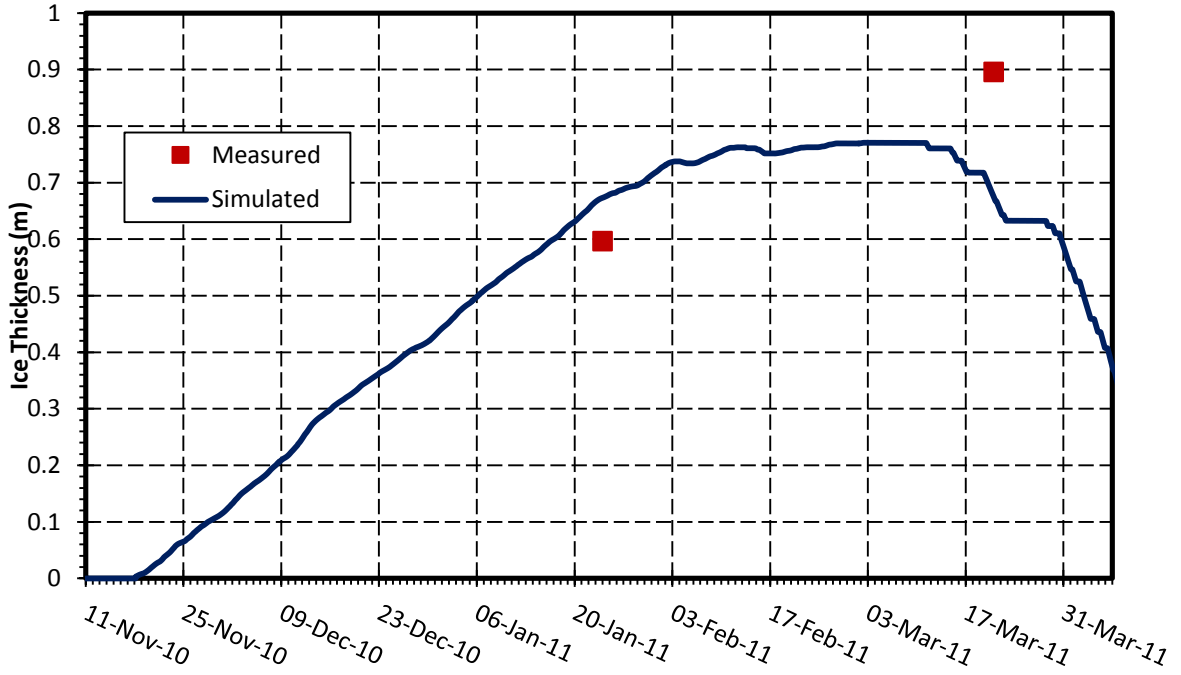


Figure A. 9: Dynamic ice verification at Netley Creek in 2010-2011.

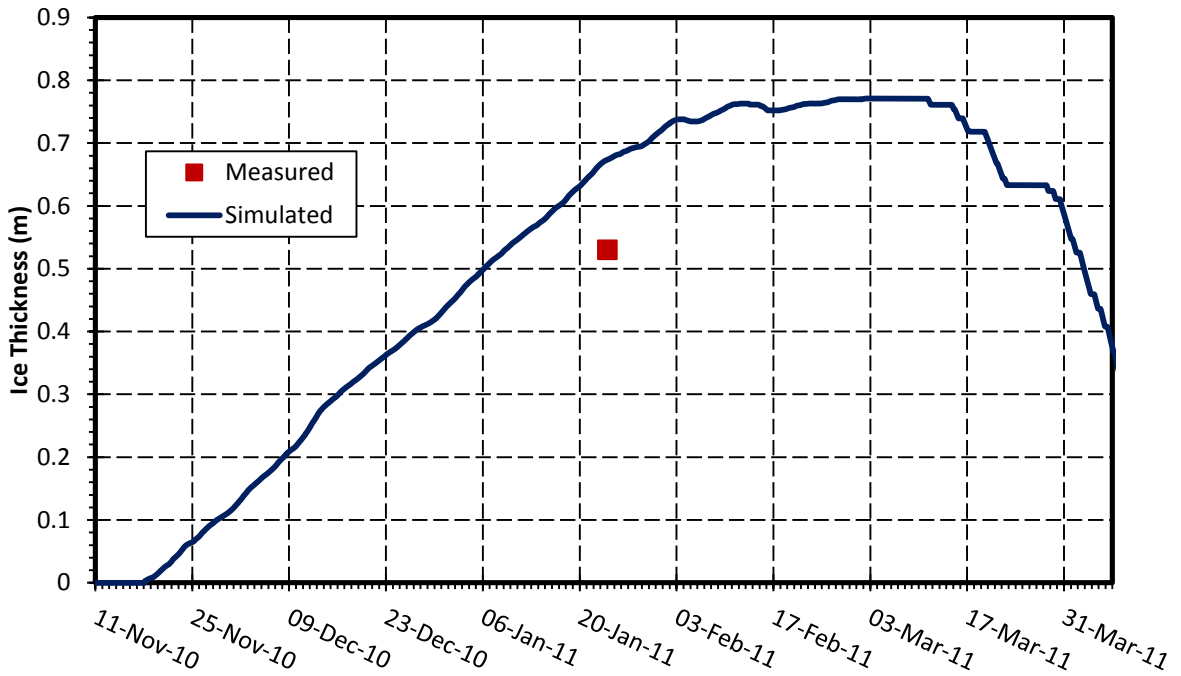


Figure A. 10: Dynamic ice verification downstream of Netley Creek in 2010-2011.

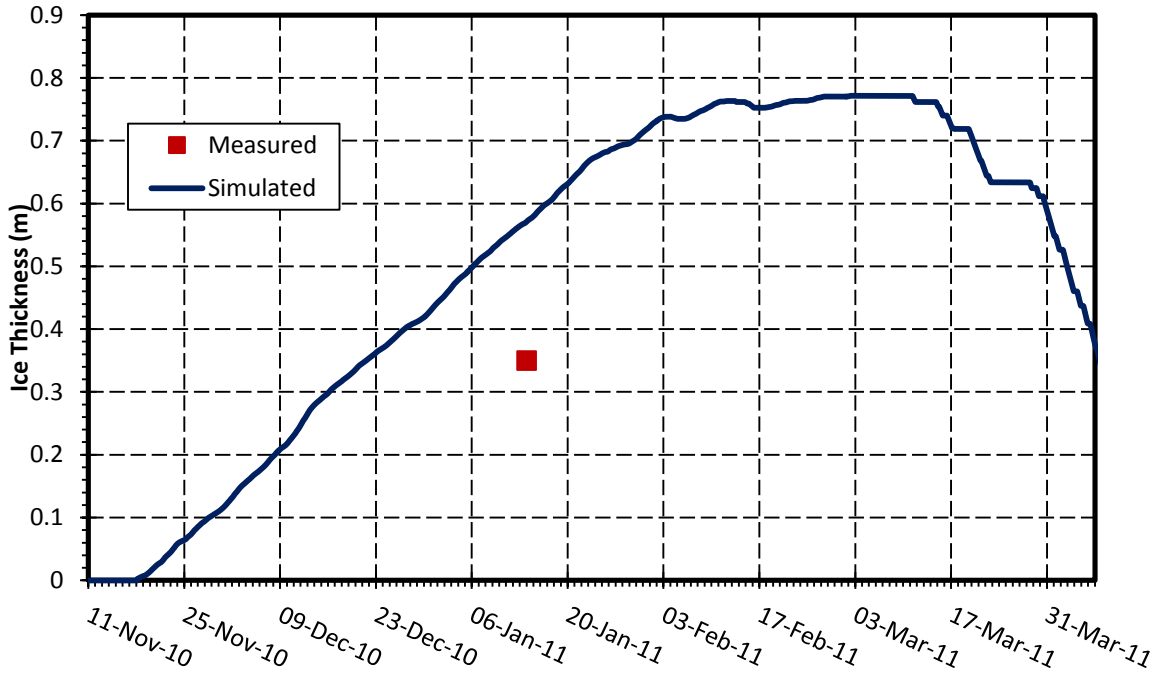


Figure A. 11: Dynamic ice verification upstream of Netley Cut in 2010-2011.

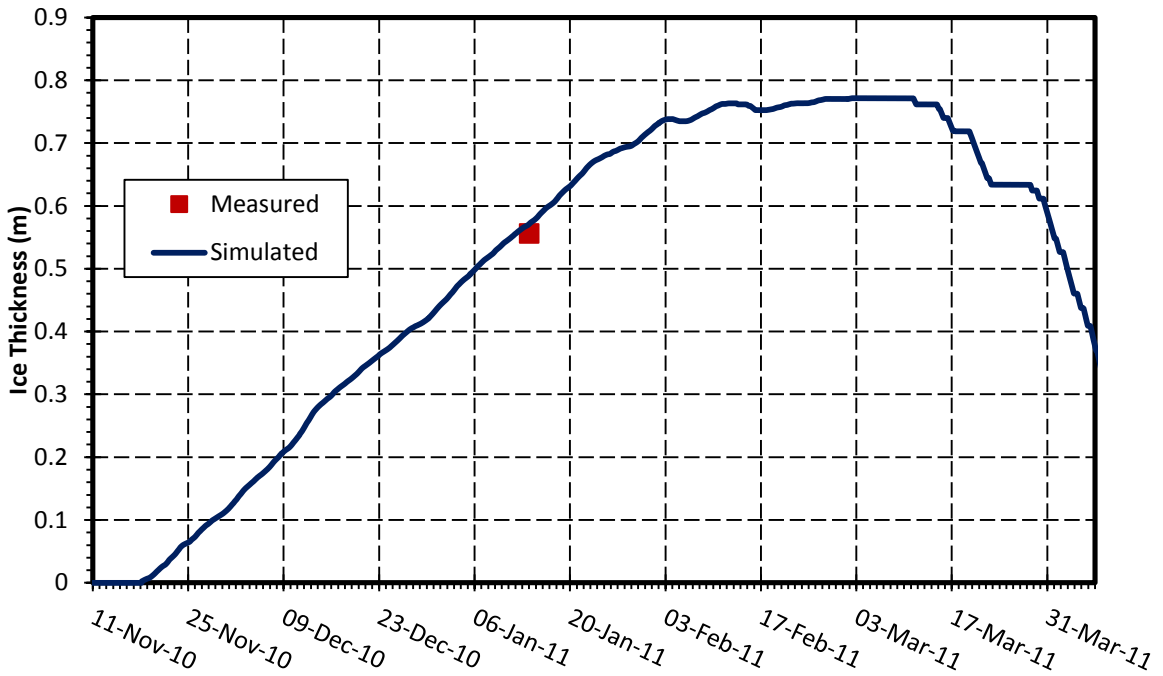


Figure A. 12: Dynamic ice verification downstream of Netley Cut in 2010-2011.

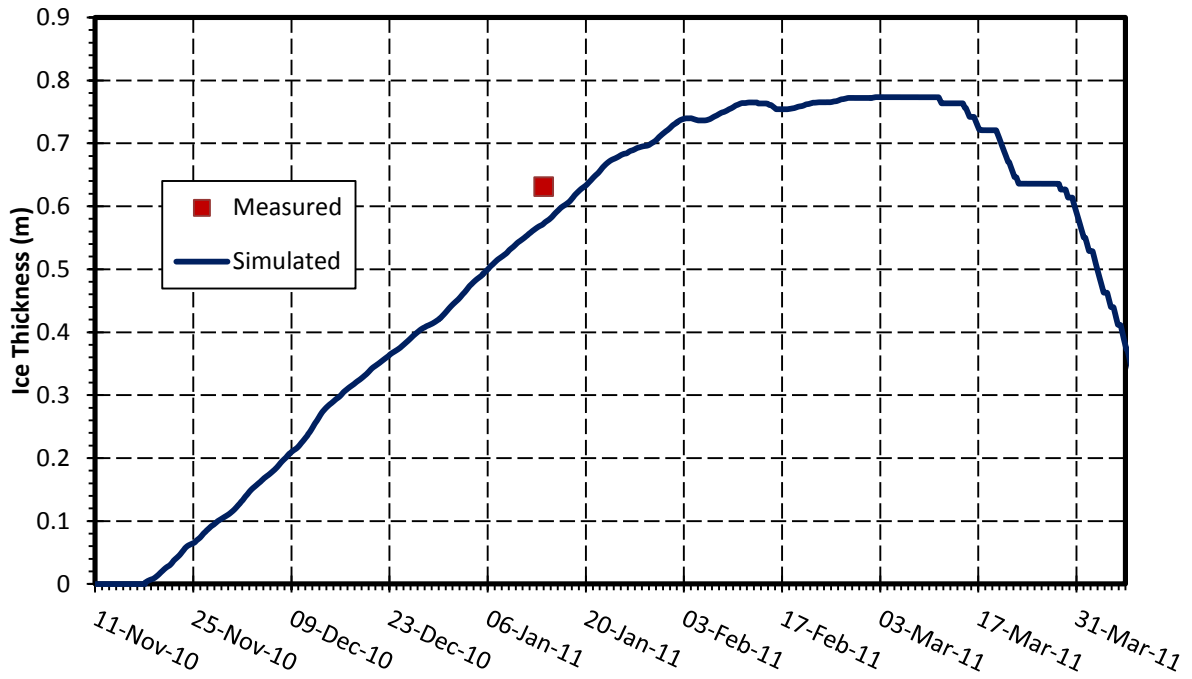


Figure A. 13: Dynamic ice verification at Netley Lake in 2010-2011.

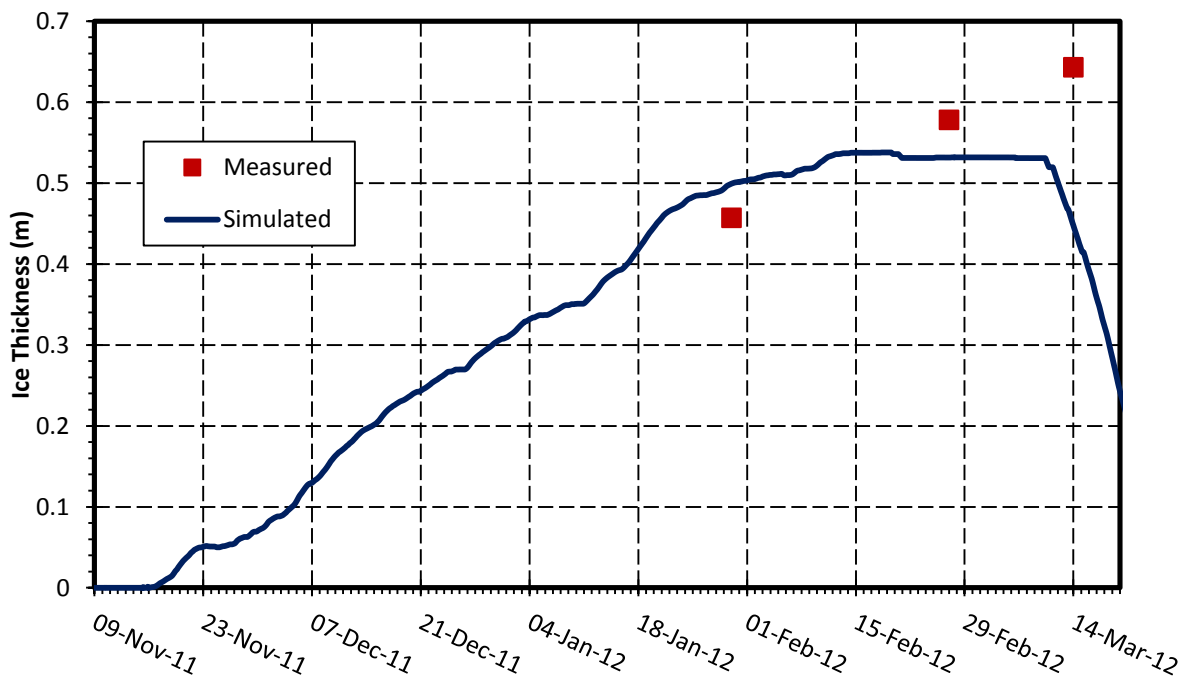


Figure A. 14: Dynamic ice verification at Breezy Point in 2011-2012.

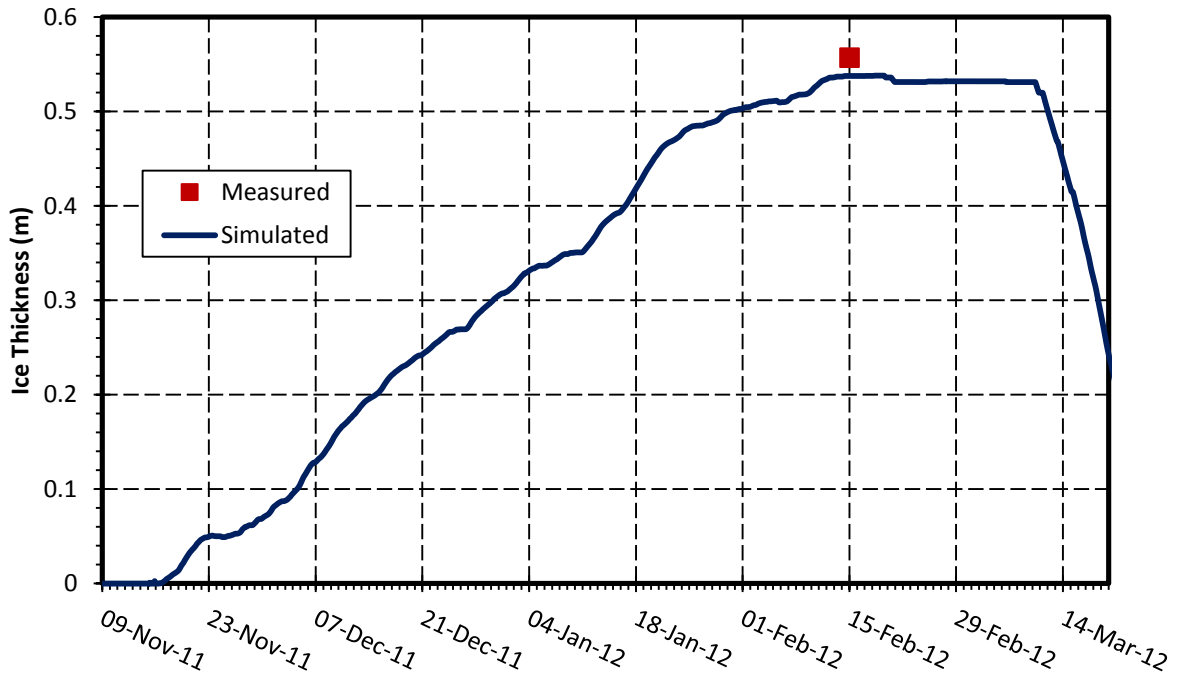


Figure A. 15: Dynamic ice verification upstream of Netley Cut in 2011-2012

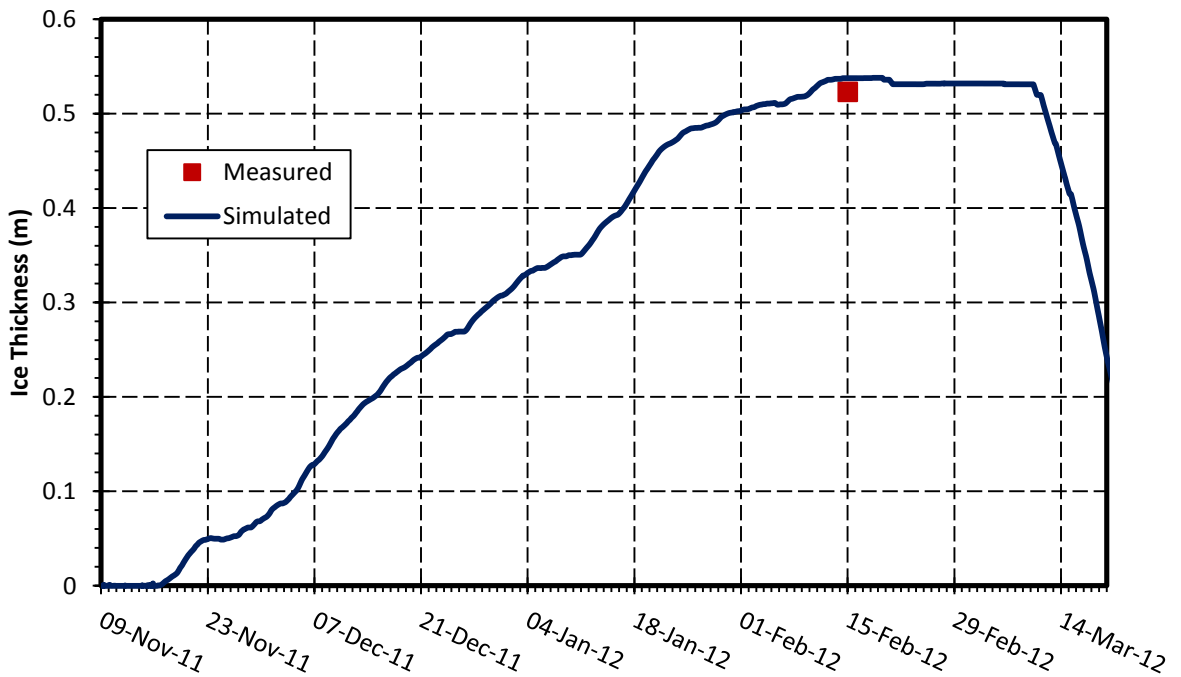


Figure A. 16: Dynamic ice verification downstream of Netley Cut in 2011-2012

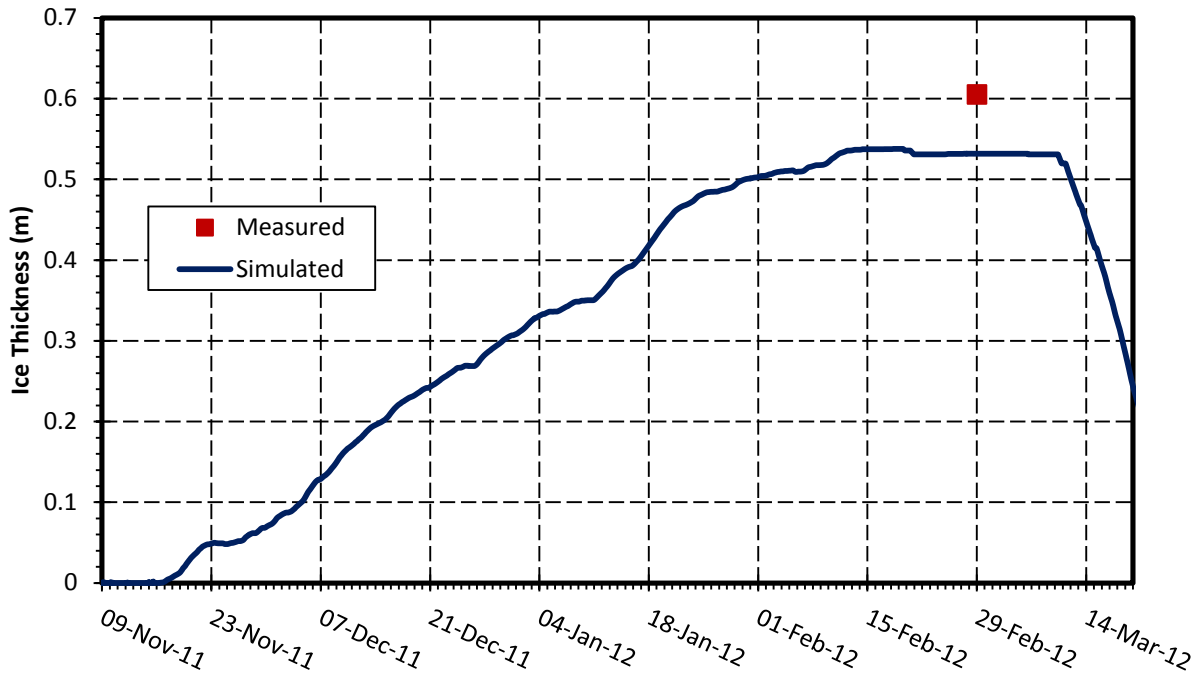


Figure A. 17: Dynamic ice verification in main channel in 2011-2012

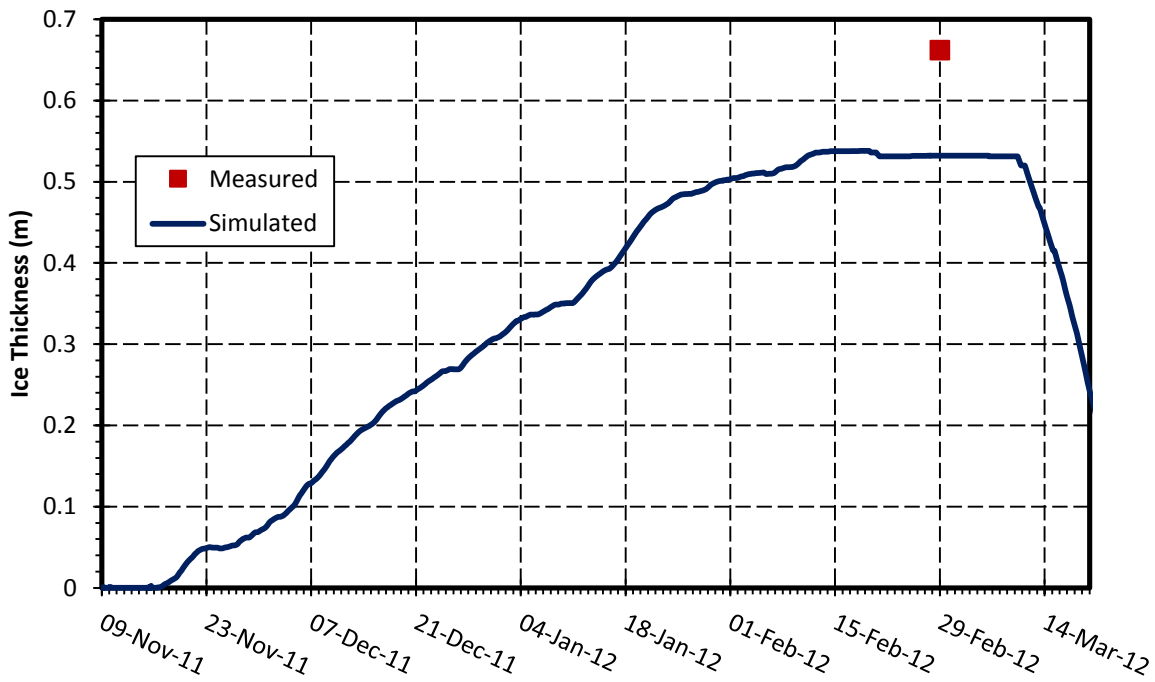


Figure A. 18: Dynamic ice verification in east channel in 2011-2012

April 16, 2012

Melissa Haresign  
Department of Civil Engineering, Faculty of Engineering  
University of Manitoba, Winnipeg, Manitoba  
Canada R3T 2N2

Dear Ms. Haresign,

I have no issues with your use of the requested figures, and grant you permission to include the requested copyright material as outlined below in your M.Sc. thesis:

Grosshans, R. E., D. A. Wrubleski and L. G. Goldsborough 2004. Changes in the Emergent Plant Community of Netley-Libau Marsh Between 1979 and 2001. *Delta Marsh Field Station (University of Manitoba) Occasional Publication No. 4, Winnipeg, Canada. 52 pp.*

- Figure 3: Netley-Libau Marsh 2001 color infrared photomosaic, based on a compilation of 106 1:10000 color infrared serial photos acquired on 3 August 2001 (Page 7).
- Figure 4: Netley-Libau Marsh, 1979 (Page 14).
- Figure 5: Netley-Libau Marsh, 2001 (Page 15).
- Figure 11: Conceptual diagram of some of the factors thought to be contributing to the decline of emergent vegetation in Netley-Libau Marsh (Page 23).
- Figure 13: This oblique, serial view (looking southwest) of the Red River, Netley Cut, and Netley Lake was taken on 8 October 2003 (Page 27).

Your graduate research is an important addition to the ongoing research efforts at Netley-Libau Marsh and the understanding of human-induced impacts to this freshwater coastal wetland. I congratulate you on your efforts, and I look forward to reading the completed thesis.

Sincerely,

Richard Grosshans  
Research Associate  
International Institute for Sustainable Development (IISD)  
Winnipeg, Manitoba, Canada  
phone: 204-958-7718, [www.iisd.org](http://www.iisd.org)

WEBSITE: [www.iisd.org](http://www.iisd.org)

E-MAIL: [info@iisd.ca](mailto:info@iisd.ca)

161 Portage Avenue East, 6th Floor  
Winnipeg, Manitoba  
Canada R3B 0Y4

TEL: (204) 958-7700  
FAX: (204) 958-7710

MIE 2  
9, chemin de Balexert  
1219 Châteline, Geneva, Switzerland

TEL: (41-22) 917-8683  
FAX: (41-22) 917-8054

300 East 56th Street, #11D  
New York, NY  
10022 USA

TEL: (646) 536-7556  
FAX: (646) 219-0955

75 Albert Street, Suite 903  
Ottawa, Ontario  
Canada K1P 5E7

TEL: (613) 238-2296  
FAX: (613) 238-8515